UiT The Arctic University of Norway

Faculty of Engineering Science and Technology

Department of Computer Science and Computational Engineering

Some new contributions related to structural problems in engineering

Andreas Seger

A dissertation for the degree of Philosophiae Doctor, February 2020

UiT The Arctic
University of Norway

Andreas Seger

Some new contributions related to structural problems in engineering

A dissertation for the degree of Philosophiae Doctor

Faculty of Engineering Science and Technology
Department of Computer Science and Computational Engineering

SINTEF Narvik

February 2020

Abstract

The studies in this PhD thesis is focused on some problems of general interest in applied mathematics and engineering sciences. A very broad view is used; from contributions which can be directly used for solving some important structural problems in engineering sciences, to contributions which also are of interest in pure mathematics. The main body of the PhD thesis consists of five papers (Papers A – E).

In Paper A a new presentation of the mathematical theory of linear elasticity from a functional analytical standpoint is given. Moreover, a useful estimate of the Sobolev norm in R^n is given. Finally, the problem connected to non-linear beams on elastic foundation is modelled and analyzed.

In Paper B we present a new finite element method by using a simplified three dimensional model to evaluate the sliding stability of flat slab buttress dams. Moreover, we investigate the possibility of utilizing safety capacity in neighbouring pillars within a section to show that the entire section has adequate capacity against sliding in the dam-foundation interface.

In Paper C we present some new thoughts on and a discussion of an overview of different numerical methods that may be applied to evaluate the stability of dam structures. In particular, we discuss and compare with 14 different case studies from the literature where numerical methods have been used to study the behaviour of gravity and plate dams. Finally, we identify and discuss advantages and disadvantages of different methods of modeling failure modes.

In Paper D we prove and discuss some new Fourier inequalities in the general frame of Lorentz-Zygmund spaces and in the case with unbounded orthogonal systems. The derived results generalize, complement and unify several results in the literature for this general case.

In Paper E we consider some mathematical aspects of the torsion problem for anisotropic periodic plate-structures where the underlying material is monoclinic. In particular, we show in detail how the weak formulation of the problem is derived and express the torsional rigidity in terms of its solution.

These new results are put into a more general frame in an Introduction, where, in particular, a comparison with some new international research and broad view of such interplay between applied mathematics and engineering problems is presented and discussed.

Preface

This PhD thesis in Engineering Science is composed of five papers [A] – [E] and a matching Introduction. In the Introduction the papers [A] – [E] are discussed and put into a more general frame. The Introduction is also of independent interest since it contains a brief discussion on the important interplay between applied mathematics and engineering applications illustrated by comparing with some relevant international research presented in this light.

A very brief presentation of the main content of the five papers can be found in the Abstract above and a more complete description at the end of the Introduction.

List of Papers

Paper A: Andreas Seger. "Some mathematical aspects on linear and nonlinear elasticity". 32 pages. *Submitted for publication.*

Paper B: Andreas Seger and Eduardo Bretas. "A simplified three-dimensional method for stability assessment of buttress dams". 17 pages. *Submitted for publication.*

Paper C: Andreas Seger. "New thoughts on and discussion of numerical methods for assessing concrete dams under static loading". 26 pages. *Submitted for publication.*

Paper D: G. Akishev, L.E. Persson and A. Seger. "Some Fourier inequalities for orthogonal systems in Lorentz–Zygmund spaces". In: *Journal of Inequalities and Applications.* (2019), Article number: 2019:171, 18 pages, DOI: 10.1186/s13660-019-2117-4.

Paper E: Dag Lukkassen, Annette Meidell and Andreas Seger. "On the Torsion Problem for Anisotropic Periodic Plate Structures". In: *AIP Conference Proceedings*. Vol. 1637 (2014), pages 976–981. DOI: 10.1063/1.4904671.

Acknowledgements

First of all I want to express my deep gratitude to my main supervisor Professor Dag Lukkassen for introducing me to the topics covered in this PhD thesis and for his invaluable support, advice, help, encouragement and care during all of this work.

Secondly, I thank my assistant supervisors Professors Annette Meidell and Lars-Erik Persson for various complementary support, proof reading, help and encouragement during my studies.

Moreover, I am very grateful to the Faculty of Engineering Science and Technology at UiT The Arctic University of Norway, Campus Narvik, as well SINTEF Narvik, for providing me the economic possibility to work with the questions studied and presented in this PhD thesis.

I also thank my colleagues at the Department of Mathematics and Engineering Sciences and SINTEF Narvik for the very good atmosphere and support of various kinds.

Last but not least, my deepest thanks go to my partner Marte Bergmann and my parents Arve Seger and Randi Moldestad for the support and love during this work.

Andreas Seger
Narvik, February 2020

Chapter 1

Introduction

This PhD thesis in Engineering Science is mainly focused on some problems of general interest in engineering sciences. It contains a broad spectrum; from contributions which can be directly used for solving some important structural problems, to contributions which are of interest also in pure mathematics.

Such broad view of science and in particular the interplay between mathematics, applied mathematics and engineering sciences are increasingly important for several reasons, e.g. for the technical development. Correspondingly, nowadays there exists even some international Journals which invites papers on such a broad scale of science. As an important example let us here mention the Journal "Nonlinear Studies" with P.L. Lions and S. Sivasundaram as Editors-in Chiefs (see [60], www.nonlinearstudies.com).

Especially the last issue of this Journal (December 2019) was devoted to the 75th anniversary of one of my supervisors and in the preface the Editors P.L. Lions, N. Samko and S. Sivasundaram wrote some motivation in this spirit, see [61] and c.f. also [66]. This Journal Issue contains 22 papers and as typical examples which especially well illustrates the spirit of this PhD thesis I mention the papers [3], [9], [11], [33], [36], [66], [98], [103], [104] and [109]. In particular, in the papers [33], [36], [103] and [109] important contributions to various types of Fourier analysis are given. In paper [D] of this PhD thesis some other new contributions in this area are given. All these contributions contain results of interest also in pure mathematics. The papers [98] and [104] are intended to be able to be used for direct applications. The papers [B] and [C] of this PhD thesis have mainly the same aims. Finally, the papers [A], [D] and [E] are typical papers in what we call "Engineering Mathematics", which means that they contain results of interest for concrete applications in engineering sciences but also in pure mathematics.

1.1 A short description of the results in papers A - E

1.1.1 Paper A

In Paper A, a new presentation of the mathematical theory of linear elasticity from a functional analytical standpoint is given. Some facts which have influenced our investigation are the following:

1. Advanced mathematical analysis based on nonlinear models seems to be needed in order to obtain a better understanding of the complicated structures that are involved.

2. In modern product development one often replaces testing activities with analytical and numerical methods, where complex mathematical results and advanced models are used.

3. By using more advanced mathematical tools one may be able to develop new methods and algorithms that are useful in designing railway tracks, see e.g. [65] which have substantially influenced our results and way of thinking.

The part of the paper devoted to beams on elastic foundation is deeply inspired by the interesting ideas and results presented in [65], and the paper is intended to be a step further in this direction. Many of the results obtained in [65] are explained in a new and hopefully more pedagogical light in this paper, and the same extensions are presented.

In order to make the paper readable to a broad audience, including engineers and scientists within the elasticity community, as well as pure mathematicians, we have made an effort making the presentation as easy as possible without leaving out any technicalities, which are important for the understanding of the contents. Still, those who are completely unfamiliar with functional analysis and theory concerning function spaces, are guided to look in standard literature concerning such questions for complementary information.

This paper is a typical paper in what we call engineering mathematics, i.e. that it contain results of interest for concrete applications in engineering sciences but also in pure mathematics. The paper is dived into 5 sections. After an introduction we present in Section 2 some preliminary results connected to the theory of linear and nonlinear monotone operators. In Section 3 we give a new presentation of the mathematical theory of linear elasticity from a functional analytical point of view, and discuss how strong and weak formulations can be obtained and analyzed. The main result in Section 4 is a theorem, which gives an useful estimate of the Sobolev norm in R^n. Finally, Section 5 is reserved for modelling and analysis of some problems connected to nonlinear beams on elastic foundation.

The results in Paper A are related to the following publications: [2], [8], [19], [20], [64], [65], [74], [94], [97], [110] and [111].

1.1.2 Paper B

In Paper B we present a new method to evaluate the sliding stability of flat slab buttress dams. Moreover, we investigate the possibility of utilizing safety capacity in neighbouring pillars within a section to show that the entire section has adequate capacity against sliding in the dam-foundation interface. We pronounce that within the field of dam-engineering the assessment of the safety of dams is govern by national guidelines and there is little room for new computation methods. This fact has influenced the content of this engineering focused paper. In the case of buttress dams, the current practice is to evaluate each pillar individually. A section of a flat-slab buttress dam

with three different cases of inclination in the pillar-foundation interfaces is investigated. Furthermore, we preform a comparison of how the sliding safety factors of the whole section are affected if it is supported by pillars with both satisfactory and unsatisfactory safety margins. The section was modelled with shell elements using the finite element software ANSYS Mechanical v17.2, where the geometry is based on a typical flat slab buttress dam. Here, the Mohr-Coulomb contact model was used in the dam-foundation interfaces. The combined sliding safety factor for all three pillars was computed from the results obtained from the analysis.

The sliding safety factor, $S_{sliding}$ is defined by

$$S_{sliding} = \frac{\Sigma V}{\Sigma H} \tan(\phi + \alpha),$$

where ϕ is the friction angle, α is the inclination of the interface, $\sum V$ is the sum of forces in the vertical direction and $\sum H$ is the sum of forces in the horizontal direction.

In particular, the results show that for a section with one pillar with a sliding safety factor of 1.1 and two pillars with a sliding factor of 1.4, the combined sliding safety factor for the whole section is 1.4, which is the requirement in Norway [85]. This indicates that by considering the whole section an adequate sliding safety factor can be achieved and thereby we can reduce the need for rehabilitation of the unsatisfactory pillar. In this connection we suggest that further investigation will be done in order to further verify this conjecture. This can be of great interest for the industrial applications of this type related to applied mathematics.

The results in Paper B are related to the following publications: [17], [27], [34], [37], [40], [44], [45], [70], [76], [79], [83], [84], [85], [86], [99], [101] and [106].

1.1.3 Paper C

In Paper C we present some new thoughts on and a discussion of an overview of different numerical methods that may be applied to dam structures. First we mention that in Norway 95 % of the total power production is produced from hydro-power [44]. Norway has the largest installed hydro-power capacity in Europe with 31 626 MW [44]. The Norwegian Water Resources and Energy Directorate (NVE) is the governmental authority of dams in Norway and ensures that the owners of the dams complies with the dam safety regulation (Damsikkhertsforskriften) [86]. These facts were important when we started this investigation in collaboration with SINTEF Narvik.

However, we wanted to put our investigation into a more scientific and global perspective. In particular, in this light we discuss and compare 14 different case studies from the literature, where numerical methods have been used to study the behaviour of gravity and plate dams. These case studies are from 11 different countries where 3 are from Norway. Hence, we have broaden our approach when investigating dams in Norway to a more international perspective

to analyse, treat and solve similar problems worldwide. In particular, we identified and discussed advantages and disadvantages of the following four procedures for evaluating the failure modes (overturning, sliding and overstressing) of concrete dams:

- Increasing the head water level until failure.
- Push-over.
- Reducing the friction angle.
- Resultant forces.

Summing up, we think that our paper can be very useful as a basis when investigating such types of problems in engineering sciences.

The results in Paper C are related to the following publications: [1], [4], [5], [6], [7], [10], [12], [14], [15], [16], [18], [21], [22], [23], [24], [25], [28], [29], [30], [31], [32], [38], [39], [41], [42], [43], [44], [47], [50], [54], [55], [57], [56], [59], [62], [63], [70], [71], [75], [77], [81], [83], [84], [85], [86], [87], [88], [91], [92], [93], [95], [102], [105], [107], [108] and [112].

1.1.4 Paper D

In Paper D we prove some new Fourier inequalities. To shortly describe the background of such results we present the following results derived by Lars-Erik Persson in his PhD thesis from 1974 (see [89] and also [90]).

Theorem 1.1.1. *Let $0 < p < \infty$ and $\Phi = \left\{e^{2\pi ikt}\right\}_{k=-\infty}^{+\infty}$ be the trigonometrical system.*

a) If there exists a positive number $\delta > 0$ so that $\omega(t)\, t^{-\delta}$ is an increasing function of t and $\omega(t)\, t^{-\left(\frac{1}{2}-\delta\right)}$ is a decreasing function of t, then

$$\left(\sum_{k=1}^{\infty} \left(a_k^* \omega(k)\right)^p \frac{1}{k}\right)^{\frac{1}{p}} \leq c_{14} \|f\|_{\Lambda_p(\omega)}. \tag{1.1}$$

b) If there exists a positive number $\delta > 0$ such that $\omega(t)\, t^{-\frac{1}{2}-\delta}$ is an increasing function of t and $\omega(t)\, t^{-1+\delta}$ is a decreasing function of t, then

$$\|f\|_{\Lambda_p(\omega)} \leq \left(\sum_{k=1}^{\infty} \left(a_k^* \omega(k)\right)^p \frac{1}{k}\right)^{\frac{1}{p}}, \tag{1.2}$$

where $\{a_k^*\}_{k=0}^{\infty}$ is the non-increasing rearrangement of the sequence $\{|a_k|\}_{k=-\infty}^{\infty}$ of Fourier coefficients of f with respect to the system Φ.

Here, as usual the generalized Lorentz space $\Lambda_p(\omega)$ consists of the functions f on $[0,1]$ such that $\|f\|_{\Lambda_p(\omega)} < \infty$, where

$$\|f\|_{\Lambda_p(\omega)} := \begin{cases} \left(\int_0^1 (f^*(t)\,\omega(t))^p \frac{dt}{t}\right)^{\frac{1}{p}} & \text{for} \quad 0 < p < \infty, \\ \sup\limits_{0\le t\le 1} f^*(t)\,\omega(t) & \text{for} \quad p = \infty. \end{cases}$$

Remark 1.1.2. This result may be regarded as a unification and generalization of several classical results e.g. those by Marcinkiewicz, Zygmund, Hausdorff, Young, Paley, Riesz, Pitt and Stein. A very good description of this prehistory of Theorem 1.1.1 is given in the PhD thesis of Aigerim Kopezhanova from 2017 (see [51]).

Theorem 1.1.1 was generalized to the case with a general bounded orthogonal system (this means that $|a_n| \le k < \infty \forall n$) in [52] (see also [51]). However, it is not known whether or not Theorem 1.1.1 can be generalized to the case with unbounded orthogonal systems. But some results are known also for this case but in very restrictive cases e.g. for Lebesgue spaces, see for example various contributions by Marcinkiewicz and Zygmund [72], Kolyada [49] and Kirillow [48]. In Paper D we generalize and complement these results by considering the more general case with so called Lorentz-Zygmund spaces as defied below:

Let $q \in (1, +\infty)$, $r \in (0, +\infty)$ and $\alpha \in \mathbb{R}$. Moreover, let $L_{q,r}(\log L)^{\alpha}$ denote the Lorentz-Zygmund space, which consists of all measurable functions f on $[0, 1]$ such that

$$\|f\|_{q,r,\alpha} := \left\{\int_0^1 (f^*(t))^r (1 + |\ln t|)^{\alpha r} \cdot t^{\frac{r}{q}-1} dt\right\}^{\frac{1}{r}} < +\infty,$$

where f^* is the non- increasing rearrangement of the function $|f|$ (see e.g. [96]).

If $\alpha = 0$, then the Lorentz-Zygmund spaces coincides with the Lorentz space: $L_{q_1,q_2}(\log L)^{\alpha} = L_{q_1,q_2}$. If $\alpha = 0$ and $q_1 = q_2 = q$, then $L_{q_1,q_2}(\log L)^{\alpha}$ space coincides with the Lebesgue space $L_q[0, 1]$ (see e.g. [80]) with the norm

$$\|f\|_q := \left(\int_0^1 |f(x)|^q dx\right)^{\frac{1}{q}}, 1 \le q \le +\infty.$$

We consider an unbounded orthogonal system $\{\varphi_n\}$ in $L_2[0, 1]$ such that

$$\|\varphi_n\|_s \le M_n, n \in \mathbb{N}, \tag{1.3}$$

and

$$\mu_n = \sup\left\{\left\|\sum_{k=1}^n c_k\varphi_k\right\| : \sum_{k=1}^n c_k^2 = 1\right\}, \rho_n = \left(\sum_{k=n}^{\infty} |a_k|^2\right)^{\frac{1}{2}}, \tag{1.4}$$

for some $s \in (2, +\infty)$. Here $M_n \uparrow$ and $M_n \ge 1$ (see [113], [72, p.313]).

Two main results in paper D reads as follows:

Theorem 1.1.3. *Let $2 < q < s \leq +\infty$, $\alpha \in \mathbb{R}$, $r > 0$ and $\delta = \frac{rs(q-2)}{q(s-2)}$. If $\{a_n\} \in l_2$ and*

$$\Omega_{q,r,\alpha}(a) = \left\{ \sum_{n=1}^{\infty} \left(\rho_n^r - \rho_{n+1}^r\right) \mu_n^{\delta} \left(1 + \frac{2s}{s-2} \ln \mu_n\right)^{\alpha r} \right\}^{\frac{1}{r}} < +\infty,$$

where ρ_n and μ_n are defined by (1.3), then the series

$$\sum_{n=1}^{\infty} a_n \varphi_n(x)$$

with respect to an orthogonal system $\{\varphi_n\}_{n=1}^{\infty}$, which satisfies the condition (1.3), converges to some function $f \in L_{q,r}(\log L)^a$ and $\|f\|_{q,r,\alpha} \leq C\Omega_{q,r,\alpha}$.

Remark 1.1.4. For the case $\alpha = 0$ Theorem 1.1.3 contains the previously mentioned results of Kolyada [49] and Kirillow [48].

Theorem 1.1.5. *Let $s \in (2, +\infty]$, $\frac{s}{s-1} < q < 2$, $r > 1$, $\alpha \in \mathbb{R}$ and $\delta = \frac{r(q-2)s}{q(s-2)}$. If $f \in L_{q,r}(\log L)^a$, then the inequality*

$$\left[\sum_{n=1}^{\infty} \left(\sum_{k=v_n}^{v_{n+1}-1} a_k^2(f) \right)^{\frac{r}{2}} (1 + \log \mu_{v_n})^{r\alpha} \mu_{v_n}^{\delta} \right] \leq C \|f\|_{q,r,\alpha}$$

holds, where μ_{v_n} are defined by (1.4) and $a_n(f)$ denote the Fourier coefficients of f with respect to an orthogonal system $\{\varphi_n\}_{n=1}^{\infty}$ satisfying condition (1.3).

Remark 1.1.6. Theorem 1.1.5 complements the previously mentioned results by Marcinkiewicz and Zygmund and in a more general frame.

Remark 1.1.7. Fourier analysis is an important tool for applications in signal and image analysis. However, it has also in the last decades been used for various problems (crack analysis, strength capacity etc) connected to dams, bridges, and tunnels. This was the main motivation for me to study also this subject and I hope to use also these theoretical results in my further research, where also applications of this type in our artic region is in focus.

The results in Paper D are related to the following publications: [13], [35], [46], [48], [49], [51], [52], [53], [58] [72], [73], [78], [80], [82], [90], [96], [100] and [113].

1.1.5 Paper E

In Paper E we consider a periodic plate structure. The plate structure is assumed to be a connected set bounded by an upper s^+ and lower surface s^-, which are non-intersecting and periodic in the x-variable with period $2x_0$, see Figure 1 in Paper E. We investigate some mathematical aspects of the torsion problem for this anisotropic periodic plate structure, where the underlying material is monoclinic. In particular, we show in detail how the weak

formulation of the problem is derived and express the torsional rigidity in terms of its solution. By an monoclinic material we mean that it has a stiffness matrix of a special form including some symmetry and zeros involved (see formula (1) in Paper E). Also this paper is a typical paper within engineering mathematics.

The results in Paper E are related to the following publications: [2], [26], [67], [68], [69] and [111].

1.2 Additional paper

In addition to the papers included in the main body of this PhD thesis the following paper is related to this PhD thesis:

- A. Seger and D. Bista, Finite element analysis of a physical experiment of a pillar in a flat slab buttress dam, Research Report 2019, UiT The Artic University of Norway, Campus Narvik, 2019, 25 pages (submitted).

However, we have chosen not to include this paper into the main body of this PhD thesis since it does not contribute essentially to the main content.

Bibliography

[1] Abaqus. *Theory manual. Abaqus 6.6*. Simulia, Providence, RI, USA., 2006.

[2] Adams, R. *Sobolev Spaces*. Academic Press, 1975.

[3] Adiyeva, A. and Oinarov, R. "Weighted inequality and oscillatory properties of a class of fourth order differential equations". *Nonlinear Studies* vol. 26, no. 4 (2019), pp. 741–753.

[4] Anderson, C. et al. *Concrete Dams Case Histories of Failures and Nonfailures with Back Calculations*. Tech. rep. DSO-98-05. U.S. Department of Interior Bureau of Reclamation, Dam Safety Office, 1998.

[5] Ansell, A. et al. *Crack propagation in buttress dams Application of non-linear models – Part II*. Tech. rep. Elforsk AB, 2010.

[6] Ansell, A. et al. *Spricktillväxt i lamelldamm Tillämpning av icke-linjära modeller – Del I*. Swedish. Tech. rep. Elforsk AB, 2007.

[7] ANSYS Inc. *ANSYS Mechanical APDL Theory Reference 14.5*. 2012.

[8] ASCE-AREA Special Committee on Stresses in Railroad Track. *Bulletin of the AREA, First Progress Report Vol 19,1918, Second Progress Report Vol 21, 1920.* Tech. rep.

[9] Barza, S. and Nikolova, L. "Carleson– and Hardy–type inequalities in some Banach function spaces". *Nonlinear Studies* vol. 26, no. 4 (2019), pp. 755–766.

[10] Bhattacharjee, S. S. and Léger, P. "Application of NLFM Models to Predict Cracking in Concrete Gravity Dams". *Journal of Structural Engineering* vol. 120, no. 4 (1994), pp. 1255–1271.

[11] Birnir, B. "The turbulence problem". *Nonlinear Studies* vol. 26, no. 4 (2019), pp. 767–781.

[12] Björström, J., Ekström, T., and Hassanzadeh, M. *Spruckna betongdammar - Översikt och beräkningsmetoder*. Swedish. Vol. 06:29. Elforsk, 2006.

[13] Bochkarev, S. "The Hausdorff – Young – Riesz theorem in Lorentz spaces and multiplicative inequalities." *Tr. Mat. Inst. Steklova* vol. 219 (1997), pp. 103–114. (Translation in Proc. Steklov Inst. Math. 219(1997), No. 4, 96 – 107).

[14] Bolzon, G. et al. "Boundary element and finite element fracture analysis of dams by the cohesive crack model: a comparative study". In: *The International Workshop on Dam Fracture and Damage*. Ed. by Bourdarot, E., Mazars, J., and Saouma, V. Champery, France: A.A Balkema, 1994, pp. 69–78.

[15] Brand, B. et al. *Selecting Analytic Tools for Concrete Dams Adressing Key Events Along Potential Failure Mode Paths*. Tech. rep. FEMA P-1016. Federal Emergency Management Agency, 2014.

[16] Bretas, E. M., Léger, P., and Lemos, J. V. "Analysis Of Gravity Dam Considering The Application Of Passive Reinforcement". In: *Dam Maintenance and Rehabilitation II*. Ed. by García, R. R. et al. CRC Press, 2010, pp. 809–819.

[17] Bretas, E. M. "Discrete element modeling of concrete and masonry dams". In: *Workshop on numerical modeling and alternative computation methods of concrete dams.* Narvik, Norway, 2017.

[18] Bretas, E. M. and Jenssen, T. A. "A DEM-Based Tool For Safety Analysis of Gravity Dams Q. 99 – R. 25". In: *25th ICOLD Congress*. Stavanger, Norway, 2015, pp. 331–348.

[19] Browder, F. E. "Nonlinear elliptic boundary value problems". *Bull. Amer. Math. Soc.* vol. 69 (1963), pp. 862–874.

[20] Browder, F. E. "Variational boundary value problems for quasi-linear elliptic equations I-III". *Proc. Nat. Acad. Sci.U.S.A.* vol. 50 (1963), pp. 31–37, 592–598, 794–798.

[21] Carpinteri, A. et al. "Cohesive crack model description of ductile to brittle size-scale transition: dimensional analysis vs. renormalization group theory". *Engineering Fracture Mechanics* vol. 70, no. 14 (Sept. 2003), pp. 1809–1839.

[22] Carpinteri, A. et al. "Experimental and Numerical Fracture Modelling of a Gravity Dam". In: *Special Publication*. Ed. by Bazant, Z. Vol. 143. Breckenridge, Colorado, 1992, pp. 351–360.

[23] Červenka, V., Jendele, L., and Červenka, J. *ATENA Program Documentation Part 1 - Theory*. Prague,Czech Republic: Červenka Consulting s.r.o., 2018.

[24] Clough, R. W. *The stress distribution of Norfork dam*. Tech. rep. Institute of Engineering Research University of California Berkeley, 1962, p. 133.

[25] Clough, R. W. and Wilson, E. L. "Stress Analysis of a Gravity Dam by the Finite Element Method". *RILIM Bull.* vol. 19 (1963), pp. 45–54.

[26] Cook, R. D., Malkus, D. S., and Plesha, M. E. *Concepts and applications of finite element analysis*. J. Wiley and Sons Inc., 1989.

[27] Creager, W. P., Justin, J. D. W., and Hinds, J. *Engineering for Dams: Concrete dams*. Vol. 2. John Wiley & Sons, 1945.

[28] Cundall, P. A. "A Computer Model for Simulating Progressive, Large-Scale Movements in Blocky Rock Systems, Symposium Soc". *Internat. Mechanique des Roches, Nancy, Paper II–8* (1971).

[29] Dassault Systemes. *CAA V5 Encyclopaedia*. Dassault Systemes, 2009.

[30] Elguedj, T. et al. “Abaqus user element implementation of NURBS based isogeometric analysis”. In: *6th European Congress On Computational Methods In Applied Sciences And Engineering, Vienna, Austria*. Vienna, Austria, Sept. 2012, pp. 10–14.

[31] Fallah, N. A. et al. “Comparison of finite element and finite volume methods application in geometrically nonlinear stress analysis”. *Applied Mathematical Modelling* vol. 24, no. 7 (2000), pp. 439–455.

[32] Fauchet, B. et al. “Poroplastic analysis of concrete dams and their foundations”. *Dam engineering* vol. II, no. 3 (1991), pp. 165–192.

[33] Feichtinger, H. “Classical Fourier analysis via mild distributions”. *Nonlinear Studies* vol. 26, no. 4 (2019), pp. 783–804.

[34] FERC. *Engineering Guidelines for the Evaluation of Hydropower Projects - Chapter 10 - Other Dams*. Federal Energy Regulatory Commission, 1997.

[35] Flett, T. “On a theorem of Pitt”. *J. London Math. Soc.* vol. 2, no. 7 (1973), pp. 376–384.

[36] Goginava, U. “Subsequences of spherical sums of double Walsh-Fourier series”. *Nonlinear Studies* vol. 26, no. 4 (2019), pp. 821–830.

[37] Grøner, C. F. “Modern Techique Of Concrete Dams for wide Valleys and ancillary works. Q. 26 – R. 21”. In: *7th ICOLD Congress*. 1961.

[38] Hallquist, J. O., ed. *LS-DYNA Theory Manual*. Livermore Software Technology Corporation, 2006.

[39] Heitor, A. M. and Pedro, J. O. “Prestressed Piers For High Radial Gates – Fratel Spillweir Dam, Q.43 – R. 11”. In: *11th ICOLD Congress*. Madrid, Spain, 1973, pp. 1127–1142.

[40] Henny, D. “Stability of Straight Concrete Gravity Dams”. *Transactions of the American Society of Civil Engineers* vol. 99 (1934), pp. 1041–1061.

[41] Hughes, T. J. R., Cottrell, J. A., and Bazilevs, Y. “Isogeometric analysis: CAD, finite elements, NURBS, exact geometry and mesh refinement”. *Computer Methods in Applied Mechanics and Engineering* vol. 194, no. 39–41 (Oct. 2005), pp. 4135–4195.

[42] ICOLD. *B030A - Finite Elements Methods In Analysis And Design Of Dams*. French and English. B030A. (115 pages). International Commission On Large Dams, 1987.

[43] ICOLD. *B155 - Guidelines for use of numerical models in dam engineering*. French and English. B155. (204 pages). International Commission On Large Dams, 2013.

[44] IHA. *2017 Hydropower Status Report, Retrived feb. 2019*. The International Hydropower Association, 2017. URL: https://www.hydropower.org/2017-hydropower-status-report.

[45] Jansen, R. B. *Advanced dam engineering for design, construction, and rehabilitation*. ISSN: 9780442243975. New York, USA: Van Nostrand Reinhold, 1988.

[46] Johansson, H. *Embedding of H_p^ω in some Lorentz spaces, Research Report 6*. Department of Mathematics, Umeå University, 1975.

[47] Juliani, M. et al. "Itaipu Dam Monitoring Reevaluation Of Instrumentation Control Values, Q. 78 – R. 83". In: *20th ICOLD Congress*. Beijing, China, 2000.

[48] Kirillov, S. "Norm estimates of functions in Lorentz spaces". *Acta Sci. Math.* vol. 65, no. 1–2 (1999), pp. 189–201.

[49] Kolyada, V. "Some generalizations of the Hardy – Littlewood – Paley theorem". *Mat. Zametki* vol. 54, no. 3 (1993), pp. 48–71. (Translation in Math. Notes 51(1992), No. 3–4, 908–922).

[50] Konow, T. *Vurdering av bergrunnen*. Gardemoen, Oslo, Norway, Apr. 2018.

[51] Kopezhanova, A. "Summability of Fourier Transforms of Functions from Lorentz Spaces". PhD thesis. Department of Engineering Sciences and Mathematics, Luleå University of Technology, 2017.

[52] Kopezhanova, A. and Persson, L. E. "On summability of the Fourier coefficients in bounded orthonormal systems for functions from some Lorentz type spaces". *Eurasian Math J.* vol. 1, no. 1 (2010), pp. 76–85.

[53] Krein, S., Petunin, Y. I., and E.M, S. *Interpolation of linear operators*. Moscow: Nauka, 1978.

[54] Labuz, J. F. and Zang, A. "Mohr–Coulomb Failure Criterion". *Rock Mechanics and Rock Engineering* vol. 45, no. 6 (2012), pp. 975–979.

[55] Lacome, J. L. "Smooth particle hydrodynamics (SPH): a new feature in LS-DYNA". In: *6th International LS–DYNA Users Conference,* Dearborn, USA, 2000, pp. 29–34.

[56] Léger, P. et al. "A progressive methodology for structural safety evaluation of gravity dams subjected to floods." In: *Proceedings of Canadian Dam Safety Conference*. Niagara Falls, Ontario, 1996, pp. 2–16.

[57] Léger, P. et al. "Failure Mechanism Of Gravity Dams Subjected To Hydrostatic Overload: Influence Of Weak Lift Joints, Q. 75 – R. 2". In: *19th ICOLD Congress*. Florence, Italy, 1997.

[58] Leindler, L. "Generalization of inequalities of Hardy and Littlewood". *Acta Sci. Math.* vol. 31 (1970), pp. 279–285.

[59] Lindemark, J. et al. "Sarvsfossen Dam – Design of a Norwegian Concrete Arch Dam". In: *Hydropower'15*. June. Stavanger, Norway, 2015.

[60] Lions, P. L. and Sivasundaram, S. (Editors-in-Chiefs). *Nonlinear Studies*. www.nonlinearstudies.com. UK: I&S –Florida, USA: CSP-Cambrige.

[61] Lions, P. L., Samko, N. and Sivasundaram, S. (Editors). "Special Issue on harmonic analysis, applied mathematics and engineering problems. Dedicted to the 75th anniversary of Professor Lars-Erik Persson (Preface)". *Nonlinear Studies* vol. 26, no. 4 (2019), pp. 703–706.

[62] Liu, G. R. *Mesh Free Methods: Moving Beyond the Finite Element Method*. CRC Press, 2002.

[63] Love, A. E. H. *A treatise on the mathematical theory of elasticity*. 2. London: Cambridge University Press, 1906.

[64] Lu, S. "Real-time vertical track deflection measurement system". *ETD collection for University of Nebraska - Lincoln. Paper AAI3331436* (Jan. 2008).

[65] Lukkassen, D. and Meidell, A. "Beams on nonlinear elastic foundation". In: *AIP Conference Proceedings 1637*. Vol. 656. 2014.

[66] Lukkassen, D. and Meidell, A. "Lars-Erik Persson-the remarkable broad and innovative mathematician and unique Pers(s)on". *Nonlinear Studies* vol. 26, no. 4 (2019), pp. 707–722.

[67] Lukkassen, D., Meidell, A., and Wall, P. "Mathematical analysis and homogenization of the torsion problem". *J. Funct. Spaces Appl.* vol. 6, no. 2 (2008), pp. 155–176.

[68] Lukkassen, D., Meidell, A., and Wall, P. "New methods for estimating the torsional rigidity of composite bars". *International Journal of Engineering Science* vol. 47 (2009), pp. 524–536.

[69] Lukkassen, D. et al. "Symmetry–relations for elastically deformed periodic rod-structures". *Math. Mod. Meth. Appl. Sci.* vol. 19, no. 4 (2009), pp. 501–525.

[70] Malm, R. *Guideline for fe analyses of concrete dams*. Tech. rep. Energiforsk AB, 2016.

[71] Malm, R. et al. *Load capacity of grouted rock bolts due to degradation*. Tech. rep. Energiforsk AB, 2017.

[72] Marcinkiewicz, J. and Zygmund, A. "Some theorems on orthogonal systems". *Fund. Math.* vol. 28 (1937), pp. 309–335.

[73] Maslov, A. "Estimates of Hausdorff–Young type for Fourier coefficients". *Vestnik Moscow Univ. Ser. I Mat. Mekh* vol. 3, no. 19–22 (1982). (Russian).

[74] Minty, G. J. "On a "monotonicity" method for the solution of nonlinear equations in Banach spaces". *Proc. Nat. Acad. Sci. U.S.A.* vol. 50 (1963), pp. 1038–1041.

[75] Moës, N., Bolbow, J., and Belytschko, T. "A Finite Element Method For Crack Growth Without Remeshing". *International Journal For Numerical Methods In Engineering* vol. 46, no. 1 (1999), pp. 131–150.

[76] Møller, I. *Norske dammer : B. 1 : Norske vannkraftdammer i Østfold, Akershus, Hedmark, Oppland, Buskerud, Telemark, Aust-Agder, Vest-Agder og Rogaland*. ISSN: 9788292931011 (Norwegian). Oslo, Norway: Energi forl., 2008.

[77] Munjiza, A. A. *The Combined Finite-Discrete Element Method*. Hoboken: Wiley, 2004.

[78] Mustahaeva, V. and Akishev, G. "On the Fourier coefficients in Lorentz – Zygmund space". In: *Modern Metods of the theory of functions and problems*. Voronezh, 2013, pp. 155–156.

[79] Nicholson, G. A. *Design of gravity dams on rock foundations: sliding stability assessment by limit equilibrium and selection of shear strength*. Technical report GL-83-13. Vicksburg, Miss., USA: U S Army Corps of Engineers, Oct. 1983.

[80] Nikol'ski, S. M. *Approximation of classes of functions of several variables and embedding theorems*. Moscow: Nauka, 1977.

[81] Nonaka, M., Hara, T., and Kamimura, J. "Numerical Analysis On Displacement Behavior Of Concrete Gravity Dams Measured During Impoundment, Q. 78 – R. 76". In: *20th ICOLD Congress*. Beijing, China, 2000, pp. 1235–1260.

[82] Nursultanov, E. D. "On the coefficients of multiple Fourier series from L_p – spaces (Russian)". *Izv. Ross. Akad. Nauk. Ser. Mat.* vol. 64, no. 1 (2000), pp. 95–122. (Translation in Izv. Math. 64(2000) , No. 1, 93–120).

[83] NVE. *Damdatabasen SIV*. 2017. URL: https://www.nve.no/damsikkerhet-og-energiforsyningsberedskap/damsikkerhet/innrapportering-og-damdatabasen-siv/.

[84] NVE. *Retningslinje for laster og dimensjonering*. Norwegian. 2003. URL: https://www.nve.no/damsikkerhet-og-kraftforsyningsberedskap/damsikkerhet/regelverk/retningslinjer-for-laster-og-dimensjonering/.

[85] NVE. *Retningslinjer for betongdammer*. Norwegian. 2005. URL: https://www.nve.no/damsikkerhet-og-kraftforsyningsberedskap/damsikkerhet/regelverk/retningslinjer-for-betongdammer/.

[86] Olje- og Energidepartementet. *Forskrift om sikkerhet ved vassdragsanlegg (damsikkerhetsforskriften)*. Ed. by Olje- og Energidepartementet. 2010. URL: https://lovdata.no/pro/SF/forskrift/2009-12-18-1600.

[87] Oñate, E. et al. "The Particle Finite Element Method. An Overview." *International Journal of Computational Methods* vol. 1, no. 2 (2004), pp. 267–307.

[88] Pan, Y. et al. "Fracture Analysis of Brittle Materials Based on Nonlinear FEM and Application in Arch Dam with Fractures". *Journal of Applied Mathematics* vol. 2013 (2013), pp. 1–12.

[89] Persson, L. E. "Relations Between Summability of Functions and Their Fourier Series". PhD thesis. Department of Mathematics, Umeå University, 1974.

[90] Persson, L. E. "Relations between summability of functions and their Fourier series". *Acta Math. Acad. Sci. Hungar* vol. 27, no. 3–4 (1976), pp. 267–280.

[91] Randles, P. W. and Libersky, L. D. “Smoothed Particle Hydrodynamics: Some recent improvements and applications”. *Computer Methods in Applied Mechanics and Engineering* vol. 139, no. 1 (1996), pp. 375–408.

[92] Roth, S.-N., Léger, P., and Soulaïmani, A. “A combined XFEM–damage mechanics approach for concrete crack propagation”. *Computer Methods in Applied Mechanics and Engineering* vol. 283 (2015), pp. 923–955.

[93] Rueda, F. et al. “Thermomechanical Analysis of La Breña II Dam During its Construction Process: Evaluation Of potential Thermal Cracking, Q.84 – R. 31”. In: *22th ICOLD Congress*. Barcelona, Spain, 2006, pp. 513–523.

[94] Sadeghi, J. and Barati, P. “Evaluation of conventional methods in Analysis and Design of Railway Track System”. *Int. J. Civ. Eng.* vol. 8, no. 1 (2010), pp. 44–56.

[95] Sas, G., Bretas, E. M., and Lia, L. “Advanced Sliding Assessment of Målset Dam: Tests and Numerical Analysis of Unbonded Joints, Q. 99 – R. 30”. In: *25th ICOLD Congress*. Stavanger, Norway, 2015, pp. 331–348.

[96] Sharpley, R. “Counterexamples for classical operators on Lorentz-Zygmund spaces”. *Studia Math* vol. 58 (1980), pp. 141–158.

[97] Showalter, R. E. *Monotone operators in Banach space and nonlinear partial differential equations*. Vol. 49. Providence, USA: American Mathematical Society, 1997.

[98] Singh, H. and Grip, N. “Recent trends in operation model analysis techniques and its applications and its applications on a steel truss bridge”. *Nonlinear Studies* vol. 26, no. 4 (2019), pp. 911–927.

[99] Stangvik, R. M. “Shear strength of the rock-concrete interface at Kalhovd dam”. MA thesis. Department of Civil and Environmental Engineering, Norges teknisk-naturvitenskapelige universitet, 2017.

[100] Stein, E. “Interpolation of linear operators”. *Trans. Amer. Math. Soc.* vol. 83 (1956), pp. 482–492.

[101] Stone and Webster Engineering Corporation. *Uplift Pressures, Shear Strengths and Tensile Strengths for Stability Analysis of Concrete Gravity Dams*. 1 EPRI TR-100345. Palo Alto, California, USA: Electric Power Research Insitute, 1992.

[102] Su, K. et al. “Mechanism of Cracking in Dams Using a Hybrid FE-Meshfree Method”. *International Journal of Geomechanics* vol. 17, no. 9 (2017), pp. 1–14.

[103] Tephnadze, G. “Convergence and strong summability of the two-dimensional Vilinkin-Fourier series”. *Nonlinear Studies* vol. 26, no. 4 (2019), pp. 973–989.

[104] Thieu, T. K. T., Colangeli, M., and Muntean, A. “Weak solvability of a fluid–like driven system for active-passive pedestrian dynamics”. *Nonlinear Studies* vol. 26, no. 4 (2019), pp. 991–1006.

[105] Tucovis, M. “Djerdap 1 Dam Behaviour And Comparison With Project Predictions, Q. 78 – R. 9”. In: *20th ICOLD Congress*. Beijing, China, 2000, pp. 121–131.

[106] USACE. *Engineering and Design: Sliding Stability For Concrete Structures*. Technical Letter 1110-2-256. Washington, D.C, USA: U.S. Army Corps of Engineers, June 1981.

[107] USBR. *State-of-Practice for the Nonlinear Analysis of Concrete Dams at the Bureau of Reclamation, January 2006*. U.S. Department of the Interior, Bureau of Reclamation, 2006.

[108] Wang, Y. and Jia, J. “Experimental study on the influence of hydraulic fracturing on high concrete gravity dams”. *Engineering Structures* vol. 132 (2017), pp. 508–517.

[109] Weisz, F. “Hardy spaces with variable exponents and applications in Fourier analysis”. *Nonlinear Studies* vol. 26, no. 4 (2019), pp. 1015–1026.

[110] Zarembski, A. and Choros, J. “On the measurement and calculation of vertical track modulus”. In: *Proceedings American Railway Engineering Association*. Vol. 81. 1980, pp. 156–173.

[111] Ziemer, W. P. “Weakly Differentiable Functions”. Berlin: Springer, 1989. Chap. Sobolev Spaces and Functions of Bounded Variation.

[112] Zienkiewicz, O. C., Taylor, R. L., and Zhu, J. Z. *The Finite Element Method: Its Basis and Fundamentals*. 6th. Elsevier Butterworth-Heinemann, 2005.

[113] Zygmund, A. *Trigonometric series*. Vol. II. Moscow: Izdat. "Mir", 1965.

Papers

Paper A

Some mathematical aspects on linear and nonlinear elasticity

Andreas Seger

Submitted for publication.

Abstract

In this paper a new presentation of the mathematical theory of linear elasticity from a functional analytic standpoint is given. Moreover, an useful estimate of the Sobolev norm in R^n is given. Finally, the problem connected to non-linear beams on elastic foundation is modelled and analyzed.

AMS classification: 74B05, 74B20,26D10,47A30, 46N20,35S99
Key words and phrases: Elasticity, operators, inequalities, partial differential equations, Sobolev norm, modelling, applications.

A.1 Introduction

Structural analysis concerns the estimation and computation of the class of effects of loads on physical structures and their components. All structures which are designed to withstand loads are subject to this type of analysis, including buildings, dam structures, vehicles, furniture, train rails, prostheses and biological tissues.

It is impossible to have knowledge of all aspects of this field since it involves all types of specialists from practical engineers to pure mathematicians. In this paper we will focus on some mathematical aspects connected to existence theory in linear and nonlinear elasticity. In addition we will consider beams resting on nonlinear foundations.

Vertical deflections and rail bending moments are often determined by the Winkler model (1867). This model uses the wrong assumption that the deflection in the rail, which is obtained by the weight of the train, is proportional to the supporting forces under the rail. The linear ordinary differential equations which this assumption implies, can be solved by classical methods. However, the linear treatment neglects several important conditions. Experimental results shows that there is a substantial increase in the deflection and bending moment due to the nonlinearity of the supporting system. Several researchers

are therefore questioning the reliability of the Linear approach (c.f. [7], [1] and [9]). Advanced mathematical analysis based on nonlinear models seems to be needed in order to obtain a better understanding of the complicated structures that are involved. In this connection it should be mentioned that in modern product development one often replace testing activities with analytical and numerical methods where complex mathematical results and advanced models are used. It has been pointed out by several authors (see e.g. [5]) that by using more advanced mathematical tools one may be able to develop new methods and algorithms that are useful in designing railway tracks. More mathematical understanding of the models involved is important for getting better methods that provides more accurate analytical and numerical results in determining deflections and bending moments. The part of the paper devoted to beams on elastic foundation is deeply inspired by the interesting ideas and results presented in [5], and is intended to be a small step further in this direction. Many of the results obtained in [5] are explained in a new and hopefully more pedagogical light, and even some extensions are presented. In particular a multidimensional generalization of an equivalent Sobolev norm is proved. This generalization enable us to obtain similar results as those obtained in [5] for even more complicated structures, e.g. nonlinear plates on elastic foundation like ice on water. We aim to develop these ideas even further in forthcoming papers.

In order to make the paper readable to a broader audience, including engineers and scientist within the elasticity community, as well as pure mathematicians, we have made an effort making the presentation as easy as possible without leaving out any technicalities which are important for the understanding of the contents. Still, those who are completely unfamiliar with functional analysis and theory concerning function spaces, might find some parts difficult to penetrate.

We start in Section 2 with stating some preliminary results connected to the theory of linear and nonlinear monotone operators. In Section 3 we give a new presentation of the mathematical theory of linear elasticity from a functional analytical standpoint, and discuss how strong and the weak formulation can be obtained and analyzed. The main result in Section 4 is a theorem which gives an useful estimate of the Sobolev norm in R^n. Finally, Section 5 is reserved for modelling and analysis of problems connected to nonlinear beams on elastic foundation.

A.2 Some preliminaries

In this paper X denotes a Banach space and its dual is denoted X^*. If $f \in X^*$ and $x \in X$ we usually write $\langle f, x\rangle$ instead of $f(x)$ If A is a single-valued operator from X to X^* we let $R(A)$ denote the range of A, that is the set of all points f of X^* such that there exists $x \in X$ satisfying $Ax = f$. Let us also recall the following definitions:

a) A is called monotone if

$$\langle Ax_1 - Ax_2, x_1 - x_2\rangle \geq 0, \text{ for every } x_1, x_2 \in X. \tag{A.1}$$

b) A is called strictly monotone if, in addition to (A.1),

$$\langle Ax_1 - Ax_2, x_1 - x_2 \rangle = 0, \text{ where } x_1, x_2 \in X, \text{ implies that } x_1 = x_2.$$

c) A is called maximal monotone if for every pair $(x, y) \in X \times X^*$ satisfying the condition

$$\langle y - A\xi, x - \xi \rangle \geq 0 \text{ for every } \xi \in X,$$

it follows that $y = Ax$.

d) A is called coercive if

$$\lim_{\|x\| \to \infty} \frac{\langle Ax, x \rangle}{\|x\|} = +\infty.$$

e) A is called strongly monotone if there exists a positive constant c_1 such that

$$\langle Ax_1 - Ax_2, x_1 - x_2 \rangle \geq c_1 \|x_1 - x_2\|^2, \text{ for every } x_1, x_2 \in X. \qquad \text{(A.2)}$$

f) A is called hemicontinuous if

$$\lim_{t \to 0} A(x + ty) = Ax$$

weakly in X^* (i.e. $\lim_{t \to 0} \langle A(x + ty), v \rangle = \langle Ax, v \rangle$ for all $v \in X$) for all $x, y \in X$.

Theorem A.2.1. *Let X be a Banach space with norm $\|\cdot\|$ and assume that $A : X \to X^*$ is monotone and hemicontinuous. Then A is maximal monotone. If, in addition, X is reflexive and A is coercive, then the range $R(A) = X^*$.*

The last sentence of this theorem is usually referred to as the Browder-Minty theorem, i.e. the main theorem concerning monotone operators. Browder-Minty theorem was proved by Browder [2] and Minty [6] (we also refer to [3]). For more detailed information we refer to e.g. in the book [8].

In the special case when X is a Hilbert space with scalar product $*$ and a corresponding norm $\|\cdot\|_X$ (defined as usual as $\|v\|_X = \sqrt{v * v}$), the Browder-Minty theorem reduces to the Lax-Milgram Lemma, which we recall here, for completeness, in addition to som other basic results on the linear case. Assume that $a(.,.)$ is a bilinear form on X and assume that L is a linear functional on X. The following conditions may or may not be satisfied:

1. $a(.,.)$ is symmetric, i.e. $a(\phi, v) = a(v, \phi), \forall \phi, v \in X$.
2. $a(.,.)$ is continuous, i.e. there is a constant $\gamma > 0$ such that $|a(\phi, v)| \leq \gamma \|\phi\|_X \|v\|_X \quad \forall \phi, v \in X$.
3. $a(.,.)$ is V-elliptic, i.e. there is a constant $\alpha > 0$ such that $a(\phi, \phi) \geq \alpha \|\phi\|_X^2 \quad \forall \phi \in X$.
4. L is continuous, i.e. there is a constant $\Lambda > 0$ such that $|L(\phi)| \leq \Lambda \|\phi\|_X$ $\forall \phi \in X$.

We will now consider the following abstract minimization problem: Find $u \in X$ such that

$$F(u) = \min_{\phi \in X} F(\phi), \tag{A.3}$$

where

$$F(\phi) = \frac{1}{2} a(\phi, \phi) - L(\phi),$$

and we will also consider the following abstract weak formulation problem: Find $u \in X$ such that

$$a(u, \phi) = L(\phi), \quad \forall \phi \in X. \tag{A.4}$$

Theorem A.2.2. *[Lax-Milgram Lemma] If the conditions 2, 3 and 4 are satisfied then there exists a unique solution $u \in V$ of the problem (A.4).*

Moreover, we have the following useful result:

Theorem A.2.3. *If the conditions 1, 2, 3 and 4 are satisfied then there exists a unique solution $u \in X$ of the problem (A.3). In addition, the problems in (A.3) and (A.4) are equivalent, i.e. $u \in X$ satisfies (A.3) if and only if u satisfies (A.4).*

A proof of this result can be found in most books connected to functional analysis. Let us also recall the Friedrichs's inequality: If Ω is a bounded subset of R^n with diameter d and $u : \Omega \to R$ is a member of the Sobolev space $W_0^{k,p}(\Omega)$, then

$$\|u\|_{L^p(\Omega)} \leq d^k \left(\sum_{|\alpha|=k} \|D^\alpha u\|^p_{L^p(\Omega)} \right)^{1/p}.$$

In our beam-problem we will be interested in the case $n = 1$, $k = 2$ and $p = 2$. For this simple case we often use the notation $H_0^2(\Omega)$ instead of $W_0^{2,2}(\Omega)$. The norm of this space is defined as follows

$$\|u\|^2_{H^2(\Omega)} = \|u\|^2_{L^2(\Omega)} + \|u'\|^2_{L^2(\Omega)} + \|u''\|^2_{L^2(\Omega)}.$$

Throughout the paper $\|\cdot\|$ and $\|\cdot\|_2$ denote the H^2-norm and the L^2-norm, respectively.

A.3 Mathematical aspects of linear elasticity

Let $\mathbf{S}$ denote the space of all symmetric 3×3 matrices and let $a \cdot b$ denote the scalar product between two matrices $a = \{a_{ij}\}$ and $b = \{b_{ij}\}$ in $\mathbf{S}$, which is defined by $a \cdot b = \sum_{ij} a_{ij} b_{ij}$. The norm $|a|$ is correspondingly defined by $|a|^2 = \sum_{ij} a_{ij}^2$ (here and in the rest of the paper $\sum_{ij}$ is used in place of the more complicated symbol $\sum_{i=1}^3 \sum_{j=1}^3$). If a and b are vectors, then $a \cdot b$ will still denote the usual scalar product in $\mathbf{R}^3$.

We usually characterize the state of an elastic body by the displacement vector, the strain and the stress. If the body is deformed, a fixed point $x =$

(x_1, x_2, x_3) of the body moves to a point $x + \mathbf{u}(x)$, where the vector function $\mathbf{u}(x) = (u_1(x), u_2(x), u_3(x))$ is called the *displacement vector*, or simply the *displacement.* The strain $e(\mathbf{u})$ is a symmetric 3×3 matrix with elements $e_{ij} = e_{ij}(x)$ given by

$$e_{ij} = \frac{1}{2}(\frac{\partial u_i}{\partial x_j} + \frac{\partial u_j}{\partial x_i}).$$

We call $\mathbf{u}$ a *rigid displacement* if $e(\mathbf{u}) = \mathbf{0}$. It can be shown that any rigid displacement $\mathbf{u}(x) = (u_1(x), u_2(x), u_3(x))$ has the form

$$\begin{bmatrix} u_1(x) \\ u_2(x) \\ u_3(x) \end{bmatrix} = \begin{bmatrix} 0 & b_{12} & b_{13} \\ -b_{12} & 0 & b_{23} \\ -b_{13} & -b_{23} & 0 \end{bmatrix} \begin{bmatrix} x_1 \\ x_2 \\ x_3 \end{bmatrix} + \begin{bmatrix} c_1 \\ c_2 \\ c_3 \end{bmatrix}, \tag{A.5}$$

where b_{ij} and c_i are constants.

In continuum mechanics one considers two different kind of forces, namely *body forces* and *surface forces*. Body forces are described by a density function $\mathbf{f}(x) = [f_1(x), f_2(x), f_3(x)]$ (e.g. gravity), defined in such a way that the total force applied to a given volume Q equals $\int_Q \mathbf{f}(x)dx$. Surface forces which are applied at the boundary of the body may course deformation. The deformation of the elastic body gives surface forces that act on points inside the body. These surface forces are called *stresses* and are characterized by a symmetric matrix $\sigma(\mathbf{u})$ with elements $\sigma_{ij} = \sigma_{ij}(x)$. On every surface ∂Q of a given subdomain Q with outward normal unit normal $n = (n_1, n_2, n_3)$ we may define a vector function $\mathbf{F}(\mathbf{u}) = (F_1, F_2, F_3)$, the so-called *stress vector,* given by $F_i = \sum_{j=1}^{3} \sigma_{ij} n_j = \sigma_i \cdot n$, where $\sigma_i = (\sigma_{i1}, \sigma_{i2}, \sigma_{i3})$. The components σ_{ij} are defined such that the total force acting on Q, from the rest of the body, equals $\int_{\partial Q} \mathbf{F}(\mathbf{u})(x)ds$. By Gauss theorem (the divergence theorem) we have that

$$\int_{\partial Q} F_i \, ds = \int_{\partial Q} (\sigma_i \cdot n) \, ds = \int_Q \operatorname{div} \sigma_i \, dx. \tag{A.6}$$

In state of equilibrium of forces, the following equality must be satisfied:

$$\int_Q \mathbf{f} \, dx = -\int_{\partial Q} \mathbf{F}(\mathbf{u}) \, ds.$$

Hence, by (A.6) we obtain that

$$\int_Q f_i \, dx = -\int_Q \operatorname{div} \sigma_i \, dx.$$

Since this holds for every subdomain Q in the elastic body, we may conclude that

$$\operatorname{div} \sigma_i = -f_i,$$

i.e.

$$\frac{\partial \sigma_{i1}}{\partial x_1} + \frac{\partial \sigma_{i2}}{\partial x_2} + \frac{\partial \sigma_{i3}}{\partial x_3} = -f_i.$$

In other words, taking into account the symmetry relation $\sigma_{ij} = \sigma_{ji}$, we obtain the following three equations

$$\begin{aligned}
\frac{\partial \sigma_{11}}{\partial x_1} + \frac{\partial \sigma_{12}}{\partial x_2} + \frac{\partial \sigma_{13}}{\partial x_3} &= -f_1, \\
\frac{\partial \sigma_{12}}{\partial x_1} + \frac{\partial \sigma_{22}}{\partial x_2} + \frac{\partial \sigma_{23}}{\partial x_3} &= -f_2, \\
\frac{\partial \sigma_{13}}{\partial x_1} + \frac{\partial \sigma_{23}}{\partial x_2} + \frac{\partial \sigma_{33}}{\partial x_3} &= -f_3.
\end{aligned}$$

In elasticity theory it is often convenient to introduce the "divergence" of the stress, denoted $\operatorname{div} \sigma(\mathbf{u})$, as the vector $(\operatorname{div} \sigma_1 , \operatorname{div} \sigma_2, \operatorname{div} \sigma_3)$. Hence, the above three equations can be written on the following compact form:

$$\operatorname{div} \sigma(\mathbf{u}) \ = -\mathbf{f}. \tag{A.7}$$

The stress is related to the strain via the following relation, called the Hooks law:

$$\sigma_{ij} = \sum_{kr} c_{ijkr} e_{kr}(u)$$

where $\{C_{ijkr}\}$ satisfies the following symmetry relations $C_{ijkr} = C_{krij}$, $C_{ijkr} = C_{jikr} = C_{ijrk}$. Each coefficient C_{ijkr} may be a function of x. For each matrix ξ, let $C\xi$ denote the matrix with elements

$$(C\xi)_{ij} = \sum_{kr} c_{ijkr} \xi_{kr}.$$

Using this notation, the Hooks law can be written as follows:

$$\sigma(\mathbf{u}) = Ce(\mathbf{u}). \tag{A.8}$$

In addition to the above conditions, we will assume that there exists positive constants ν_1 and ν_2 such that

$$\nu_1 |\xi|^2 \leq \xi \cdot C\xi \leq \nu_2 |\xi|^2 \tag{A.9}$$

for all $\xi \in \mathbf{S}$.

The strain and stress can alternatively be represented as vectors:

$$\begin{aligned}
e &= [e_{11}, e_{22}, e_{33,} \gamma_{12}, \gamma_{23}, \gamma_{13}]^T , \ \gamma_{ij} = 2e_{ij} \\
\sigma &= [\sigma_{11}, \sigma_{22}, \sigma_{33,} \sigma_{12}, \sigma_{23}, \sigma_{13}]^T .
\end{aligned}$$

In this case the Hooks law takes the following form:

$$\begin{bmatrix} \sigma_{11} \\ \sigma_{22} \\ \sigma_{33} \\ \sigma_{12} \\ \sigma_{23} \\ \sigma_{13} \end{bmatrix} = \begin{bmatrix} C_{1111} & C_{1122} & C_{1133} & C_{1112} & C_{1123} & C_{1113} \\ C_{2211} & C_{2222} & C_{2233} & C_{2212} & C_{2223} & C_{2213} \\ C_{3311} & C_{3322} & C_{3333} & C_{3312} & C_{3323} & C_{3313} \\ C_{1211} & C_{1222} & C_{1233} & C_{1212} & C_{1223} & C_{1213} \\ C_{2311} & C_{2322} & C_{2333} & C_{2312} & C_{2323} & C_{2313} \\ C_{1311} & C_{1322} & C_{1333} & C_{1312} & C_{1323} & C_{1313} \end{bmatrix} \begin{bmatrix} e_{11} \\ e_{22} \\ e_{33} \\ \gamma_{12} \\ \gamma_{23} \\ \gamma_{13} \end{bmatrix}.$$

where $\gamma_{ij} = 2e_{ij}$. In the case when the underlaying material is locally orthotropic, the stiffness matrix reduces to

$$C = \begin{bmatrix} C_{1111} & C_{1122} & C_{1133} & 0 & 0 & 0 \\ C_{2211} & C_{2222} & C_{2233} & 0 & 0 & 0 \\ C_{3311} & C_{3322} & C_{3333} & 0 & 0 & 0 \\ 0 & 0 & 0 & C_{1212} & 0 & 0 \\ 0 & 0 & 0 & 0 & C_{2323} & 0 \\ 0 & 0 & 0 & 0 & 0 & C_{1313} \end{bmatrix}$$

The inverse of this matrix, called the compliance matrix, is a symmetric matrix of the form

$$C^{-1} = \begin{bmatrix} \frac{1}{E_1} & -\frac{\nu_{12}}{E_2} & -\frac{\nu_{13}}{E_3} & 0 & 0 & 0 \\ -\frac{\nu_{21}}{E_1} & \frac{1}{E_2} & -\frac{\nu_{23}}{E_3} & 0 & 0 & 0 \\ -\frac{\nu_{31}}{E_1} & -\frac{\nu_{32}}{E_2} & \frac{1}{E_3} & 0 & 0 & 0 \\ 0 & 0 & 0 & \frac{1}{G_{12}} & 0 & 0 \\ 0 & 0 & 0 & 0 & \frac{1}{G_{23}} & 0 \\ 0 & 0 & 0 & 0 & 0 & \frac{1}{G_{13}} \end{bmatrix}.$$

Here, 'E_i' are the Young's moduli, 'G_{ij}' are the shear moduli and 'ν_{ij}' are the Poisson's ratios. Inverting this matrix we find that

$$\begin{aligned} &C_{1111} = \frac{1-\nu_{23}\nu_{32}}{\Delta E_2 E_3}, \quad C_{1122} = \frac{\nu_{21}+\nu_{31}\nu_{23}}{\Delta E_2 E_3}, \quad C_{1133} = \frac{\nu_{31}+\nu_{21}\nu_{32}}{\Delta E_2 E_3} \\ &C_{2222} = \frac{1-\nu_{13}\nu_{31}}{\Delta E_1 E_3}, \quad C_{2233} = \frac{\nu_{32}+\nu_{12}\nu_{31}}{\Delta E_1 E_3}, \quad C_{3333} = \frac{1-\nu_{12}\nu_{21}}{\Delta E_1 E_2} \\ &C_{1212} = G_{12}, \quad C_{2323} = G_{23}, \quad C_{1313} = G_{13}, \end{aligned} \tag{A.10}$$

where

$$\Delta = \frac{1-\nu_{12}\nu_{21}-\nu_{23}\nu_{32}-\nu_{31}\nu_{13}-2\nu_{21}\nu_{32}\nu_{13}}{E_1 E_2 E_3}.$$

In particular, if the material is isotropic, i.e. when $E_1 = E_2 = E_3 = E$, $\nu_{12} = \nu_{21} = \nu_{23} = \nu_{32} = \nu_{31} = \nu_{13} = \nu$ and $G_{12} = G_{23} = G_{13} = E/2(1+\nu)$, we obtain that

$$C = \frac{E}{(1-2\nu)(1+\nu)} \begin{bmatrix} 1-\nu & \nu & \nu & 0 & 0 & 0 \\ \nu & 1-\nu & \nu & 0 & 0 & 0 \\ \nu & \nu & 1-\nu & 0 & 0 & 0 \\ 0 & 0 & 0 & \frac{1}{2}-\nu & 0 & 0 \\ 0 & 0 & 0 & 0 & \frac{1}{2}-\nu & 0 \\ 0 & 0 & 0 & 0 & 0 & \frac{1}{2}-\nu \end{bmatrix}.$$

Note that if $a = a(x)$ and $b = b(x)$ belong to the space $L^2(\Omega, R^{3\times 3}))$, consisting of all 3×3 matrixes with components belonging to $L^2(\Omega)$, then it is possible to prove the following version of Schwartz' inequality (for a proof, see Remark A.3.2 below):

$$\left| \int_\Omega a(x) \cdot Cb(x)\, dx \right| \leq \left(\int_\Omega a(x) \cdot Ca(x)\, dx \right)^{\frac{1}{2}} \left(\int_\Omega b(x) \cdot Cb(x)\, dx \right)^{\frac{1}{2}}, \tag{A.11}$$

(which holds even if we drop the symmetry conditions $C_{ijkr} = C_{jikr} = C_{ijrk}$). In particular, if C is the identity mapping, i.e. the mapping defined by

$$c_{ijkr} = \begin{cases} 1 & \text{if } ij = kr, \\ 0 & \text{if } ij \neq kr, \end{cases}$$

we obtain that

$$\left| \int_\Omega a(x) \cdot b(x)\, dx \right| \leq \left(\int_\Omega |a(x)|^2 \, dx \right)^{\frac{1}{2}} \left(\int_\Omega |b(x)|^2 \, dx \right)^{\frac{1}{2}},$$

or equivalently,

$$\left| \int_\Omega \sum_{ij} a_{ij}(x) b_{ij}(x)\, dx \right| \leq \left(\int_\Omega \sum_{ij} a_{ij}^2(x)\, dx \right)^{\frac{1}{2}} \left(\int_\Omega \sum_{ij} b_{ij}^2(x)\, dx \right)^{\frac{1}{2}}. \quad \text{(A.12)}$$

We are now ready to state the following useful result:

Proposition A.3.1. *It yields that*

$$a * b = \int_\Omega a(x) \cdot Cb(x)\, dx. \quad \text{(A.13)}$$

defines a scalar product on $L^2(\Omega, R^{3\times 3}))$. Use this to prove (A.11).

Proof: A.3.1 In order to prove that "$*$" is a scalar product, we have to prove that for all $a, b, c \in L^2(\Omega, R^{3\times 3}))$ and $k \in R$ we have that

1. $a * b = b * a$
2. $(ka) * b = k\,(a * b)$
3. $(a + c) * b = a * b + c * b$
4. $a * a > 0$, if $a \neq 0$
5. $a * a = 0$ only if $a = 0$.

Proof of 1):

$$a \cdot Cb = \sum_{ij} a_{ij}\,(Cb)_{ij} = \sum_{ij} a_{ij}(\sum_{kr} c_{ijkr} b_{kr}) = \sum_{ij}(\sum_{kr} c_{ijkr} a_{ij} b_{kr}) =$$

$$\sum_{kr}\sum_{ij}(c_{ijkr} a_{ij} b_{kr}) = \sum_{kr} b_{kr} \sum_{ij}(c_{ijkr} a_{ij})$$

$$= \sum_{kr} b_{kr} \sum_{ij}(c_{krij} a_{ij}) = \sum_{kr} b_{kr}\,(Ca)_{kr} = b \cdot Ca,$$

i.e. $a \cdot Cb = b \cdot Ca$. Hence,

$$a * b = \int_\Omega a(x) \cdot Cb(x)\, dx = \int_\Omega b(x) \cdot Ca(x)\, dx = b * a.$$

Proof of 2):

$$(ka) * b = \int_\Omega (ka) \cdot Cb\, dx = \int_\Omega \sum_{ij} ka_{ij} \left(Cb\right)_{ij}\, dx = k \int_\Omega \sum_{ij} a_{ij} \left(Cb\right)_{ij}\, dx =$$

$$k \int_\Omega a \cdot Cb\, dx = k\,(a * b)$$

Proof of 3):

$$(a + c) * b = \int_\Omega (a + c) \cdot Cb\, dx = \int_\Omega \sum_{ij} \left(a_{ij} + c_{ij}\right) \left(Cb\right)_{ij}\, dx$$

$$= \int_\Omega \sum_{ij} a_{ij} \left(Cb\right)_{ij}\, dx + \int_\Omega \sum_{ij} c_{ij} \left(Cb\right)_{ij}\, dx = \int_\Omega a \cdot Cb\, dx + \int_\Omega c \cdot Cb\, dx = a*b + c*b$$

Proof of 4) and 5): If $a \neq 0$ then $|a| > 0$. Using (A.9) we find that

$$\nu_1 \int_\Omega |a|^2\, dx = \int_\Omega \nu_1 |a|^2\, dx \leq \int_\Omega a \cdot Ca\, dx \leq \int_\Omega \nu_2 |a|^2\, dx = \nu_2 \int_\Omega |a|^2\, dx.$$

Hence

$$\nu_1 \int_\Omega |a|^2\, dx \leq a * a \leq \nu_2 \int_\Omega |a|^2\, dx. \tag{A.14}$$

This shows that $a * a = 0$ if $a = 0$. On the other hand, if $a \neq 0$ then $|a| > 0$. Hence $a * a > 0$ by the first inequality of (A.14). This shows that (A.13) defines a scalar product.

Remark A.3.2. Note that (A.11) follows by (A.13) and the general Schwartz inequality,

$$|a * b| \leq (a * a)^{\frac{1}{2}} (b * b)^{\frac{1}{2}}.$$

A.3.1 Greens formula for elasticity problems

Let $\mathbf{v}$ be any vector valued function of the type $\mathbf{v} = (v_1, v_2, v_3)$. If $v_i = v_i(x)$ and each component of the stress matrix σ_{ij} are sufficiently smooth, and Ω is a domain with sufficiently smooth boundary $\partial\Omega$, we obtain from the Greens formula that

$$\int_\Omega v_i \operatorname{div} \sigma_i\, dx = -\int_\Omega (\operatorname{grad} v_i) \cdot \sigma_i\, dx + \int_{\partial\Omega} v_i \left(\sigma_i \cdot n\right)\, ds.$$

Thus,

$$\int_\Omega \mathbf{v} \cdot \operatorname{div} \sigma(\mathbf{u})\, dx = \int_\Omega (v_1, v_2, v_3) \cdot (\operatorname{div} \sigma_1, \operatorname{div} \sigma_2, \operatorname{div} \sigma_3)\, dx = \int_\Omega \sum_{i=1}^{3} v_i \operatorname{div} \sigma_i\, dx =$$

$$\sum_{i=1}^{3}\int_{\Omega} v_i \operatorname{div}\sigma_i \, dx = \sum_{i=1}^{3}\left(-\int_{\Omega}(\operatorname{grad} v_i)\,\sigma_i \, dx + \int_{\partial\Omega} v_i\,(\sigma_i\cdot n)\; ds\right) =$$

$$-\int_{\Omega}\sum_{i=1}^{3}(\operatorname{grad} v_i)\,\sigma_i \, dx + \int_{\partial\Omega}\sum_{i=1}^{3} v_i\,(\sigma_i\cdot n)\; ds.$$

Hence, since

$$(\operatorname{grad} v_i)\cdot\sigma_i = \left(\frac{\partial v_i}{\partial x_1}, \frac{\partial v_i}{\partial x_2}, \frac{\partial v_i}{\partial x_2}\right)\cdot(\sigma_{i1},\sigma_{i2},\sigma_{i3}) = \sum_{j=1}^{3}\frac{\partial v_i}{\partial x_j}\sigma_{ij}$$

and

$$\sum_{i=1}^{3} v_i\,(\sigma_i\cdot n) = \sum_{i=1}^{3} v_i F_i = \mathbf{v}\cdot\mathbf{F},$$

where $\mathbf{F}$ is the stress vector on the surface $\partial\Omega$, we find that

$$\int_{\Omega}\mathbf{v}\cdot\operatorname{div}\sigma(\mathbf{u})\, dx = -\int_{\Omega}\sum_{ij}\frac{\partial v_i}{\partial x_j}\sigma_{ij}\, dx + \int_{\partial\Omega}\mathbf{v}\cdot\mathbf{F}(\mathbf{u})\, ds. \tag{A.15}$$

Moreover, since

$$\sum_{ij}\frac{\partial v_i}{\partial x_j}\sigma_{ij} = \sum_{ij}\frac{\partial v_j}{\partial x_i}\sigma_{ji}$$

(due to the fact that the sum is not changed if i and j are interchanged), and $\sigma_{ij} = \sigma_{ji}$, it is clear that

$$e(\mathbf{v})\cdot\sigma(\mathbf{u}) = \sum_{ij} e_{ij}(\mathbf{v})\sigma_{ij} = \sum_{ij}\frac{1}{2}\left(\frac{\partial v_i}{\partial x_j} + \frac{\partial v_j}{\partial x_i}\right)\sigma_{ij} =$$

$$\frac{1}{2}\sum_{ij}\frac{\partial v_i}{\partial x_j}\sigma_{ij} + \frac{1}{2}\sum_{ij}\frac{\partial v_j}{\partial x_i}\sigma_{ij} = \sum_{ij}\frac{\partial v_i}{\partial x_j}\sigma_{ji}.$$

Thus, we obtain the following version of the Green formula:

$$\int_{\Omega}\mathbf{v}\cdot\operatorname{div}\sigma(\mathbf{u})\, dx = -\int_{\Omega} e(\mathbf{v})\cdot\sigma(\mathbf{u})\, dx + \int_{\partial\Omega}\mathbf{v}\cdot F(\mathbf{u})\, ds. \tag{A.16}$$

Another version which also is useful is the following:

$$\int_{\Omega}\sum_{ij} v_i\frac{\partial\sigma_{ij}}{\partial x_j}\; dx = -\int_{\Omega}\sum_{ij}\frac{\partial v_i}{\partial x_j}\sigma_{ij}\, dx + \int_{\partial\Omega}\sum_{ij} v_i\,(\sigma_{ij}n_j)\; ds, \tag{A.17}$$

which is valid even if σ is non-symmetric. This identity follows directly from (A.15) by using the facts that

$$\sum_{ij} v_i\frac{\partial\sigma_{ij}}{\partial x_j} = \mathbf{v}\cdot\operatorname{div}\sigma(\mathbf{u}) \text{ and } \sum_{ij} v_i\,(\sigma_{ij}n_j) = v\cdot F.$$

A.3.2 Classical formulations of the Dirichlet and Neumann problems

By (A.7) and (A.8) we obtain that $\operatorname{div}(Ce(\mathbf{u})) = -\mathbf{f}$. However, similarly as for the conductivity problem, this equation does not provide us with enough information to determine the strain $e(\mathbf{u})$ (or the stress $\sigma(\mathbf{u})$) uniquely. In order to obtain uniqueness, we have to add some information concerning the boundary conditions on $\mathbf{u}$ and/or the stress vector $F(\mathbf{u})$.

The simplest case is when the elastic body, occupying a domain Ω, is fixed along its boundary, i.e. when we have the following Dirichlet problem:

$$\begin{cases} \operatorname{div}(Ce(\mathbf{u})) = -\mathbf{f} & \text{in } \Omega, \\ \mathbf{u} = \mathbf{0} & \text{on } \partial\Omega. \end{cases} \tag{A.18}$$

As we will see, the corresponding weak formulation of this problem gives a unique solution $\mathbf{u}$ if we only assume that the components of $\mathbf{f}$ belong to $L^2(\Omega)$.

If there are no boundary forces at $\partial\Omega$ we have the following Neumann problem:

$$\begin{cases} \operatorname{div}(Ce(\mathbf{u})) = -\mathbf{f} & \text{in } \Omega, \\ F(\mathbf{u}) = \mathbf{0} & \text{on } \partial\Omega, \end{cases} \tag{A.19}$$

Also here it turns out that the corresponding weak formulation gives a solution $\mathbf{u}$ if Ω is sufficiently smooth (e.g. Lipschitz continuous), the components of $\mathbf{f}$ belong to $L^2(\Omega)$ and $\int_\Omega \mathbf{f}\cdot\mathbf{v}\,dx = 0$ for every rigid displacement $\mathbf{v}$ (for a physical intepretation of the latter property, see Proposition A.3.3 below). However, in contrast to the Dirichlet problem the solution is not unique, since $\mathbf{w} = \mathbf{u} + \mathbf{v}$ also is a solution for any rigid displacement $\mathbf{v}$. This follows from the fact that $e(\mathbf{v}) = \mathbf{0}$ and $F(\mathbf{v}) = \mathbf{0}$, thus $e(\mathbf{w}) = e(\mathbf{u}+\mathbf{v}) = e(\mathbf{u})$ and $F(\mathbf{w}) = F(\mathbf{u}+\mathbf{v}) = F(\mathbf{u})$, which shows that $\operatorname{div}(Ce(\mathbf{w})) = -\mathbf{f}$ in Ω and $F(\mathbf{w}) = \mathbf{0}$ on $\partial\Omega$. In order to obtain a unique solution we have to search in a function space which do not contain any rigid displacements (except the zero displacement, which must be present since any vector space must contain the o-vector). We will come back to this issue. Next, we state the following:

Proposition A.3.3. *The condition $\int_\Omega \mathbf{f}\cdot\mathbf{v}\,dx = 0$, for every rigid displacement $\mathbf{v}$, simply means that the resultant force in each direction $F_i = \int_\Omega f_i dx$ and the resultant moments $M_1 = \int_\Omega (x_3 f_2 - x_2 f_3)\,dx$, $M_2 = \int_\Omega (x_3 f_1 - x_1 f_3)\,dx$, $M_3 = \int_\Omega (-x_2 f_1 + x_1 f_2)\,dx$, applied to whole domain Ω, are all equal 0.*

Proof Assume that $\int_\Omega \mathbf{f}\cdot\mathbf{v}\,dx = 0$ for all rigid displacements. Let $\mathbf{v} = (v_1, v_2, v_3)$ be a rigid displacement, i.e. of the form

$$\begin{bmatrix} v_1(x) \\ v_2(x) \\ v_3(x) \end{bmatrix} = \begin{bmatrix} 0 & b_{12} & b_{13} \\ -b_{12} & 0 & b_{23} \\ -b_{13} & -b_{23} & 0 \end{bmatrix} \begin{bmatrix} x_1 \\ x_2 \\ x_3 \end{bmatrix} + \begin{bmatrix} c_1 \\ c_2 \\ c_3 \end{bmatrix}.$$

Setting $c_1 = 1$ and all other constants equal to zero, i.e. $\mathbf{v} = \mathbf{v}_1 = (1,0,0)$, we obtain that

$$\int_\Omega \mathbf{f}\cdot\mathbf{v}\,dx = \int_\Omega (f_1, f_2, f_3)\cdot(1,0,0)\;dx = \int_\Omega f_1(x)\,dx,$$

which shows that $F_1 = \int_\Omega f_1(x)\ dx = 0$. Similarly, we obtain that $F_2 = \int_\Omega f_2(x)\ dx = 0$ and $F_3 = \int_\Omega f_3(x)\ dx = 0$.

Setting e.g. $b_{23} = 1$ and all other constants equal to zero, i.e. $\mathbf{v} = \mathbf{v}_{23} = (0, x_3, -x_1)$, we obtain that

$$\int_\Omega \mathbf{f} \cdot \mathbf{v}\ dx = \int_\Omega (f_1, f_2, f_3) \cdot (0, x_3, -x_1)\ dx = \int_\Omega x_3 f_2 - x_1 f_3\ dx.$$

Hence, $M_1 = \int_\Omega (x_3 f_2 - x_2 f_3)\ dx = 0$. Similarly, by first setting $b_{13} = 1$ (and all other constants equal to zero), and next setting $b_{12} = 1$ (and all other constants equal to zero) we obtain that $M_2 = 0$ and $M_3 = 0$.

Conversally, assume that the resultant forces and moments are zero. Let $\mathbf{v}_1, \mathbf{v}_2, \mathbf{v}_3, \mathbf{v}_{12}, \mathbf{v}_{13}, \mathbf{v}_{23}$ denote the six rigid displacements considered above. It is clear that any rigid displacement can be written in the form

$$\mathbf{v} = c_1\mathbf{v}_1 + c_2\mathbf{v}_2 + c_3\mathbf{v}_3 + b_{12}\mathbf{v}_{12} + b_{13}\mathbf{v}_{13} + b_{23}\mathbf{v}_{23}.$$

Hence,

$$\int_\Omega \mathbf{f} \cdot \mathbf{v}\ dx = \int_\Omega \mathbf{f} \cdot (c_1\mathbf{v}_1 + c_2\mathbf{v}_2 + c_3\mathbf{v}_3 + b_{12}\mathbf{v}_{12} + b_{13}\mathbf{v}_{13} + b_{23}\mathbf{v}_{23})\ dx =$$

$$c_1 \int_\Omega \mathbf{f} \cdot \mathbf{v}_1\ dx + c_2 \int_\Omega \mathbf{f} \cdot \mathbf{v}_2\ dx + c_3 \int_\Omega \mathbf{f} \cdot \mathbf{v}_3\ dx +$$

$$b_{12} \int_\Omega \mathbf{f} \cdot \mathbf{v}_{12}\ dx + b_{13} \int_\Omega \mathbf{f} \cdot \mathbf{v}_{13}\ dx + b_{23} \int_\Omega \mathbf{f} \cdot \mathbf{v}_{23}\ dx =$$

$$c_1F_1 + c_2F_2 + c_3F_3 + b_{12}M_3 + b_{13}M_2 + b_{23}M_1 = 0.$$

Therefore, $\int_\Omega \mathbf{f} \cdot \mathbf{v}\ dx = 0$ for any rigid displacement $\mathbf{v}$. This completes the proof that the two statements are equivalent.

Next we present the following example of application of Proposition A.3.3:

Proposition A.3.4. *A flywheel is a rotating mass used to store energy mechanically in the form of kinetic energy. Figure A.1 shows an example of a flywheel occupying a domain Ω and rotating around the x_3-axis. We assume that there are no boundary forces present. Moreover, the density function $\mathbf{f}$ (the centrifugal force) points in the radial direction with magnitude proposional to the distance from the x_3-axis. More precizely,*

$$\mathbf{f}(x) = (f_1(x), f_2(x), f_3(x)) = (\omega^2\rho x_1, \omega^2\rho x_2, 0),$$

where ω is the angular velocity and ρ is the density of the material. Then $\mathbf{f}$ satisfies the conditions required to obtain a solution of the corresponding Neumann problem.

Proof We see that $f_i(x)$ is bounded (i.e. $f_i(x) \leq C < \infty$ for some constant C). Hence

$$\int_\Omega f_i^2(x)\ dx \leq \int_\Omega C^2\ dx = C^2 \int_\Omega 1 dx = C^2(\text{volume of } \Omega) < \infty,$$

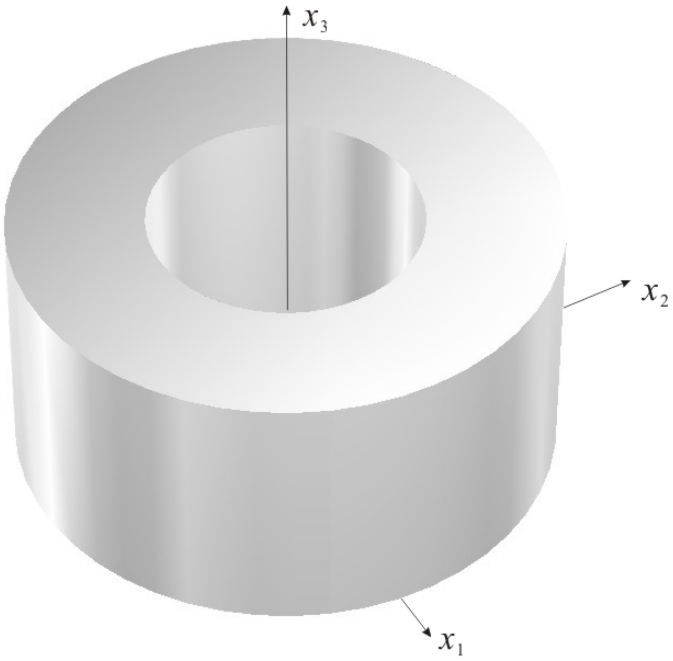

Figure A.1: A flywheel occupying a domain Ω.

which shows that f_i belongs to $L^2(\Omega)$. In order to prove that $\int_\Omega \mathbf{f} \cdot \mathbf{v}\, dx = 0$ for every rigid displacement $\mathbf{v}$, it is enough to show that the resultant forces and moments are zero (according to Proposition A.3.3). Due to the fact that Ω is symmetric in the x_1-direction, and $f_1(x)$ is anti-symmetric in the x_1-direction, it follows that $F_1 = \int_\Omega f_1(x)\, dx = 0$. Similarly we obtain that $F_2 = \int_\Omega f_2(x)\, dx = 0$. The fact that $F_3 = \int_\Omega f_3(x)\, dx = 0$ is trivial. Of the same symmetry-reasons we find that

$$M_1 = \int_\Omega (x_3 f_2 \ - x_2 f_3)\, dx = \omega^2 \rho \int_\Omega x_3 x_2\, dx = 0,$$

and

$$M_2 = \int_\Omega (x_3 f_1 \ - x_1 f_3)\, dx = \omega^2 \rho \int_\Omega x_3 x_1\, dx = 0.$$

Moreover, we obtain that

$$M_3 = \int_\Omega (-x_2 f_1 \ + x_1 f_2)\, dx = \int_\Omega \underbrace{\left(-x_2 \omega^2 \rho x_1 \ + x_1 \omega^2 \rho x_2\right)}_{=0} dx = 0.$$

This show that $\mathbf{f}$ satisfies the conditions required to obtain a solution of the corresponding Neumann problem.

A.3.3 Weak formulation of the Dirichlet problem

Let $\mathbf{L}^2(\Omega)$, $\mathbf{W}^{1,2}(\Omega)$, $\mathbf{W}_0^{1,2}(\Omega)$, $\mathbf{W}_{per}^{1,2}(Y)$ denote the spaces of vector valued functions $\mathbf{u} = (u_1, u_2, u_3)$ with components in $L^2(\Omega)$, $W^{1,2}(\Omega)$, $W_0^{1,2}(\Omega)$, $W_{per}^{1,2}(Y)$, respectively. The scalar product in these spaces are defined by

$$\mathbf{u} \star \mathbf{v} = (u_1, u_2, u_3) \star (v_1, v_2, v_3) = u_1 * v_1 + u_2 * v_2 + u_3 * v_3,$$

where "$*$" on the right side denotes the scalar product between the components, which has been defined previously. Thus, the norm $\|\mathbf{u}\|$ is given by

$$\|\mathbf{u}\| = \left(\sum_{i=1}^{3} \|u_i\|^2 \right)^{\frac{1}{2}}.$$

More precisely, the norm in $\mathbf{L}^2(\Omega)$ is given by

$$\|\mathbf{u}\|_{\mathbf{L}^2} = \left(\sum_{i=1}^{3} \|u_i\|_{L^2}^2 \right)^{\frac{1}{2}} = \left(\sum_{i=1}^{3} \int_\Omega u_i^2 \, dx \right)^{\frac{1}{2}} = \left(\int_\Omega \sum_{i=1}^{3} u_i^2 \, dx \right)^{\frac{1}{2}} = \left(\int_\Omega |\mathbf{u}|^2 \, dx \right)^{\frac{1}{2}}$$

and the norm in the $\mathbf{W}$-spaces is given by

$$\|\mathbf{u}\|_{\mathbf{W}^{1,2}} = \left(\sum_{i=1}^{3} \|u_i\|_{W^{1,2}}^2 \right)^{\frac{1}{2}} = \left(\sum_{j=1}^{3} \left(\int_\Omega u_i^2 \, dx + \sum_{i=1}^{3} \int_\Omega \left(\frac{\partial u_i}{\partial x_j} \right)^2 dx \right) \right)^{\frac{1}{2}} =$$

$$\left(\int_\Omega \sum_{j=1}^{3} u_i^2 \, dx + \sum_{ij} \int_\Omega \left(\frac{\partial u_i}{\partial x_j} \right)^2 dx \right)^{\frac{1}{2}} = \left(\int_\Omega |\mathbf{u}|^2 \, dx + \sum_{ij} \left(\int_\Omega \left(\frac{\partial u_i}{\partial x_j} \right)^2 dx \right) \right)^{\frac{1}{2}}.$$

Similarly as above we let $\mathbf{C}^\infty(\Omega)$ and $\mathbf{C}_0^\infty(\Omega)$ denote the spaces of vector valued functions $\mathbf{u} = (u_1, u_2, u_3)$ with components in $C^\infty(\Omega)$ and $C_0^\infty(\Omega)$, respectively. Since we already know that Sobolev-functions can be approximated by smooth functions in the scalar case, it is clear that this also is true in the vector-valued case.

Assume that $\mathbf{f} \in \mathbf{L}^2(\Omega)$. By muliplying both sides of the above equation with an arbitrary vector function $\mathbf{v} \in \mathbf{W}_0^{1,2}(\Omega)$, and next integrating, we obtain that

$$\int_\Omega \mathbf{v} \cdot \operatorname{div} \sigma(\mathbf{u}) \, dx = -\int_\Omega \mathbf{v} \cdot \mathbf{f} \, dx. \tag{A.20}$$

By using Greens formula we find that

$$\int_\Omega \mathbf{v} \cdot \operatorname{div} \sigma(\mathbf{u}) \, dx = -\int_\Omega e(\mathbf{v}) \cdot \sigma(\mathbf{u}) \, dx + \underbrace{\int_{\partial\Omega} \mathbf{v} \cdot F(\mathbf{u}) \, ds}_{= 0, \text{ since } \mathbf{v}=\mathbf{0} \text{ on } \partial\Omega}$$

$$= -\int_\Omega e(\mathbf{v}) \cdot \sigma(\mathbf{u}) \, dx = -\int_\Omega e(\mathbf{v}) \cdot Ce(\mathbf{u}) \, dx.$$

Thus, (A.20) gives that

$$\int_\Omega e(\mathbf{v}) \cdot Ce(\mathbf{u})\, dx = \int_\Omega \mathbf{v} \cdot \mathbf{f}\, dx. \tag{A.21}$$

Hence, the weak formulation of (A.18) takes the following form: Find $\mathbf{u} \in \mathbf{W}_0^{1,2}(\Omega)$ such that

$$a(\mathbf{u}, \mathbf{v}) = L(\mathbf{v}) \text{ for all } \mathbf{v} \in \mathbf{W}_0^{1,2}(\Omega), \tag{A.22}$$

where

$$a(\mathbf{u}, \mathbf{v}) = \int_\Omega e(\mathbf{v}) \cdot Ce(\mathbf{u})\, dx, \quad L(\mathbf{v}) = \int_\Omega \mathbf{v} \cdot \mathbf{f}\, dx.$$

We are now ready to state our next result.

Proposition A.3.5. *It yields that $a(\mathbf{u}, \mathbf{v}) = \int_\Omega e(\mathbf{v}) \cdot Ce(\mathbf{u})\, dx$ defines a symmetric bilinear form.*

Proof It is clear that $e(\cdot)$ is a linear transformation, i.e. that $e(\mathbf{u} + \mathbf{v}) = e(\mathbf{u}) + e(\mathbf{v})$ and $e(k\mathbf{v}) = ke(\mathbf{v})$, for all $\mathbf{u}, \mathbf{v} \in \mathbf{W}^{1,2}(\Omega)$ and $k \in R$. Moreover, due to the fact that (A.13) defines a scalar product $*$, we know that

$$a(\mathbf{u}, \mathbf{v}) = \int_\Omega e(\mathbf{v}) \cdot Ce(\mathbf{u})\, dx = e(\mathbf{v}) * e(\mathbf{u}) = e(\mathbf{u}) * e(\mathbf{v}) = \int_\Omega e(\mathbf{u}) \cdot Ce(\mathbf{v})\, dx = a(\mathbf{v}, \mathbf{u}).$$

Hence, $a(\mathbf{u}, \mathbf{v})$ is symmetric. Similarly, we obtain that

$$a(\mathbf{u} + \mathbf{v}, \mathbf{w}) = \int_\Omega e(\mathbf{u} + \mathbf{v}) \cdot Ce(\mathbf{w})\, dx = e(\mathbf{w}) * e(\mathbf{u} + \mathbf{v}) = e(\mathbf{w}) * (e(\mathbf{u}) + e(\mathbf{v})) =$$

$$e(\mathbf{w}) * e(\mathbf{u}) + e(\mathbf{w}) * e(\mathbf{v}) = \int_\Omega e(\mathbf{w}) \cdot Ce(\mathbf{u})\, dx + \int_\Omega e(\mathbf{w}) \cdot Ce(\mathbf{v})\, dx = a(\mathbf{u}, \mathbf{w}) + a(\mathbf{v}, \mathbf{w}),$$

and

$$a(k\mathbf{v}, \mathbf{w}) = \int_\Omega e(\mathbf{w}) \cdot Ce(k\mathbf{v})\, dx = e(\mathbf{w}) * e(k\mathbf{v}) = e(\mathbf{w}) * (ke(\mathbf{v})) = k\,(e(\mathbf{w}) * e(\mathbf{v})) =$$

$$k \int_\Omega e(\mathbf{w}) \cdot Ce(\mathbf{v})\, dx = ka(\mathbf{v}, \mathbf{w}).$$

This proves the linearity of $a(\mathbf{u}, \mathbf{v})$ in the first variable. The linearity of $a(\mathbf{u}, \mathbf{v})$ in the second variable follows by the fact that $a(\mathbf{u}, \mathbf{v})$ is symmetric.

By Proposition A.3.5 we observe that $a(\mathbf{u}, \mathbf{v})$ satisfies condition 1) in the abstract theory formulated in Theorem A.2.2 and Theorem A.2.3. Let us show that $a(\mathbf{u}, \mathbf{v})$ and $L(\mathbf{v})$ also satisfy the remaining conditions 2), 3), and 4). For simplicity we let $\|\cdot\|$ denotes the norm $\|\cdot\|_{\mathbf{W}^{1,2}}$. For the proof of condition 2) let $\varphi \in \mathbf{W}^{1,2}(\Omega)$. By (A.12) and the fact that

$$\sum_{ij} (\frac{\partial \varphi_i}{\partial x_j})^2 = \sum_{ij} (\frac{\partial \varphi_j}{\partial x_i})^2,$$

(due to the fact that the sum is not changed if i and j are interchanged) we obtain that

$$\int_\Omega \sum_{ij} (\frac{\partial \varphi_i}{\partial x_j} \frac{\partial \varphi_j}{\partial x_i})\, dx \leq$$

$$\left(\int_\Omega \sum_{ij} (\frac{\partial \varphi_i}{\partial x_j})^2\, dx \right)^{\frac{1}{2}} \left(\int_\Omega \sum_{ij} (\frac{\partial \varphi_j}{\partial x_i})^2\, dx \right)^{\frac{1}{2}} = \int_\Omega \sum_{ij} (\frac{\partial \varphi_i}{\partial x_j})^2\, dx.$$

Thus,

$$\int_\Omega |e(\varphi)|^2\ dx = \frac{1}{4} \int_\Omega \sum_{ij} (\frac{\partial \varphi_i}{\partial x_j} + \frac{\partial \varphi_j}{\partial x_i})^2\, dx =$$

$$\frac{1}{2} \int_\Omega \sum_{ij} (\frac{\partial \varphi_i}{\partial x_j})^2\, dx + \frac{1}{2} \int_\Omega \sum_{ij} (\frac{\partial \varphi_i}{\partial x_j} \frac{\partial \varphi_j}{\partial x_i})\, dx \tag{A.23}$$

$$\leq \frac{1}{2} \int_\Omega \sum_{ij} (\frac{\partial \varphi_i}{\partial x_j})^2\, dx + \frac{1}{2} \int_\Omega \sum_{ij} (\frac{\partial \varphi_i}{\partial x_j})^2\, dx = \int_\Omega \sum_{ij} (\frac{\partial \varphi_i}{\partial x_j})^2\, dx,$$

i.e.

$$\int_\Omega |e(\varphi)|^2\ dx \leq \int_\Omega \sum_{ij} (\frac{\partial \varphi_i}{\partial x_j})^2\, dx. \tag{A.24}$$

Moreover, by (A.11), (A.9) and (A.24) we obtain that

$$|a(\mathbf{u}, \mathbf{v})| \leq \left(\int_\Omega e(\mathbf{u}) \cdot Ce(\mathbf{u})\, dx \right)^{\frac{1}{2}} \left(\int_\Omega e(\mathbf{v}) \cdot Ce(\mathbf{v})\, dx \right)^{\frac{1}{2}} \leq$$

$$\left(\nu_2 \int_\Omega e(\mathbf{u}) \cdot e(\mathbf{u})\, dx \right)^{\frac{1}{2}} \left(\nu_2 \int_\Omega e(\mathbf{v}) \cdot e(\mathbf{v})\, dx \right)^{\frac{1}{2}} =$$

$$\nu_2 \left(\int_\Omega |e(\mathbf{u})|^2\ dx \right)^{\frac{1}{2}} \left(\int_\Omega |e(\mathbf{v})|^2\ dx \right)^{\frac{1}{2}} \leq$$

$$\nu_2 \left(\int_\Omega \sum_{ij} (\frac{\partial u_i}{\partial x_j})^2\, dx \right)^{\frac{1}{2}} \left(\int_\Omega \sum_{ij} (\frac{\partial v_i}{\partial x_j})^2\, dx \right)^{\frac{1}{2}} \leq$$

$$\nu_2 \left(\int_\Omega |\mathbf{u}|^2\ dx + \int_\Omega \sum_{ij} (\frac{\partial u_i}{\partial x_j})^2\, dx \right)^{\frac{1}{2}} \left(\int_\Omega |\mathbf{v}|^2\ dx + \int_\Omega \sum_{ij} (\frac{\partial v_i}{\partial x_j})^2\, dx \right)^{\frac{1}{2}}$$

$$= \nu_2 \|\mathbf{u}\| \|\mathbf{v}\|,$$

i.e.

$$|a(\mathbf{u}, \mathbf{v})| \leq \nu_2 \|\mathbf{u}\| \|\mathbf{v}\|, \tag{A.25}$$

which proves condition 2).

For the proof of condition 3) we let we $\varphi \in \mathbf{C}_0^\infty(\Omega)$ and use the Green formula

$$\int_\Omega \sum_{ij} v_i \frac{\partial \sigma_{ij}}{\partial x_j}\, dx = -\int_\Omega \sum_{ij} \frac{\partial v_i}{\partial x_j}\sigma_{ij}\, dx + \int_{\partial\Omega} \sum_{ij} v_i \left(\sigma_{ij} n_j\right)\, ds,$$

(see (A.17)) first with $v_i = \varphi_i$ and $\sigma_{ij} = \partial\varphi_j/\partial x_i$, next with $v_i = \partial\varphi_i/\partial x_i$ and $\sigma_{ij} = \varphi_j$. This yield the two equations

$$\int_\Omega \sum_{ij} \varphi_i \frac{\partial\left(\partial\varphi_j/\partial x_i\right)}{\partial x_j}\, dx = -\int_\Omega \sum_{ij} \frac{\partial\varphi_i}{\partial x_j}\frac{\partial\varphi_j}{\partial x_i}\, dx + \underbrace{\int_{\partial\Omega} \sum_{ij} \varphi_i \left(\frac{\partial\varphi_j}{\partial x_i} n_j\right)\, ds}_{=0,\ \text{since } \varphi_i = 0 \text{ on } \partial\Omega},$$

$$\int_\Omega \sum_{ij} \frac{\partial\varphi_i}{\partial x_i}\frac{\partial\varphi_j}{\partial x_j}\, dx = -\int_\Omega \sum_{ij} \frac{\partial\left(\partial\varphi_i/\partial x_i\right)}{\partial x_j}\varphi_j\, dx + \underbrace{\int_{\partial\Omega} \sum_{ij} \frac{\partial\varphi_i}{\partial x_i}\left(\varphi_j n_j\right)\, ds}_{=0,\ \text{since } \varphi_i = 0 \text{ on } \partial\Omega},$$

which, by using the fact that

$$\frac{\partial\left(\partial\varphi_j/\partial x_i\right)}{\partial x_j} = \frac{\partial\left(\partial\varphi_j/\partial x_j\right)}{\partial x_i},$$

reduce to the equations

$$\int_\Omega \sum_{ij} \varphi_i \frac{\partial\left(\partial\varphi_j/\partial x_j\right)}{\partial x_i}\, dx = -\int_\Omega \sum_{ij} \frac{\partial\varphi_i}{\partial x_j}\frac{\partial\varphi_j}{\partial x_i}\, dx,$$

and

$$\int_\Omega \sum_{ij} \varphi_j \frac{\partial\left(\partial\varphi_i/\partial x_i\right)}{\partial x_j}\, dx = -\int_\Omega \sum_{ij} \frac{\partial\varphi_i}{\partial x_i}\frac{\partial\varphi_j}{\partial x_j}\, dx.$$

Observing that the left sides of these equations are identical, we obtain that right sides also are identical, i.e. that

$$\int_\Omega \sum_{ij} \frac{\partial\varphi_i}{\partial x_j}\frac{\partial\varphi_j}{\partial x_i}\, dx = \int_\Omega \sum_{ij} \frac{\partial\varphi_i}{\partial x_i}\frac{\partial\varphi_j}{\partial x_j}\, dx.$$

Now, using that

$$\sum_{ij} \frac{\partial\varphi_i}{\partial x_i}\frac{\partial\varphi_j}{\partial x_j} = \left(\frac{\partial\varphi_1}{\partial x_1} + \frac{\partial\varphi_2}{\partial x_2} + \frac{\partial\varphi_3}{\partial x_3}\right)^2 = \left(\operatorname{div}\varphi\right)^2,$$

the last identity and (A.23) we find that

$$\int_\Omega \left|e(\varphi)\right|^2\, dx = \frac{1}{2}\int_\Omega \sum_{ij} \left(\frac{\partial\varphi_i}{\partial x_j}\right)^2 dx + \frac{1}{2}\int_\Omega \sum_{ij} \left(\frac{\partial\varphi_i}{\partial x_j}\frac{\partial\varphi_j}{\partial x_i}\right) dx =$$

$$\frac{1}{2}\int_\Omega \sum_{ij}(\frac{\partial \varphi_i}{\partial x_j})^2\ dx + \frac{1}{2}\int_\Omega (\operatorname{div}\varphi)^2\ dx \geq \frac{1}{2}\int_\Omega \sum_{ij}(\frac{\partial \varphi_i}{\partial x_j})^2\ dx =$$

$$\frac{1}{2}\int_\Omega \sum_{i=1}^{3} |\operatorname{grad}\varphi_i|^2\ dx = \frac{1}{2}\sum_{i=1}^{3}\int_\Omega |\operatorname{grad}\varphi_i|^2\ dx \geq$$

$$\frac{1}{2}\frac{1}{C_0+1}\sum_{i=1}^{3}\|\varphi_i\|^2_{W^{1,2}} = \frac{1}{2}\frac{1}{C_0+1}\|\varphi\|^2,$$

where C_0 is a positive constant (the last inequality is due to Friedrich's inequality), i.e.

$$\int_\Omega |e(\varphi)|^2\ dx \geq \frac{1}{2}\frac{1}{C_0+1}\|\varphi\|^2.$$

Using (A.9) we therefore obtain that

$$a(\varphi,\varphi) = \int_\Omega e(\varphi)\cdot Ce(\varphi)\ dx \geq \nu_1\int_\Omega |e(\varphi)|^2\ dx \geq \frac{1}{2}\frac{\nu_1}{C_0+1}\|\varphi\|^2. \qquad \text{(A.26)}$$

Now, if $\mathbf{u} \in \mathbf{W}^{1,2}(\Omega)$, then we can find functions $\varphi_h \in \mathbf{C}_0^\infty(\Omega)$ such that $\|\mathbf{u}-\varphi_h\| \to 0$ as $h\to\infty$. Since (A.26) holds if φ is replaced by φ_h, i.e.,

$$a(\varphi_h,\varphi_h) \geq \frac{1}{2}\frac{\nu_1}{C_0+1}\|\varphi_h\|^2$$

we obtain that

$$a(\mathbf{u},\mathbf{u}) \geq \frac{1}{2}\frac{\nu_1}{C_0+1}\|\mathbf{u}\|^2,$$

from the the convergences $\|\varphi_h\| \to \|\mathbf{u}\|$ and $a(\varphi_h,\varphi_h) \to a(\mathbf{u},\mathbf{u})$. Hence, in order to complete the proof of condition 3) it just remains to prove these convergences. For the proof that $\|\varphi_h\| \to \|\mathbf{u}\|$, we just use the reverse triangle inequality

$$|\|\mathbf{u}\| - \|\varphi_h\|| \leq \|\mathbf{u}-\varphi_h\|.$$

In the same way we obtain that $\|\mathbf{u}+\varphi_h\| \to 2\|\mathbf{u}\|$ (just use that

$$|\|2\mathbf{u}\| - \|\mathbf{u}+\varphi_h\|| \leq \|2\mathbf{u} - (\mathbf{u}+\varphi_h)\| = \|\mathbf{u}-\varphi_h\| \to 0)$$

Hence,

$$|a(\varphi_h,\varphi_h) - a(\mathbf{u},\mathbf{u})| = \left| a(\varphi_h,\varphi_h) + \underbrace{a(\varphi_h,\mathbf{u}) - a(\mathbf{u},\varphi_h)}_{=0,\text{ due to symmetry}} - a(\mathbf{u},\mathbf{u})\right| =$$

$$|a(\varphi_h-\mathbf{u},\varphi_h+\mathbf{u})| \leq \nu_2\|\varphi_h-\mathbf{u}\|\,\|\varphi_h+\mathbf{u}\| \to \nu_2\cdot 0\cdot 2\|\mathbf{u}\| = 0,$$

where the last inequality follows from (A.25). Hence, $a(\varphi_h,\varphi_h)\to a(\mathbf{u},\mathbf{u})$.

For the prove of condition 4) we use the Schwartz inequality and obtain that

$$|L(\mathbf{v})| = \left|\int_\Omega \mathbf{v}\cdot\mathbf{f}\ dx\right| \leq \left(\left|\int_\Omega |\mathbf{v}|^2\ dx\right|\right)^{\frac{1}{2}}\left(\left|\int_\Omega |\mathbf{f}|^2\ dx\right|\right)^{\frac{1}{2}} \leq$$

$$\left(\int_\Omega |\mathbf{v}|^2 \, dx + \sum_{ij} \left(\int_\Omega \left(\frac{\partial v_i}{\partial x_j}\right)^2 dx\right)\right)^{\frac{1}{2}} \left(\left|\int_\Omega |\mathbf{f}|^2 \, dx\right|\right)^{\frac{1}{2}} = \|\mathbf{v}\| \left(\left|\int_\Omega |\mathbf{f}|^2 \, dx\right|\right)^{\frac{1}{2}}.$$

Hence,.

$$|L(\mathbf{v})| \leq \Lambda \|\mathbf{v}\|,$$

where

$$\Lambda = \left(\left|\int_\Omega |\mathbf{f}|^2 \, dx\right|\right)^{\frac{1}{2}}.$$

This proves condition 4.

A.3.4 Weak formulation of the Neumann problem

Similarly as we use the Poincaré inequality in the proof of the coercivity for the conductivity problem with Neumann boundary conditions, we use the so-called Korn's inequality in case of the elasticity problems. It takes the following form:

$$\int_\Omega |e(\varphi)|^2 \, dx \geq c_0 \|\varphi\|^2_{\mathbf{W}^{1,2}}, \tag{A.27}$$

where c_0 is some positive constant. However, it is easy to see that this inequality is not valid in the whole space $\mathbf{W}^{1,2}(\Omega)$. For example, for any rigid displacement φ (e.g. a constant vector), we have that $e(\varphi) = 0$, so (A.27) is clearly violated if φ is a non-zero rigid displacement. On the other hand, it is possible to prove that if Ω be a bounded domain with Lipschitz continuous boundary and $\mathbf{V}$ is a closed (i.e. a complete) subspace of $\mathbf{W}^{1,2}(\Omega)$ that does not contain any rigid displacements except 0, then there exists a constant $c_0 > 0$ such that (A.27) holds for all $\varphi \in \mathbf{V}$.

In almost the same way as we derived (A.22) we obtain the following weak formulation of the Neumann problem: Find $\mathbf{u} \in \mathbf{W}^{1,2}_0(\Omega)$ such that

$$a(\mathbf{u}, \mathbf{v}) = L(\mathbf{v}) \text{ for all } \mathbf{v} \in \mathbf{W}^{1,2}(\Omega), \tag{A.28}$$

where $a(\mathbf{u}, \mathbf{v})$ and $L(\mathbf{v})$ are given above. Let $\mathfrak{R}$ denote the subspace of all rigid displacements and let $\mathbf{V}$ be the subspace

$$\mathbf{V} = \left\{\varphi \in \mathbf{W}^{1,2}(\Omega) \colon \int_\Omega \varphi \cdot \mathbf{r} \, dx = 0 \text{ for all } \mathbf{r} \in \mathfrak{R}\right\}. \tag{A.29}$$

It is clear that $\mathbf{V}$ does not contain any rigid displacements except 0. We have already proved that $a(\mathbf{u}, \mathbf{v})$ and $L(\mathbf{v})$ satisfy the conditions 1), 2) and 4) for all $\mathbf{u}, \mathbf{v} \in \mathbf{W}^{1,2}(\Omega)$, hence, also for all $\mathbf{u}, \mathbf{v} \in \mathbf{V}$. Moreover, by (A.9) and Korn's inequality (A.27) we have that

$$a(\varphi, \varphi) = \int_\Omega e(\varphi) \cdot Ce(\varphi) \, dx \geq \nu_1 \int_\Omega |e(\varphi)|^2 \, dx \geq \nu_1 c_0 \|\varphi\|^2_{\mathbf{W}^{1,2}}.$$

for all $\varphi \in \mathbf{V}$, which shows that condition 3) in Lax-Milgrams lemma is fullfilled. Hence, the problem

$$a(\mathbf{u}, \mathbf{v}) = L(\mathbf{v}) \text{ for all } \mathbf{v} \in \mathbf{V}, \tag{A.30}$$

admits a unique solution $\mathbf{u}$ in $\mathbf{V}$. It remains to prove that this solution also is a solution to the problem (A.28) provided that

$$L(\mathbf{r}) = \mathbf{0} \tag{A.31}$$

for all $\mathbf{r} \in \mathfrak{R}$. From (A.5) we see that $\mathfrak{R}$ is a 6-dimensional space. It is easy to find a basis for this space $(\mathbf{v}_1, ..., \mathbf{v}_6)$ which is orthonormal with respect to the scalar product in $\mathbf{L}^2(\Omega)$ given by $\varphi * \mathbf{v} = \int_\Omega \varphi \cdot \mathbf{v}\, dx$. If $\varphi \in \mathbf{W}^{1,2}(\Omega)$ we let $\varphi_\mathfrak{R}$ denote the orthogonal projection of φ onto $\mathfrak{R}$, i.e. the function

$$\varphi_\mathfrak{R} = \sum_{i=1}^{6} (\varphi * \mathbf{v}_i)\, \mathbf{v}_i.$$

Clearly, the function $\mathbf{v} = \varphi - \varphi_\mathfrak{R}$ belongs to $\mathbf{V}$. Inserting this function into (A.30) we obtain that

$$a(\mathbf{u}, \varphi) - a(\mathbf{u}, \varphi_\mathfrak{R}) = L(\varphi) - L(\varphi_\mathfrak{R})$$

for all $\mathbf{v} \in \mathbf{W}^{1,2}(\Omega)$. Since $L(\varphi_\mathfrak{R}) = \mathbf{0}$ by (A.31) and

$$a(\mathbf{u}, \varphi_\mathfrak{R}) = \int_\Omega \underbrace{e(\varphi_\mathfrak{R})}_{=\,0} \cdot Ce(\mathbf{u})\, dx = 0,$$

this shows that

$$a(\mathbf{u}, \varphi) = L(\varphi).$$

Hence, $\mathbf{u}$ is a solution of the problem (A.28). We complete this subsection with the following useful information about the space V defined by (A.29):

Proposition A.3.6. *The space V defined by (A.29) defines a closed subspace of $\mathbf{W}^{1,2}(\Omega)$ so that, in particular, $\mathbf{V}$ is a Hilbert space with respect to the norm $\|\|_{\mathbf{W}^{1,2}}$.*

Proof: Let $\mathbf{u}, \mathbf{v} \in \mathbf{V}$ and let $k \in \mathbb{R}$. Then,

$$\int_\Omega (\mathbf{u} + \mathbf{v}) \cdot \mathbf{r}\, dx = \int_\Omega \mathbf{u} \cdot \mathbf{r}\, dx + \int_\Omega \mathbf{v} \cdot \mathbf{r}\, dx = 0$$

and

$$\int_\Omega k\mathbf{u} \cdot \mathbf{r}\, dx = k \int_\Omega \mathbf{u} \cdot \mathbf{r}\, dx = 0$$

for all $\mathbf{r} \in \mathfrak{R}$. Hence, $\mathbf{u} + \mathbf{v} \in \mathbf{V}$ and $k\mathbf{u} \in \mathbf{V}$. This shows that $\mathbf{V}$ is a vector space.

In order to see that $\mathbf{V}$ is closed in $\mathbf{W}^{1,2}(\Omega)$, let $\varphi_h \in \mathbf{V}$ such that $\varphi_h \to \varphi$ in $\mathbf{W}^{1,2}(\Omega)$. We only have to show that $\varphi \in \mathbf{V}$. By the Schwartz inequality,

$$\left| \int_\Omega (\varphi - \varphi_h) \cdot \mathbf{r}\, dx \right| \leq \left(\left| \int_\Omega |\varphi - \varphi_h|^2\, dx \right| \right)^{\frac{1}{2}} \left(\left| \int_\Omega |\mathbf{r}|^2\, dx \right| \right)^{\frac{1}{2}}$$

$$\leq \|\varphi - \varphi_h\|^2 \left(\left| \int_\Omega |\mathbf{r}|^2 \, dx \right| \right)^{\frac{1}{2}} \to 0,$$

i.e.

$$\int_\Omega (\varphi - \varphi_h) \cdot \mathbf{r} \, dx \to 0.$$

Hence,

$$\int_\Omega \varphi \cdot \mathbf{r} \, dx = \int_\Omega \varphi \cdot \mathbf{r} \, dx - \underbrace{\int_\Omega \varphi_h \cdot \mathbf{r} \, dx}_{=0, \text{ since } \varphi_h \in \mathbf{V}} = \int_\Omega (\varphi - \varphi_h) \cdot \mathbf{r} \, dx \to 0,$$

which shows that $\int_\Omega \varphi \cdot \mathbf{r} \, dx = 0$, i.e. $\varphi \in \mathbf{V}$. This completes the proof that $\mathbf{V}$ is closed in $\mathbf{W^{1,2}}(\Omega)$.

A.4 On the Sobolev norm in R^n

Let $\Omega \subset R^n$ be an open set and let $H^m(\Omega)$ denote the usual Sobolev space with norm $\|\cdot\|$ given by

$$\|u\|^2 = \|u\|_2^2 + \sum_{r=1}^{m} \|D^r u\|_2^2,$$

where $\|\cdot\|_2$ is the $L^2(\Omega)$-norm and $D^r u$ denotes the vector $\{D^\alpha u\}_{|\alpha|=r}$. We recall that Ω is called an *open extension domain* if there exists a bounded linear operator $F : H^m(\Omega) \to H^m(R^n)$ such that $F(u)|_\Omega = u$ for all $u \in H^m(\Omega)$ (see e.g. [10, p. 63]). For example, if Ω is open and bounded with sufficiently smooth boundary (e.g. Lipschitz) it turns out to be of this type. It is possible to show (c.f. [10, p. 183]) that for any bounded open extension domain Ω, $\varepsilon > 0$ and $1 \leq |\alpha| \leq m-1$, there exists a positive constant $C(\varepsilon) < \infty$ such that

$$\|D^\alpha u\|_2 \leq C(\varepsilon) \|u\|_2 + \varepsilon \|D^m u\|_2 \tag{A.32}$$

for all $u \in H^m(\Omega)$. The purpose of this section is to show that this inequality holds even for $\Omega = R^n$.

Theorem A.4.1. *The inequality (A.32) holds for all* $u \in H^m(R^n)$.

Proof. We may assume that $0 \leq \varepsilon \leq 1$ (otherwise, just let $C(\varepsilon)$ be equal to that valid for the case $\varepsilon = 1$). If $0 < p \leq q-1$, and $x > 0$ then the following inequality holds

$$x^p \leq \varepsilon x^q + \frac{1}{\varepsilon^{q-1}}. \tag{A.33}$$

This follows by observing that the the left side is less than the right side for $x \leq 1/\varepsilon$ and that the same holds for its derivatives for $x \geq 1/\varepsilon$.

For all $u \in L^2(R^n)$ the Fourier transform $\mathcal{F}u(\xi) = \widehat{u}(\xi)$ is given by

$$\widehat{u}(\xi) = \frac{1}{(2\pi)^{\frac{n}{2}}} \int_{R^n} u(x) \, e^{-ix\xi} dx, \text{ for all } \xi \in R^n,$$

where $x\xi$ is the scalar product of x with ξ. The Plancherel equation implies that

$$\|u\|_2^2 = \|\mathcal{F}u\|_2^2 = \int_{R^n} |\widehat{u}(\xi)|^2 \, d\xi \tag{A.34}$$

Replacing u with $D^\beta u$ in (A.34) and using the formula

$$\mathcal{F}\left(D^\beta u\right) = i^{|\beta|}\xi^\beta \mathcal{F}(u), \tag{A.35}$$

where ξ^β denotes the number $\xi_1^{\beta_1} \cdots \xi_n^{\beta_n}$, we obtain that

$$\left\|D^\beta u\right\|_2^2 = \left\|\mathcal{F}\left(D^\beta u\right)\right\|_2^2 = \int_{R^n} \left|\xi^\beta \widehat{u}(\xi)\right|^2 d\xi. \tag{A.36}$$

We note that (A.35) and (A.36) are valid as long as $|\beta| \leq m$ and $u \in H^m(R^n)$.

Let $|\alpha| = r$ and let $\alpha^{[0]}, \alpha^{[1]}, ..\alpha^{[n]}$ and $\beta^{[1]}, ..\beta^{[n]}$ be the multi-indices defined by $\alpha^{[0]} = \alpha$, $\alpha^{[1]} = (0, \alpha_2, \alpha_3, ...\alpha_n)$, $\alpha^{[2]} = (0, 0, \alpha_3, ...\alpha_n)$,...$\alpha^{[n]} = (0, 0, ..., 0)$ and $\beta^{[1]} = (\alpha_1 + m - r, \alpha_2, \alpha_3, ...\alpha_n)$, $\beta^{[2]} = (0, \alpha_1 + \alpha_2 + m - r, \alpha_3, ..., \alpha_n)$,... $\beta^{[n]} = (0, 0, , ..., 0, \sum_{k=1}^n \alpha_k + m - r)$. Note that for each j the multi-indices $\alpha^{[j]}$, $\alpha^{[j+1]}$ and $\beta^{[j+1]}$ are equal except for the $j+1$-th component which is

$$\alpha_{j+1}^{[j]} = \alpha_{j+1},\ \alpha_{j+1}^{[j+1]} = 0 \text{ and } \beta_{j+1}^{[j+1]} = \left(\sum_{k=1}^{j+1} \alpha_k\right) + m - r \leq m,$$

respectively. This implies that

$$\xi^{\alpha^{[j]}} = \xi^{\alpha^{[j+1]}} \xi_{j+1}^{\alpha_{j+1}^{[j]}} \text{ and } \xi^{\beta^{[j+1]}} = \xi^{\alpha^{[j+1]}} \xi_{j+1}^{\beta_{j+1}^{[j+1]}}. \tag{A.37}$$

Replacing x with $|\xi_{j+1}|$, p with $\alpha_{j+1}^{[j]}$ and q with $\beta_{j+1}^{[j+1]}$ in (A.33), we obtain that

$$\left|\xi_{j+1}^{\alpha_{j+1}^{[j]}}\right| \leq \varepsilon \left|\xi_{j+1}^{\beta_{j+1}^{[j]}}\right| + \frac{1}{\varepsilon^{\beta_{j+1}^{[j+1]}-1}} \leq \varepsilon \left|\xi_{j+1}^{\beta_{j+1}^{[j]}}\right| + \frac{1}{\varepsilon^{m-1}}.$$

Multiplying this inequality with

$$\left|\xi^{\alpha^{[j+1]}}\right|$$

we obtain from (A.37) that

$$\left|\xi^{\alpha^{[j]}}\right| \leq \varepsilon \left|\xi^{\beta^{[j+1]}}\right| + \left|\xi^{\alpha^{[j+1]}}\right| \frac{1}{\varepsilon^{m-1}}. \tag{A.38}$$

Let $a_{j+1} = m^j$. Replacing ε with $\varepsilon^{a_{j+1}}$ in (A.38) and using that

$$\left(\varepsilon^{m^j}\right)^{m-1} = \frac{\varepsilon^{m^{j+1}}}{\varepsilon^{m^j}}$$

we obtain that

$$\left|\xi^{\alpha^{[j]}}\right| \leq \varepsilon^{m^j} \left|\xi^{\beta^{[j+1]}}\right| + \left|\xi^{\alpha^{[j+1]}}\right| \frac{\varepsilon^{m^j}}{\varepsilon^{m^{j+1}}},$$

i.e.

$$\frac{1}{\varepsilon^{m^j}}\left|\xi^{\alpha^{[j]}}\right| \leq \left|\xi^{\beta^{[j+1]}}\right| + \frac{1}{\varepsilon^{m^{j+1}}}\left|\xi^{\alpha^{[j+1]}}\right|.$$

Iterative use of this inequality gives that

$$\frac{1}{\varepsilon^{m^0}}\left|\xi^{\alpha^{[0]}}\right| \leq \left|\xi^{\beta^{[1]}}\right| + \frac{1}{\varepsilon^{m^1}}\left|\xi^{\alpha^{[1]}}\right|$$

$$\leq \left|\xi^{\beta^{[1]}}\right| + \left|\xi^{\beta^{[2]}}\right| + \frac{1}{\varepsilon^{m^2}}\left|\xi^{\alpha^{[2]}}\right| \leq \left|\xi^{\beta^{[1]}}\right| + \left|\xi^{\beta^{[2]}}\right| + \left|\xi^{\beta^{[3]}}\right| + \frac{1}{\varepsilon^{m^3}}\left|\xi^{\alpha^{[3]}}\right| \leq ....$$

$$\leq \sum_{j=1}^{n}\left|\xi^{\beta^{[j]}}\right| + \frac{1}{\varepsilon^{m^n}}\left|\xi^{\alpha^{[n]}}\right|.$$

Thus, using that $\left|\alpha^{[n]}\right| = 0$, we obtain that

$$|\xi^{\alpha}| = \left|\xi^{\alpha^{[0]}}\right| \leq \varepsilon\sum_{j=1}^{n}\left|\xi^{\beta^{[j]}}\right| + \frac{1}{\varepsilon^{m^n-1}}$$

By multiplying both sides with $\widehat{u}(\xi)$ we obtain by integration and the Minkowski inequality that

$$\left\|\xi^{\alpha}\widehat{u}(\xi)\right\|_2 \leq \varepsilon\sum_{j=1}^{n}\left\|\xi^{\beta^{[j]}}\widehat{u}(\xi)\right\|_2 + \frac{1}{\varepsilon^{m^n-1}}\left\|\widehat{u}(\xi)\right\|_2$$

Hence, using (A.34) and (A.36) (with $\beta = \beta^{[j]}$ and $\beta = \alpha$) gives that

$$\left\|D^{\alpha}u\right\|_2 = \left\|\xi^{\alpha}\widehat{u}(\xi)\right\|_2 \leq \varepsilon\sum_{j=1}^{n}\left\|D^{\beta^{[j]}}u\right\|_2 + \frac{1}{\varepsilon^{m^n-1}}\left\|u\right\|_2.$$

Accordingly, the Jensen inequality

$$\frac{1}{n}\sum_{j=1}^{n}|a_i| \leq \left(\frac{1}{n}\sum_{j=1}^{n}|a_i|^2\right)^{\frac{1}{2}}$$

together with the fact that $\left|\beta^{[j]}\right| = m$, implies that

$$\left\|D^{\alpha}u\right\|_2 \leq \varepsilon\sqrt{n}\left\|D^{m}u\right\|_2 + \frac{1}{\varepsilon^{m^n-1}}\left\|u\right\|_2.$$

By replacing ε with $\varepsilon/\sqrt{n}$, we obtain that (A.32) holds for all $u \in H^m(R^n)$. The proof is complete.

Corollary A.4.2. *It holds that*

$$\frac{1}{\sqrt{s}}\left\|u\right\|^2 \leq \int_R u^2dx + \int_R\left|\frac{d^su}{dx^s}\right|^2dx,$$

for all $u \in H^s(R)$.

Corollary A.4.2 follows from Theorem A.4.1. However, it can be proved independently by even easier arguments than for the general case. We therefore outline some details above its proof. which are of independent interest. The ideas are basically obtained from [5] with some small changes for pedagogical purposes.

Proof. We can find a sequence of smooth functions $\{\varphi_m\}$, converging to u where φ_m has support in the interval $(-\pi m, \pi m)$. These functions have Fourier series representation of the form

$$\varphi_m(x) = \frac{a_{0,m}}{2} + \sum_{l=1}^{\infty} a_{l,m} \cos\left(\frac{l}{m}x\right) + b_{l,j} \sin\left(\frac{l}{m}x\right).$$

Let $r \leq s$ be a fixed integer. By differentiating we obtain that $d^r\varphi_m(x)/dx^r$ has a similar series representation with Fourier coefficients of magnitude

$$a_{l,m}\left(\frac{l}{m}\right)^r \text{ and } b_{l,m}\left(\frac{l}{m}\right)^r.$$

Parseval's theorem applied to the corresponding series gives that

$$\frac{1}{2\pi m}\int_{-\pi m}^{\pi m} (\varphi_m(x))^2\, dx = \left(\frac{a_{0,m}}{2}\right)^2 + \sum_{l=1}^{\infty} c_{l,m}^2$$

and

$$\frac{1}{2\pi m}\int_{-\pi m}^{\pi m} \left(\frac{d^r\varphi_m(x)}{dx^r}\right)^2 dx = \sum_{l=1}^{\infty}\left(\frac{l}{m}\right)^{2r} c_{l,m}^2, \tag{A.39}$$

where

$$c_{l,j}^2 = \left(\frac{a_{l,j}}{2}\right)^2 + \left(\frac{b_{l,j}}{2}\right)^2.$$

According to our assumtion $r \leq s$. Thus we see, by adding the two inequalities, that

$$\sum_{l=1}^{m}\left(\frac{l}{m}\right)^{2r} c_{l,j}^2 \leq \sum_{l=1}^{m}\left(\frac{l}{m}\right)^{2s} c_{l,j}^2 \leq \sum_{l=1}^{\infty}\left(\frac{l}{m}\right)^{2s} c_{l,j}^2 = \frac{1}{2\pi m}\int_{-\pi m}^{\pi m}\left(\frac{d^s\varphi_m(x)}{dx^s}\right)^2 dx$$

and

$$\sum_{l=m+1}^{\infty}\left(\frac{l}{m}\right)^{2r} c_{l,j}^2 \leq \sum_{l=m+1}^{\infty} c_{l,j}^2 \leq \sum_{l=1}^{\infty} c_{l,j}^2 \leq \frac{1}{2\pi m}\int_{-\pi m}^{\pi m}(\varphi_m(x))^2\, dx,$$

so we obtain from (A.39) that

$$\int_{-\pi m}^{\pi m}\left(\frac{d^r\varphi_m(x)}{dx^r}\right)^2 dx \leq \int_{-\pi m}^{\pi m}(\varphi_m(x))^2 + \left(\frac{d^s\varphi_j(x)}{dx^s}\right)^2 dx.$$

Since φ_j has support in the interval $(-\pi m, \pi m)$, this gives that

$$\int_R \left(\frac{d^r \varphi_m(x)}{dx^r}\right)^2 dx \leq \int_R (\varphi_m(x))^2 + \left(\frac{d^s \varphi_m(x)}{dx^s}\right)^2 dx. \tag{A.40}$$

Using that $\varphi_m \to u$ in $H^s(R)$ we find that φ_m and $d^r\varphi_m/dx^r$ converges (in $L^2(R)$) to u and $d^r u/dx^r$, respectively. Hence, it follows from (A.40) that

$$\int_R \left(\frac{d^r u(x)}{dx^r}\right)^2 dx \leq \int_R (u(x))^2 + \left(\frac{d^s u(x)}{dx^s}\right)^2 dx.$$

Thus,

$$\int_R u^2 dx + \sum_{r=1}^{s} \int_R \left|\frac{d^r u}{dx^r}\right|^2 dx \leq s \int_R (u(x))^2 + \left(\frac{d^s u(x)}{dx^s}\right)^2 dx,$$

i.e.

$$\|u\|^2 \leq s \|u\|_1^2$$

and the proof follows.

Remark A.4.3. The above result shows that the norm $\|\cdot\|_*$ given by

$$\|u\|_*^2 = \|u\|_2^2 + \|D^m u\|_2^2$$

is equivalent to $\|\cdot\|$ on $H^m(R^n)$.

A.5 Beams resting on nonlinear foundation

Let us now investigate the case of a straight beam of stiffness EI resting on some nonlinear elastic foundation. We assume that the beam is subjected to a distributed force $q(x)$ from above (an illustration is found in Figure A.2). The letter y stands for the vertical deflection of the beam downwards. The slope $\tan\theta = dy/dx$, is approximately equal to the angle of the slope θ, since we are assuming small deflection. Moreover, we only assume that vertical forces are transmitted between the beam and the foundation. In addition, we ignore any resultant tensile force in the beam. The function $p = [p(y)](x)$ denotes the distributed load between the beam and the foundation and we assume that it is purely dependent of the deflection $y(x)$. The linear model assumes a relation of the form $p(y) = ky$, where k is called the modulus of the foundation. Most of the previous analysis is based on this simplified model. In this paper we relax the linearity assumption. A much weaker assumption is to assume that

$$H(r)H(s)C_1 (r-s)^2 \leq (p(r) - p(s))(r-s) \leq C_2 (r-s)^2 \tag{A.41}$$

for some constants $C_1, C_2 \in \langle 0, \infty \rangle$ for all $r, s \in R$. Here, H is the Heaviside step function (which is zero for negative arguments and 1 for positive arguments).

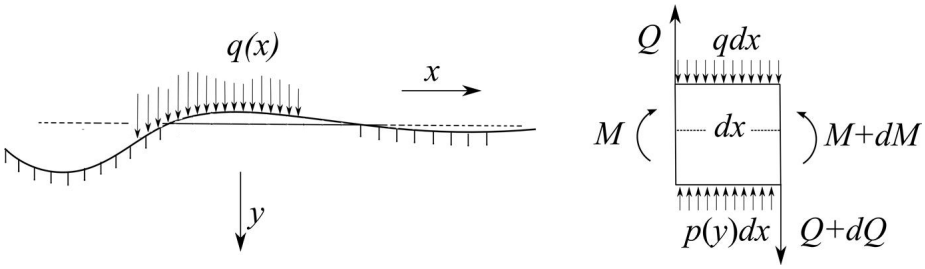

Figure A.2: Straight beam resting on an elastic foundation and subjected to some distributed force $q(x)$.

This criteria covers several interesting cases of practical importance. In the case of rail bending, for example, experimental data indicates a cubic relation of the form $p(y) = H(y)\left(k_0 y + k_1 y^3\right)$, (see [4]), where k_0 and k_1 are positive constants. The presence of the Heaviside step function is often ignored, due to the fact that it makes the analysis more complicated. However, from a practical point of view it is hard to explain why we ignore the fact that there are obviously no negative forces preventing the beam from being separated (lifted) from the foundation. This important obstacle with previous models of the problem has never been discussed previously, not even in the paper [5]. The problem with this generalization is that the corresponding partial differential operators does not satisfy the monotonicity assumption above. This makes the analysis much harder. There are ways to overcome this hindrance, but for the sake of limitation we will use the following more strict assumption on p:

$$C_1 (r-s)^2 \leq (p(r) - p(s))(r-s) \leq C_2 (r-s)^2 \tag{A.42}$$

In order to let the empirical formula $p(y) = H(y)\left(k_0 y + k_1 y^3\right)$ fit our setting, we may replace $H(y)$ by 1 and modify $p(y)$ such that the expression becomes linear for $|y| \geq r_0$ for a sufficiently large constant $r_0 > 0$, e.g. by putting

$$p(y) = \begin{cases} 0 & \text{for} \quad y < 0, \\ k_0 y + k_1 y^3 & \text{for} \quad 0 \leq y \leq r_0, \\ \frac{p(r_0)}{r_0} y & \text{for} \quad y > r_0. \end{cases}$$

Replacing $H(y)$ by 1 is certainly questionable, but necessary if to ensure monotonicity. The last simplification is easier to except since we from experience know that too large deflections can not happen before the beam structure collapses of other reasons. In Figure A.2 we have illustrated an infinitely small beam element enclosed between two vertical cross sections of distance dx from each other.

The shear force Q is often considered to be positive if it is acting upward on the left side of the element. The moment M is considered to be positive if it is clockwise on the left side of the element. Using that the anticlockwise moment

$M+dM$ is equal to the sum of clockwise moments about any point on the right side of the element, we obtain that

$$M + dM = M + Qdx + (p(y) - q)dx\frac{1}{2}(dx)^2.$$

By using that the resultant force is zero in the vertical direction we obtain

$$Q + p(y)dx = Q + dQ + qdx.$$

Thus,

$$\frac{dM}{dx} = Q \text{ and } \frac{dQ}{dx} = p(y) - q.$$

Accordingly, it yields that

$$\frac{d^2M}{dx^2} = p(y) - q \tag{A.43}$$

Using the beam bending equation

$$M = -EI\left(\frac{d^2y}{dx^2}\right) \tag{A.44}$$

(valid for small deformations) this gives us the following fourth order equation

$$\frac{d^2}{dx^2}\left(EI\frac{d^2y}{dx^2}\right) = -p(y) + q. \tag{A.45}$$

Note that this equation is valid in regions free from concentrated forces and moments only. Moreover, it is assumed that EI is a smooth function of x. Let us consider a single concentrated force P_0, which is directed downward acts at some point $x = a$. Moreover, assume that a concentrated clockwise moment M_0 is applied at that point as well. Now, the left and right parts of the beam which are separated by the point $x = a$ can be coupled together via the following conditions for the shear force

$$Q_+ - Q_- = -P_0 \tag{A.46}$$

and the moment

$$M_+ - M_- = M_0. \tag{A.47}$$

Here, $Q_\pm$ and $M_\pm$ stands for the right and left limits, i.e.

$$Q_\pm = \lim_{x\to a^\pm} Q \text{ and } M_\pm = \lim_{x\to a^\pm} M,$$

respectively (see Figure A.3).

As usual we obtain a corresponding weak formulation of this problem, by multiplying (A.43) with a general smooth function v with compact support, and afterwords integrate as follows:

$$\int_R \frac{d^2M}{dx^2} v\, dx = \int_R (p(y) - q)\, v\, dx. \tag{A.48}$$

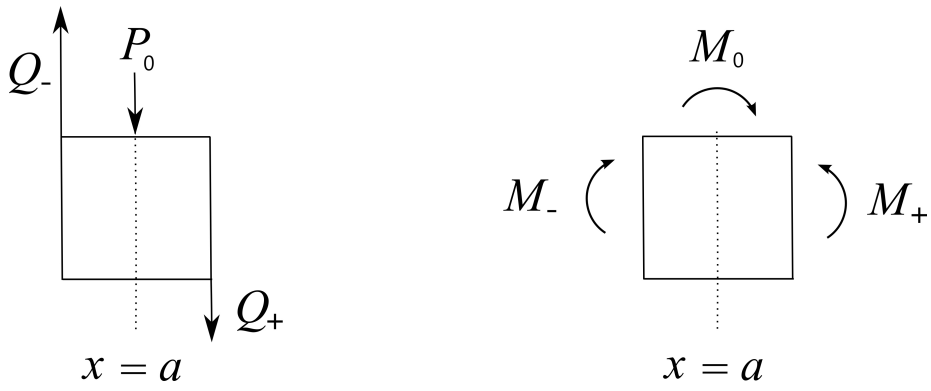

Figure A.3: The figure illustates the shear force and moments on both sides close to the point $x = a$, at which the consentrated force P_0 and moment M_0 are applied. This explains the discontinuity conditions given in (A.46) and (A.47).

By using the product rule we obtain that

$$\frac{d^2M}{dx^2}v = M\frac{d^2v}{dx^2} - \left(M\frac{dv}{dx}\right)' + \left(\frac{dM}{dx}v\right)' = M\frac{d^2v}{dx^2} - \left(M\frac{dv}{dx}\right)' + (Qv)'.$$

Assume first that a is the only point where we have concentrated forces and moments. By adding the two integrals

$$\int_{-\infty}^{a} \frac{d^2M}{dx^2}v\,dx = \int_{-\infty}^{a} M\frac{d^2v}{dx^2}\,dx - \left(\lim_{x\to a^-} M\right)\frac{dv}{dx}(a) + \left(\lim_{x\to a^-} Q\right)v(a),$$

and

$$\int_{a}^{\infty} \frac{d^2M}{dx^2}v\,dx = \int_{a}^{\infty} M\frac{d^2v}{dx^2}\,dx + \left(\lim_{x\to a^+} M\right)\frac{dv}{dx}(a) - \left(\lim_{x\to a^+} Q\right)v(a),$$

we obtain that

$$\int_R \frac{d^2M}{dx^2}v\,dx = \int_R M\frac{d^2v}{dx^2}dx + M_0\frac{dv}{dx}(a) + P_0v(a).$$

More generally we can consider several concentrated forces P_i and moments M_i at points a_i, for $i = 0, 1, ..., K$, (see Figure A.4), and obtain the following:

$$\int_R \frac{d^2M}{dx^2}v\,dx = \int_R M\frac{d^2v}{dx^2}dx + \sum_{i=0}^{K}\left(M_i\frac{dv}{dx}(a_i) + P_iv(a_i)\right).$$

$$\int_R EI\left(\frac{d^2y}{dx^2}\right)\frac{d^2v}{dx^2}dx = \int_R -\left(p(y)+q\right)v\,dx + \sum_{i=0}^{K}\left(M_i\frac{dv}{dx}(a_i) + P_iv(a_i)\right).$$

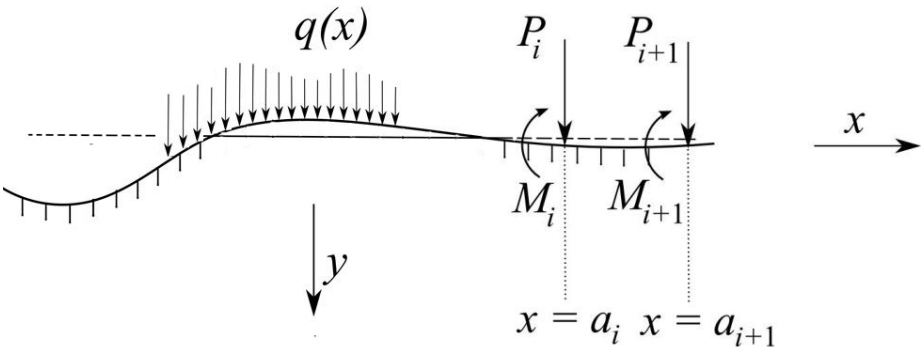

Figure A.4: The beam is subjected to some distributed force $q(x)$, together with concentrated forces P_i and moments M_i. The figure is borrowed from [5]

By (A.44) and (A.48) we then find that

$$\int_R EI\left(\frac{d^2y}{dx^2}\right)\frac{d^2v}{dx^2}dx + \int_R p(y)v\,dx = \int_R qv\,dx + \sum_{i=0}^{K}\left(M_i\frac{dv}{dx}(a_i) + P_iv(a_i)\right). \tag{A.49}$$

Let us consider the the usual Sobolev space $H^s(R)$ on the real line R with the following norm $\|\cdot\|$

$$\|u\|^2 = \int_R u^2dx + \sum_{i=1}^{s}\int_R\left|\frac{d^iu}{dx^i}\right|^2 dx.$$

According to a standard result (see e.g. the book [10, p. 56]) it holds that $H^s(R) = H_0^s(R)$ where

$$H_0^s(R) = \{u : \exists\{\varphi_j\} \subset \mathcal{D}(R) \text{ such that } \varphi_j \to u\}.$$

Above, $\mathcal{D}(R)$ denotes the space consisting of all smooth functions with compact support. If $q \in L^2(R)$ and $y \in H^2(R)$ the left side of (A.49) makes sense even for all $v \in H^2(R)$. Using the fact that every $v \in H^2(R)$ and its first order derivative is continuous [10, p. 62] we obtain that the right hand side also makes sense for all $v \in H^2(R)$.

If we also account for the weight (per unit length) of the beam w_0, the value of q must be replaced by $q + w_0$. For simplicity we assume that w_0 is constant. Letting u denote the function $u = y - y_0$, where y_0 is the (constant) deflection corresponding to the case when the beam is resting on the foundation under

the influence of its own weight only, i.e. $p(y_0) = w_0$,we obtain from (A.45) the equation

$$\frac{d^2}{dx^2}\left(EI\frac{d^2u}{dx^2}\right) = q - \rho'(u),$$

where

$$\rho'(u) = p(u + y_0) - p(y_0).$$

Note that according to (A.42), ρ' satisfies the following condition

$$C_1\left(r-s\right)^2 \leq \left(\rho'(r) - \rho'(s)\right)\left(r-s\right) \leq C_2\left(r-s\right)^2 \tag{A.50}$$

for all $r, s \in R$. Moreover the last inequality implies that

$$\left|\rho'(r) - \rho'(s)\right| \leq C_2\left|r-s\right| \tag{A.51}$$

It might feel natural to just let the weight w_0 be a part of the distributed load q, as we do for finitely long beams. However, for an infinitely long beam, w_0 is not a member of $L^2(R)$, and neither is the solution y. A slightly different weak formulation is therefore needed. Let Ω be a connected open set of R (not necessarily bounded).The problem is stated is as follows: Find $u \in H_0^2(\Omega)$ such that

$$\langle Au, v\rangle = L(v) \text{ for all } v \in H_0^2(\Omega), \tag{A.52}$$

where

$$\langle Au, v\rangle = \int_\Omega EI\left(\frac{d^2u}{dx^2}\right)\frac{d^2v}{dx^2}dx + \int_\Omega \rho'(u)v\,dx$$

and

$$L(v) = \int_\Omega qv\,dx + \sum_{i=0}^{K}\left(M_i\frac{dv}{dx}(a_i) + P_iv(a_i)\right)$$

In [5] the mentioned weight issue was not addressed. Thus we consider the modified formulation to be one of the major contributions of this paper since it improves the presentation without making it significantly more complicated. The right side, $L(v)$, defines a linear functional which turns out to be continuous on $H^2(\Omega)$. In order to see this we consider each term separately. The first term is continuous due to the Schwartz inequality:

$$\left|\int_\Omega qv\,dx\right| \leq \|q\|_2\,\|v\|_2 \leq \|q\|_2\,\|v\|\,, \tag{A.53}$$

where $\|\cdot\|_2$ denotes the $L^2(R)$-norm. For the other terms, we extend v to zero outside Ω and use that

$$v(a) = -\int_a^\infty (e^{a-x}v(x))'dx = \int_a^\infty (e^{a-x}v(x) - e^{a-x}v'(x))dx$$

and

$$v'(a) = -\int_a^\infty (e^{a-x}v'(x))'dx = \int_a^\infty (e^{a-x}v'(x) - e^{a-x}v''(x))dx.$$

Hence, by using Schwartz inequality, we obtain that

$$|v(a)| \leq c\,\|v\| \text{ and } |v'(a)| \leq c\,\|v\|\,,$$

where

$$c = \sqrt{\int_a^\infty e^{2(a-x)}dx}.$$

Thus, we obtain that $L(v)$ is a sum of finitely many continuous functionals on $H^2(\Omega)$ and is therefore continuous. Moreover, it is clear that A is continuous on $H^2(\Omega)$, i.e. there exists a constant $C > 0$ such that

$$|\langle Au_1 - Au_2, \varphi\rangle| \leq C\,\|\varphi\|\,\|u_1 - u_2\| \tag{A.54}$$

for all $u_1, u_2, \varphi \in H^2(\Omega)$. Indeed,

$$|\langle Au_1 - Au_2, \varphi\rangle| \leq \int_\Omega \left| EI\left(\frac{d^2\,(u_1 - u_2)}{dx^2}\right)\frac{d^2\varphi}{dx^2}\right| dx + \int_\Omega |(\rho(u_1) - \rho(u_2))\,\varphi|\;dx.$$

Hence, using the Schwartz inequality, (A.51), and the fact that the L^2-norm of a function (and its second derivatives) is less than the H^2-norm, we obtain that

$$|\langle Au_1 - Au_2, \varphi\rangle| \leq (EI + C_2)\,\|\varphi\|\,\|u_1 - u_2\|\,,$$

all u and v in $H^2(R)$, i.e. A is continuous. If we use the following stronger condition on the monotonicity of p (compared with that given in (A.42))

$$C_1\,(r-s)^2 \leq (p(r) - p(s))\,(r-s)\,,$$

i.e.

$$C_1\,(r-s)^2 \leq (\rho'(r) - \rho'(s))\,(r-s)\,, \tag{A.55}$$

then the operator A becomes strongly monotone. To see this, let k_0 be a positive constant less than EI and C_1. Then by (A.55) we obtain that

$$\langle Au_1 - Au_2, u_1 - u_2\rangle \geq EI\left\|(u_1 - u_2)''\right\|_2^2 + C_1\,\|u_1 - u_2\|_2^2 \geq \tag{A.56}$$

$$k_0\left(\left\|(u_1 - u_2)''\right\|_2^2 + \|(u_1 - u_2)\|_2^2\right) \geq \frac{k_0}{\sqrt{2}}\,\|u_1 - u_2\|^2\,,$$

where the last inequality is due to Proposition A.4.2. Thus, A is strongly monotone. We note that continuity (of A) implies hemicontinuity and the strong monotonicity implies strict monotonicity and coercivity. The existence of a solution of (A.52) then follows by Theorem A.2.1. The uniqueness follows by the strict monotonicity of A.

Let us turn back to the weaker case when

$$H\left(r+y_0\right)H\left(s+y_0\right)C_1\left(r-s\right)^2 \leq \left(\rho'(r)-\rho'(s)\right)\left(r-s\right).$$

In this case the term $C_1\left\|u_1-u_2\right\|_2^2$ in (A.56) may vanish. However, if Ω is bounded, then the operator A still becomes strongly monotone. In order to prove this, let $\Omega_k = [-k,k]$, where k is a positive integer. By Friedrichs inequality we have that

$$\|v\|_2 \leq (2k)^2 \left\|v''\right\|_2$$

and

$$\|v'\|_2 \leq 2k \left\|v''\right\|_2,$$

for any $v \in H_0^2(\Omega_k)$, which implies that

$$\left\|v''\right\|_2^2 \leq \|v\|^2 \leq C\left(\left\|v''\right\|_2^2\right),$$

for some positive constant C_N (e.g. $C_k = 3\left(2k\right)^4$). This proves that $\left\|(\cdot)''\right\|_2$ is an equivalent norm on $H_0^2(\Omega)$. Hence, we obtain the strong monotonicity of the operator A from a weaker statement (compared with that given in (A.56)),

$$\langle Au_1 - Au_2, u_1-u_2\rangle \geq EI\left\|(u_1-u_2)''\right\|_2^2.$$

Acknowledgements. I thank professor Dag Lukkassen for several things related to this paper. In particular, the presentation of the mathematical aspects of linear elasticity presented here is strongly motivated by the insight of Dag, who has shared his deep knowledge on this issue through many years, partly by some unpublished manuscripts which has been a great motivation for the current presentation. Moreover, the proof of Theorem A.4.1 is strongly motivated by discussions with Dag, who shared his thoughts on the basic idea behind the proof.

References

[1] ASCE-AREA Special Committee on Stresses in Railroad Track. *Bulletin of the AREA, First Progress Report Vol 19,1918, Second Progress Report Vol 21, 1920.* Tech. rep.

[2] Browder, F. E. "Nonlinear elliptic boundary value problems". *Bull. Amer. Math. Soc.* vol. 69 (1963), pp. 862–874.

[3] Browder, F. E. "Variational boundary value problems for quasi-linear elliptic equations I-III". *Proc. Nat. Acad. Sci.U.S.A.* vol. 50 (1963), pp. 31–37, 592–598, 794–798.

[4] Lu, S. "Real-time vertical track deflection measurement system". *ETD collection for University of Nebraska - Lincoln. Paper AAI3331436* (Jan. 2008).

[5] Lukkassen, D. and Meidell, A. “Beams on nonlinear elastic foundation”. In: *AIP Conference Proceedings 1637*. Vol. 656. 2014.

[6] Minty, G. J. “On a "monotonicity" method for the solution of nonlinear equations in Banach spaces”. *Proc. Nat. Acad. Sci. U.S.A.* vol. 50 (1963), pp. 1038–1041.

[7] Sadeghi, J. and Barati, P. “Evaluation of conventional methods in Analysis and Design of Railway Track System”. *Int. J. Civ. Eng.* vol. 8, no. 1 (2010), pp. 44–56.

[8] Showalter, R. E. *Monotone operators in Banach space and nonlinear partial differential equations*. Vol. 49. Providence, USA: American Mathematical Society, 1997.

[9] Zarembski, A. and Choros, J. “On the measurement and calculation of vertical track modulus”. In: *Proceedings American Railway Engineering Association*. Vol. 81. 1980, pp. 156–173.

[10] Ziemer, W. P. “Weakly Differentiable Functions”. Berlin: Springer, 1989. Chap. Sobolev Spaces and Functions of Bounded Variation.

Authors' addresses

A. Seger UiT, Lodve Langesgate, N-8505 Narvik, Norway and Sintef Narvik, Rombaksveien 47, N-8517 Narvik, Norway

Paper B

A simplified three-dimensional method for stability assessment of buttress dams

Andreas Seger, Eduardo Bretas

Submitted for publication.

B

A simplified three-dimensional method for stability assessment of buttress dams

Andreas Seger[1,2] and Eduardo Bretas[2]
[1]UiT, Lodve Langesgate, N-8505 Narvik, Norway
[2]Sintef Narvik, Rombaksveien 47, N-8517 Narvik, Norway

Abstract

The aim of this paper is to present the development of a new method to evaluate the sliding stability of flat slab buttress dams. The possibility of utilizing safety capacity in neighbouring pillars within a section to show that the entire section has adequate capacity against sliding in the dam-foundation interface is explored. Within the field of dam-engineering the assessment of the safety of dams is govern by national guidelines and there is little room for new computation methods. In the case of buttress dams, the current practice is to evaluate each pillar individually. A section of a flat-slab buttress dam with three different cases of inclination in the pillar-foundation interfaces is considered. A comparison of how the safety factor of the whole section is affected if it is supported by pillars with both satisfactory and unsatisfactory safety margins. The section was modelled with shell elements using a finite element software where the geometry is based on a typical flat slab buttress dam, Mohr-Coulomb contact model was used in the dam-foundation interfaces. The combined safety factor for all three pillars was computed from the results obtained from the analysis. The results show that for a section with one pillar with the safety factor of 1.1 and two pillars with 1.4. The combined safety factor for the whole section is 1.4, which is requirement in Norway. This shows that by considering the whole section an adequate safe factor can be achieved by and thereby reduce the need for rehabilitation of the unsatisfactory pillar.

Keywords: dam; stability; FEM; flat slab dam

1 Introduction

Norway has the largest installed hydropower capacity in Europe, hydropower accounts for 95 % of its total power production [1]. The country has many steep mountains and high rainfall, so its topography and climate are very well suited for hydroelectric generation. There is currently ca. 4000 registered dams in Norway of which 336 are buttress dams [2]. A buttress dam consists of a sloping upstream deck that restricts the flow of water and vertical walls (buttresses or pillars) that transfer loads from the deck to the foundation. The benefit of a sloping deck is that the weight of the water contributes to the dam's stability. Flat slab dams are common in Norway. The reason is the low volume of concrete needed to build such dams when compared to that required for comparable gravity dams. Mainly because this helps alleviate the logistical problems caused by the remoteness of such dam sites [3]. Buttress dams are best suited for use where the dam site's topography is characterized by a wide valley with limited variation in the height of the foundation. Due to the high stresses under the buttresses, these dams require strong foundations [4]. In Norway, there are many dams that incorporate buttress dam sections, typically combined with gravity dam sections close to the abutments or arch dams if there are large grooves in the foundation.

The International Commission on Large Dams (ICOLD) defines three types of buttress dam: flat slab dams, multiple arch dams, and massive head dams. This paper focuses solely on flat slab buttress dams; for information about the other types, the reader is referred to earlier publications [5], [6] and the references therein. The goal of this paper is present a simplified method for safety analysis of flat slab dams. The method is based on the gravity method which is assumed as a conservative approach. In this work the scenario of the dam sliding over the foundation plane is considered. In a general case, others sliding planes should be investigated trough out the foundation mass.

2 Flat slab dams in Norway

As mentioned above, flat slab dams consist of a relatively thin reinforced concrete slab supported by buttresses on the downstream side. The slab may be continuous in the cross-valley direction or divided into sections with a vertical joint between adjacent sections. An individual slab section may be supported by multiple buttresses or may just span the space between two adjacent buttresses. The buttress spacing depends on the slab's thickness: thin slabs require closer spacing. The slab and buttresses may be integrated or independent, depending on how they were joined during construction. The oldest registered flat slab dam in Norway is at Møsvatn in the Telemark region. It was built in 1908 and partly decommissioned in 2004 [7]. Many other flat slab dams built between 1950 and 1970 are now being reassessed based on modern regulations.

While this design is necessarily adapted on a case-by-case basis to account for the conditions at the site where the dam is to be located, all dams based on this design have some common structural principles. Notably, the vertical joints in the slab are placed at positions of zero moment, reducing the need for joint reinforcement. The slab thickness increases linearly with the depth, from about 30 cm at the crest and 3 cm/m vertically. Slabs span two or three pillars with a vertical joint between them, often strengthened where they connect to a pillar [3]. The distance between the vertical center lines of adjacent pillars is usually 5 m. The upstream slab has an inclination of 5:4, and an insulation wall is installed on the downstream side to reduce stresses induced by temperature changes. Figure 1 shows how the plates are connected, one resting on the other, and Figure 2 depicts a typical buttress profile.

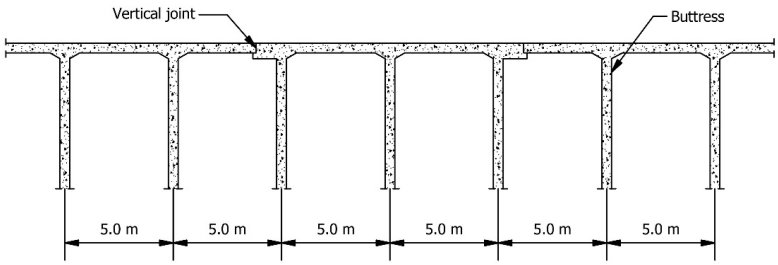

Figure 1: Plates of a typical Norwegian buttress dam.

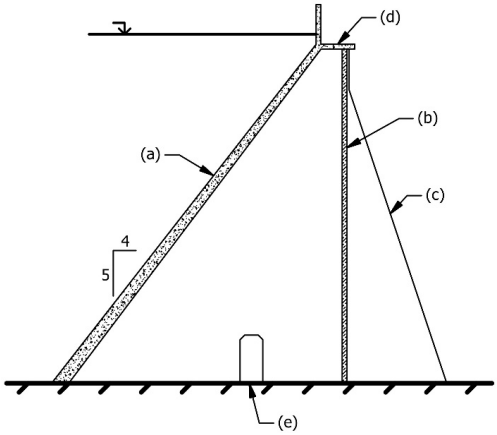

Figure 2: Profile of a typical Norwegian flat slab dam. (a) Slab with variable thickness. (b) Insulating wall. (c) Buttress/pillar. (d) Footway. (e) Foundation.

3 Stability analysis of buttress dams

All registered dams in Norway have been classified based on the severity of the damage expected in the event of their failure, from class 0 to class 4 [8] Dams in consequence class 4 would cause severe damage upon failure, while a failure of dam in consequence class 0 would have minor consequences. There are 17 dams in consequence class 4, 43 in class 3, 66 in class 2, 90 in class 1, and 96 flat slab dams in consequence class 0. Norwegian dams in consequence classes 2 to 4 are reassessed every 15 years. For class 1 dams, assessments are performed every 20 years. Each assessment includes an evaluation of the dam's stability based on the current regulations.

Most Norwegian flat slab dams are less than 15 m tall. Such dams are normally found to be stable towards overturning but unstable towards sliding when evaluated according to Norwegian regulations [9]. The load case corresponding to the normal design reservoir elevation and ice load very often becomes the design load case. According to the Norwegian regulation, a flat slab buttress dam is required to achieve a sliding and overturning safety factors of at least 1.4 if cohesion is neglected in the calculation. If cohesion is assumed in the dam-foundation interface, the required safety factors are 3 for serviceability and ultimate limit states, and 2 for accidental limit state, as in case of extreme flooding. If the cohesion at the interface has been assessed and proven to be adequate using reliable tests, these required safety factors are reduced to 2.5 and 1.5, respectively. In addition, the dam should be design according to the current national building standards [9].

3.1 Historical review of methods of dam sliding analysis

Briefly reviewing current and historical methods for estimating the sliding stability of dams, the "sliding resistance method" was used from around 1900 and during 30 years to evaluate the sliding stability of gravity dams [10] This method is based on the experiences of early dam engineers, who found that the shear resistance of very sound foundation material did not need to be further investigated if the ratio of horizontal to

vertical forces acting on the dam was below 0.65 for static loading (and 0.85 for seismic loading). The "shear-friction method" was introduced by Henny in 1934 [11]. The original method only considered a single horizontal failure plane, but it was later extended to include inclined failure planes. The original method defined the safety factor as the ratio of the total resisting shear force acting along a horizontal failure plane to the maximum horizontal driving force. The assumptions made in the method's development were:

- The sliding of the dam is a two-dimensional problem.
- Failure along the assumed failure plane is kinematically possible.
- The Mohr-Coulomb failure criteria can be used to describe failure between the interfaces in the assumed failure plane.

The safety factor for the shear-friction method is

$$S_{SFM} = \frac{F}{\sum H} \tag{1}$$

where $\sum H$ is the sum of the horizontal forces acting on the dam and the resisting shear force acting along the horizontal plane, and F is given by the expression

$$F = \frac{cA}{\cos\alpha(1-\tan\varphi\tan\alpha)} + \sum V\tan(\varphi+\alpha) \tag{2}$$

where c is the cohesion, α is the inclination angle of the assumed failure plane, φ is the friction angle, A is the area of the failure plane and $\sum V$ is the sum of the vertical forces acting on the failure plane.

The "limit equilibrium method" was presented in 1981 by the U.S. Corps of Engineers [10] is a way to compute sliding safety factors. The method has its origin in soil engineering and is now commonly used in dam engineering. The sliding safety factor is defined as the ratio between the shearing strength and the applied shear stress. The method's development was partly motivated by the need to include multiple sliding planes and to represent the effects of wedges (asperities) better than is done by the shear-friction method. The assumptions and simplifications of the limit equilibrium method are:

- As the method's name suggests, it is based on limit equilibrium, i.e. it assumes sliding will occur in the assumed failure plane if the applied shear is greater than the resting shear.
- It is assumed plane surfaces of failure.
- Sliding must be kinematically possible in the assumed failure planes.
- It assumed that the sliding of the dam is a two-dimensional problem.
- Force equilibrium is satisfied, moment equilibrium is not used.
- The method neglects displacements, so differences in rigidity between materials are not accounted for.
- The relationship between the resisting shear stress and normal stress acting on the failure plane is assumed to be linear and described by the Mohr-Coulomb failure criterion.

Because of the last assumption, the shear strength is $\tau_a = c + \sigma_n \tan\varphi$. This gives the safety factor for the limit equilibrium method as,

$$S_{LEM} = \frac{\tau_a}{\tau} = \frac{c+\sigma_n \tan\varphi}{\tau}, \quad (3)$$

where τ_a is the shear strength of the plane, τ is the shear stress, c is the cohesion, σ_n is the normal stress acting on the plane and φ is the friction angle.

Nicholson showed in [12] that for a given c and φ and an inclined failure plane (i.e. one for which $\alpha > 0$), two cases are possible, as shown below:

$$\text{if } \tan\varphi < \frac{\sum V}{\sum H} \text{ then } S_{LEM} > S_{SFM}, \text{ otherwise } S_{LEM} < S_{SFM} \quad (4)$$

Hence if the failure plane is inclined and the friction coefficient ($\tan\varphi$) is less than $\sum V / \sum H$, the shear-friction method will give a more conservative safety factor. If the friction coefficient is greater than $\sum V / \sum H$, the limit equlibrim method gives a more conservative safety factor. Similarly, two cases exist for a downward-sloping failure plane ($\alpha < 0$):

$$\text{if } \tan\varphi < \frac{\sum V}{\sum H} \text{ then } S_{LEM} < S_{SFM}, \text{ otherwise } S_{LEM} > S_{SFM} \quad (5)$$

Thus, when the failure plane is downward sloping and the friction coefficient is less than $\sum V / \sum H$, the limit equilibrium method will give the more conservative safety factor. If the friction coefficient is greater than $\sum V / \sum H$, the shear friction method will give a more conservative safety factor.

When numerical models are employed, the methodology of reducing the friction angle until failure [13] is a valid strategy. The main objective is to evaluate safety with respect to sliding in the dam-foundation interface or other known failure planes. The downside of this method is that it requires many runs of the analysis, one for each tested friction angle. This is an iterative method whereby the friction angle is reduced until the dam starts sliding. The safety factor is defined as the ratio between the lowest friction angle that do not cause sliding and the actual friction angle. This method can be used in numerical analyses (such as FEM or DEM analyses).

Malm presented in [14] a “push-over method” to obtain the global failure modes of the dam, i.e. overturning and sliding. The driving loads acting on the dam are increased until failure, loads that act in a stabilising manner are kept constant. The safety factor is then defined as the ratio between the load that causes failure and the actual load case scenario under consideration. A drawback of this method is that is difficult to predict how changes in load will affect the results, since the stabilising loads are kept constant but the loads that are pushing the dam downstream is increased.

3.2 The proposed method for sliding assessment of flat slab dams

The current practice for checking the stability of flat slab dams is similar to that used for gravity dams, i.e. the stability of each pillar is evaluated separately with respect to

overturning and sliding. The pillar is assumed to be a rigid body, and the potential for overturning about the toe (and any other point about which the body can rotate) is checked. Sliding stability should be checked along all potential failure planes. The NVE stipulates that at least the dam-foundation interface should be checked for sliding [9]. For flat slab dams, the loads applied to a pillar are the loads acting on the dam plate that can be assumed to act on the pillar in question around its influence area, as showed in Figure 3a. The alternative approach proposed in this paper is illustrated in Figure 3b.

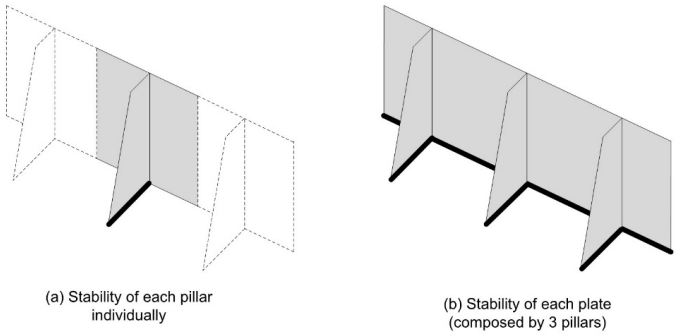

Figure 3: Dam sections considered in (a) two- and (b) three-dimensional analyses of flat slab buttress dams.

Basically the idea is to do the assessment of the entire plate composed by 3 pillars. The following steps should be implemented to apply successfully this method, considering a plate that comprises three pillars:

- The 3 pillars are assessed independently as is done in the traditional practice;
- If the 3 pillars are safe, the plate is assumed as safe, or if the 3 pillars are unsafe the plate is assumed as unstable;
- If one or two of the pillars are not safe, the unbalance loads are transferred to the neighbour pillars belong to the same plate, and the pillars are reassessed;
- If the new analysis gives a stable scenario the plate, as a set of pillars, a safe structure otherwise is considered unstable.

The next section presents rigid body analyses (also known as gravity method analyses) for pillars in which the slope angle at the dam-foundation interface (α) is $\alpha = 0°$ and $\alpha = 10°$. In addition, finite element analyses are presented for three multi-pillar sections with different inclinations at the dam-foundation interface. The goal of these 3D finite element models is verify the level of stress in the plate, check if it is able to transfer the loads between the pillars, and then certify this simplify method as it was proposed.

The results of these analyses are used to derive combined sliding safety factors for multi-pillar sections of a flat slab buttress dam. The stability of every pillar supporting one plate segment is evaluated by performing finite element calculations to determine the load distribution between the pillars and then computing combined sliding safety factors for all three pillars in a way that accounts for potential load transfer between

pillars. The approach was tested by simulating the behaviour of a dam segment with three pillars under three different conditions, each involving different combinations of slope angles in the dam-foundation interface.

4 Case study: Two-dimensional analysis of flat-slab buttress dams

This section applies the current method for evaluating the stability of a section of a flat slab dam for cases in which $\alpha = 0°$ and $\alpha = 10°$ [6]. The pillar geometry considered in these studies is shown in Figure 4.

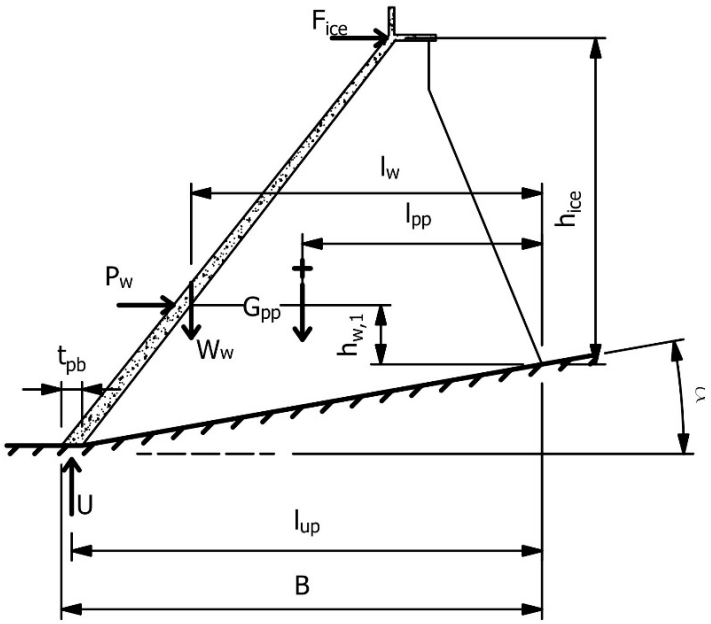

Figure 4: The dimensions and loads acting on a pillar.

4.1 Loads acting on the dam

The hydrostatic pressure is the pressure exerted by the water on the dam in the direction normal to the dam's surface. In this case, the headwater level was set to $\mathrm{h_w} = 15\ \mathrm{m}$. The density of water is $\rho_w = 1000\ \mathrm{kg/m^3}$. The hydrostatic pressure varies linearly from zero at the headwater level to $\mathrm{p_{w,15}} = \mathrm{h_w}\rho_w$ at the heel of the dam. In Norway, the ice load is specified as 100 kN/m acting 0.25 m below the head water level, or the pressure acting in the topmost 0.5 m ($\mathrm{t_{ice}}$) of the headwater, according to the NVE [15] In both cases, it is assumed that the ice acts in the horizontal direction. The ice pressure is $\mathrm{p_{ice}} = 200\ \mathrm{kPa}$. For flat slab dams, it is normally assumed that the uplift pressure acts only on the slab and not the pillars. This assumption is only valid if there is good drainage around the pillar and there is no accumulation of water around the pillar. In this paper, full uplift under the plate is assumed; the uplift pressure is set to $\mathrm{p_{up}} = 147.15\ \mathrm{kPa}$. This is a conservative assumption because it is often assumed that the uplift declines linearly from the headwater pressure on the upstream side to the tail water pressure on the downstream side [16]. In addition, gravity acts on the dam; the acceleration due to gravity is $\mathrm{g} = 9.81\ \mathrm{m/s^2}$. The dam-foundation interface is modelled

using the Mohr-Column failure criteria. This contact model is currently used in both the shear friction and limit equilibrium methods to calculate sliding safety factors in dam engineering. The friction angle was set to $\varphi = 45^{\circ}$, giving a friction coefficient of $\mu = 1$. Finally, it was assumed that there was no cohesion between the dam and the foundation, i.e. $c = 0$.

4.2 Sliding stability

The safety against sliding (i.e. the sliding safety factor) was computed as

$$S_{\text{sliding}} = \frac{\sum V}{\sum H}\tan(\theta + \alpha) \tag{6}$$

where $\sum V$ and $\sum H$ are the sums of the vertical and horizontal forces. The vertical forces are

$$\sum V = G_{pp} + W_w - U_r \tag{7}$$

where G_{pp} is the combined weight of the pillar and the sections of the plate and crest that are assumed to influence the pillar. According to current practice, the plate and crest sections affecting a single pillar are sections of width equal to the distance between the centers of adjacent pillars. W_w is the weight of the water contained by a plate section, and U is the uplift force acting on a plate section. The weight of the pillar is

$$G_{pp} = V_{pp} \cdot \rho_c \cdot g, \tag{8}$$

where V_{pp} is the volume of the pillar and the plate and crest sections. The weight of the water is

$$W_w = V_w \cdot \rho_w \cdot g, \tag{9}$$

where V_w is the volume of water contained by a plate section and a crest section. The uplift force is:

$$U = c_c \cdot t_{pb} \cdot h_w \cdot \rho_w \cdot g, \tag{10}$$

Because the uplift force acts in the upward direction, it has a negative sign. c_c is the distance between the centers of adjacent pillars, and t_{pb} is the plate's thickness at the heel of the pillar. The sum of the horizontal forces is

$$\sum H = P_w + F_{ice}, \tag{11}$$

where P_w is the resultant force of the horizontal water pressure and F_{ice} is the ice force. The resultant force of the horizontal water pressure is

$$P_w = c_c \cdot \rho_w \cdot g \int_0^{h_w} (h_w - y)\, dy = \frac{c_c \cdot \rho_w \cdot g \cdot h_w^2}{2} \tag{12}$$

The ice force is

$$F_{ice} = c_c \cdot t_{ice} \cdot p_{ice}. \tag{13}$$

4.3 Overturning

A dam is considered safe against overturning if the position of the resultant force, x_R, is in the middle third of the dam's width, B. The dam is thus safe if

$$\frac{B}{3} < x_R < \frac{2B}{3}. \tag{14}$$

Where the position of the resultant force is

$$x_R = \frac{\sum M}{\sum V}. \tag{15}$$

The moment, $\sum M$, is calculated about the toe of the pillar, with the positive direction being anti-clockwise. This results in the following expression:

$$\sum M = G_{pp} \cdot l_{pp} + W_w \cdot l_w - P_w \cdot h_{w,1} - F_{ice} \cdot h_{ice} - U \cdot l_{up}, \tag{16}$$

where l_{pp}, l_w, $h_{w,1}$, h_{ice} and l_{up} are the moment arms for the forces indicated by the subscripts (see Figure 4). The geometric properties used in these calculations are listed in Table 1, and the material properties are listed in Table 2.

Table 1: Geometric properties used in the calculations.

	$\alpha = 0^\circ$	$\alpha = 10^\circ$
V_{pp}	109.61 m^3	95.68 m^3
V_w	450 m^3	
c_c	5 m	
t_{pb}	0.75 m	
l_{pp}	9.25 m	8.77 m
l_w	13.78 m	12.84 m
$h_{w,1}$	5 m	2.16 m
h_{ice}	14.75 m	11.91 m
l_{up}	17.41 m	16.46 m
B	17.78 m	16.84 m

Table 2: Material properties of linear elastic concrete.

Young's modules, E_c,	35 GPa
Density, ρ_c,	2300 kg/m^3
Poisson's ratio	0.2

The typical crushing strength of concrete in dams is 20-30 MPa, but may be higher in some cases as demonstrated by recent tests on the Kalhovd dam in Norway, whose concrete exhibited a compressive strength of 41.2 MPa [17]. The sliding safety factor (6) for a pillar with an inclination of $\alpha = 0^\circ$ is thus

$$S_{sliding} = 1.1. \tag{17}$$

The position of the resultant force (14) is

$$x_R = 11.59 \text{ m}, \quad (18)$$

which is within the middle third of the base. For a pillar with an inclination of $\alpha = 10^\circ$ the sliding safety factor (6) becomes

$$S_{\text{sliding}} = 1.4. \quad (19)$$

The poison of the resultant force (14) is

$$x_R = 8.759 \text{ m} \quad (20)$$

Which also is within the middle third of the base. The pillar with an inclination of $\alpha = 10^\circ$ is thus safe with respect to both sliding and overturning. Conversely, the pillar with an inclination of $\alpha = 0^\circ$ is safe with respect to overturning but does not achieve the required sliding safety factor of 1.4. The inadequate sliding stability of the pillar when $\alpha = 0^\circ$ suggested that it would be interesting to determine how sliding stability is affected when an otherwise unstable pillar is connected to a stable pillar by a concrete slab. The following section presents finite element analysis calculations conducted to evaluate sliding stability in three cases featuring different combinations of pillar inclination where the pillars are connected via a concrete slab.

5 Case study: Three-dimensional finite element analysis model

This section describes the model used in the three-dimensional analysis and the loads acting on the studied dam sections. Three cases are considered:

- Case 1: All three pillars have zero inclination.
- Case 2: One side pillar has an inclination $\alpha = 10^o$, the other two have zero inclination.
- Case 3: The center pillar has zero inclination and both side pillars have inclinations of $\alpha = 10^o$.

The details of the geometry in each case are shown in Figure 1 and Figure 4. The geometric properties and material properties used in the calculations are presented in Table 1and Table 2, respectively.

To reduce the number of parameters affecting the sliding stability, the foundation is assumed to be rigid. For dams lower than 15 m, the foundation's stiffness will not affect the stress distribution in the dam. Therefore, the foundation's stiffness has a negligible effect on the normal stress distribution under the pillars.

The finite element analysis was performed using ANSYS Mechanical APDL Release 17.2 [18].

5.1 Loading and boundary conditions

In addition to the hydrostatic pressure, gravity, ice pressure, and uplift, dam sections are subject to loads from neighbouring sections. As shown in Figure 1 the sections alternate in terms of how they rest upon one-another, and every other three-pillar

section supports two neighbouring sections. The transmitted load from a neighbouring section is approximated by considering a strip of the plate and assuming that the displacement is zero at the edge of the section. It is also assumed that there is no moment in the vertical joint. Finally, it is assumed that plate strip is fixed at the pillar in the neighbouring section. Therefore, the plate strip can be treated as a propped cantilever beam, and the transferred load can be determined by calculating the reaction force, R_T, at the vertical joint, which is

$$R_T = \frac{3}{8} \ (3.9 \cdot \rho_w \cdot g \cdot y) \tag{21}$$

This force acts normal to the plate where $0 \leq y \leq (h_w - 0.5\ m)$. The part on which ice pressure acts is also subject to an additional transmitted load acting in the horizontal direction:

$$R_{T,ice} = \frac{3}{8} \ (3.9 \cdot p_{ice}) \tag{22}$$

for $h_w - t_{ice} \leq y \leq h_w$.

5.2 Elements used in the analysis

Information about element types was obtained from an earlier publication [19]. The dam body was modelled using a shell element called SHELL181. This is a 4-node structural shell element based on the Mindlin-Reissner shell theory. The quadratic form of the element was used, and nodes were placed in each corner, with an additional node in the middle of each of the element's sides. Each node has six degrees of freedom corresponding to translation in the x, y and z directions, and rotation about the x, y and z-axes. The contact between the dam and rigid foundation was modelled using the contact element CONTA175 and the target element TARGE170. The CONTA175 element was placed at the bottom of the pillars and the plate to model Mohr-Coulomb contact, using the material properties defined for the underlying element to determine the contact stiffness. The rigid foundation was modelled using the quadratic form of TARGE170 with 4 nodes, one in each corner. The calculations were performed with a uniform mesh, using the numbers of elements and nodes listed in Table 3.

Table 3: Number of elements and nodes used in the FE-analysis for the different cases.

	SHELL181	**CONTA175**	**TARGE170**	**Total no. nodes**
Case 1	108255	805	15	108933
Case 2	44812	526	127	45392
Case 3	43452	521	240	44152

5.3 Finite element analysis results

Figure 5 shows the total deformation for all three cases. The maximum deformation in case 1 was 1.69 mm and occurred in the top of the section. In case 2, the maximum of 2.13 mm occurred above pillar 1. In case 3, the maximum deformation was 1.5 mm and occurred above pillar 2.

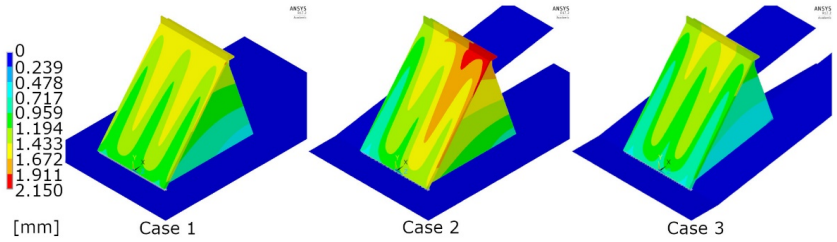

Figure 5: The total deformation in cases 1, 2, and 3 [mm].

The first principal stresses are shown in Figure 6. The highest tension stress in case 1 was 6.64 MPa and occurred in the plate perpendicular to the pillars. In case 2, the maximum tension stress was 6.37 MPa. In case 3, the highest tension stress occurred over pillars 1 and 3, and was 6.40 MPa.

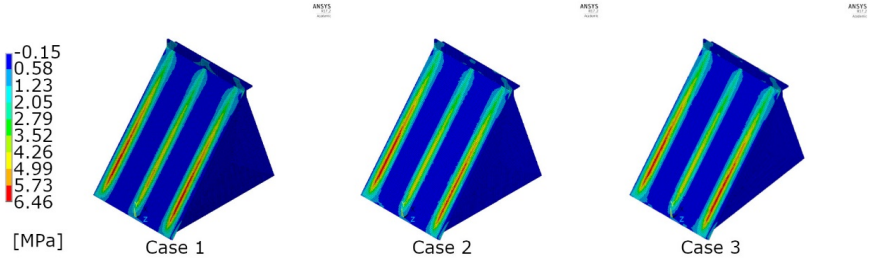

Figure 6: The principal tension stresses in cases 1, 2, and 3 [MPa].

Figure 7 shows the principal compression stresses in cases 1, 2 and 3. In case 1, the highest compression stress was -7.04 MPa and occurred in the toe of the pillars. In case 2, the highest compression stress was -6.36 MPa, and occurred in the toe of pillar 1. In case 3, the highest compression stress was -6.39 MPa and occurred in the toe of pillars 1 and 3.

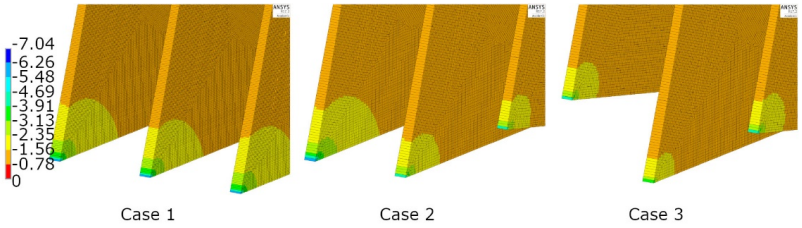

Figure 7: The principal compression stresses in cases 1, 2 and 3 [MPa].

Figure 8 shows the normal stress distributions under the pillars for cases 1, 2 and 3. In case 1, the maximum normal stresses in pillars 1, 2, and 3 were 1.32 MPa, 1.29 MPa, and 1.32 MPa, respectively. The corresponding values for case 2 were 2.1 MPa, 1.63 MPa, and 1.82 MPa, respectively. In case 3, the maximum normal stresses in pillars 1 and 3 were 1.87 MPa, while that in pillar 2 was somewhat lower (1.34 MPa). For all three cases, the maximum normal stress occurred in the toe of the pillars.

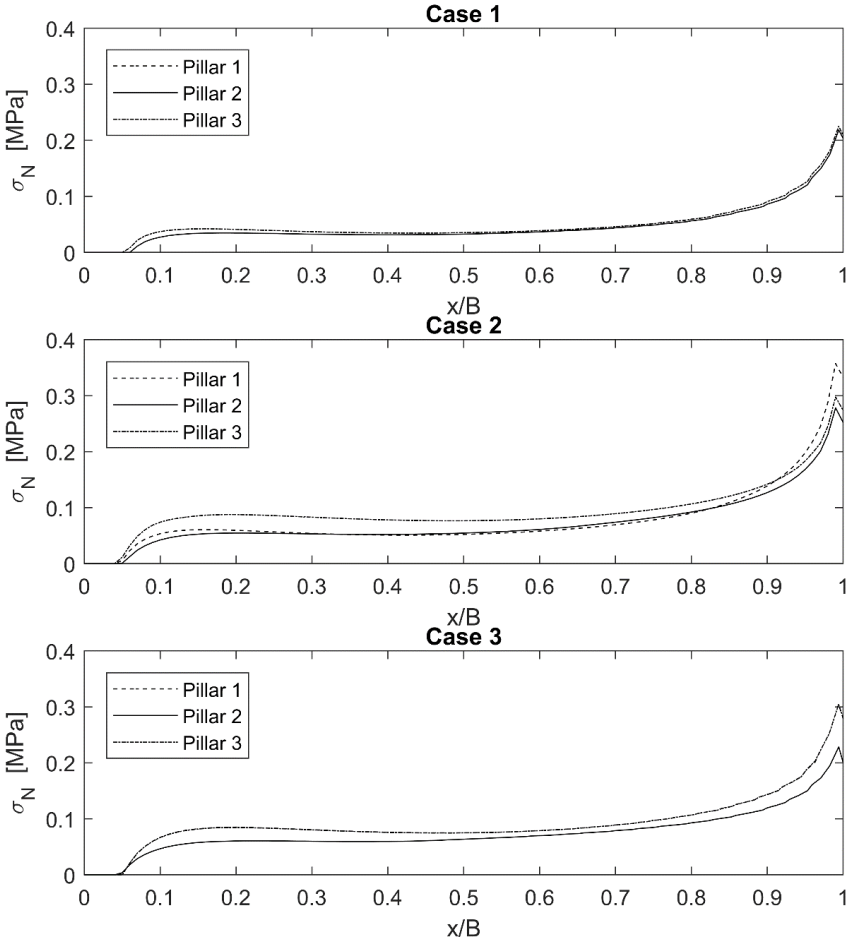

Figure 8: Normal stress distributions under pillar 1 (dashed lines), pillar 2 (solid lines) and pillar 3 (dash-dotted lines) in cases 1-3.

The sliding safety factors for each pillar are shown in Table 4, Table 5 and Table 6, for cases 1, 2, and 3, respectively. The safety factors were calculated using the Shear Friction Method (SFM) and Limit Equilibrium Method (LEM) based on the stress distributions obtained from the FEA.

Table 4: Safety factors for case 1.

	Pillar 1: $\alpha = 0^{\circ}$	**Pillar 2: $\alpha = 0^{\circ}$**	**Pillar 3: $\alpha = 0^{\circ}$**
H_i	5970 kN	5490 kN	5970 kN
V_i	6620 kN	6090 kN	6620 kN
N_i	6612 kN	6083 kN	6612 kN
T_i	5967 kN	5488 kN	5967 kN
S_{SFM}	**1.1**	**1.1**	**1.1**
S_{LEM}	**1.1**	**1.1**	**1.1**

Table 5: Safety factors for case 2.

	Pillar 1: $\alpha = 0^{\circ}$	**Pillar 2: $\alpha = 0^{\circ}$**	**Pillar 3: $\alpha = 10^{\circ}$**
H_i	6014 kN	5306 kN	6086 kN
V_i	6576 kN	6176 kN	6271 kN
N_i	6563 kN	6163 kN	7236 kN
T_i	6017 kN	5305 kN	4907 kN
S_{SFM}	**1.1**	**1.2**	**1.4**
S_{LEM}	**1.1**	**1.2**	**1.5**

Table 6: Safety factors for case 3.

	Pillar 1: $\alpha = 10^{\circ}$	**Pillar 2: $\alpha = 0^{\circ}$**	**Pillar 3: $\alpha = 10^{\circ}$**
H_i	6170 kN	5060 kN	6160 kN
V_i	6180 kN	6350 kN	6190 kN
N_i	7142 kN	6337 kN	7148 kN
T_i	5008 kN	5056 kN	4997 kN
S_{SFM}	**1.4**	**1.3**	**1.4**
S_{LEM}	**1.4**	**1.3**	**1.4**

Table 4, Table 5 and Table 6 show that there was limited variation in the vertical and horizontal forces acting on the dam-foundation interface. In case 1, this variation was probably due to the transfer of applied loads from neighbouring plate sections, which would increase the load carried by the side pillars. In cases 2 and 3, this variation would be augmented by variation in the slope angle between the pillars. Furthermore, in cases 2 and 3, it is clear that the safety factors obtained by considering complete sections differ from those obtained by considering individual pillars in isolation, as is done in rigid body analysis.

In all cases, the compression stress in the pillars was less than the normal compressive strength of concrete. The highest compression stress (6.4 MPa) was observed in case 3. The tension stresses in the plate where it is in contact with the pillars are assumed to be taken up in the reinforcement (not included in the analysis). In addition, the capital in the plate-pillar joint is not included, so the peak stresses predicted in these analyses are higher than they would have been if the capital were included. It is therefore assumed that the risk of cracking in the slab is minimal.

The normal stress distributions shown in Figure 8 deviate from the normal load distribution assumed in a rigid body analysis, where the normal stress increases linearly from the heel of the dam (or the end of the crack if there is cracking in the dam-foundation interface). Consequently, a greater proportion of the sliding resistance is activated in the toe area when using a numerical method to compute the normal stress in the dam-foundation interface. These results indicate that if an asperity in the dam-foundation interface is located near the toe of the pillar, it could significantly affect the pillar's sliding stability because more of the normal pressure would act directly on the asperity.

Overall, the FE analysis shows that the studied section is structurally sound with respect to stresses under the given assumptions, loadings, and boundary conditions.

6 The combined safety factor for all pillars in a section

As demonstrated by the FEA results, there were some differences between the safety factors for individual pillars, making it unclear which safety factor should be used. This section therefore presents a method for computing safety factors for multi-pillar dam sections.

Using the shear friction method, the safety factor for all three pillars can be calculated as

$$S_{SFM,tot} = \frac{\sum_{i=1}^{3} V_i \cdot \tan(\varphi_i + \alpha_i)}{\sum_{i=1}^{3} H_i}, \quad (25)$$

where H_i is the sum of the horizontal forces acting on the bottom pillars and the index i denotes the pillar number. For the limit equilibrium method, the safety factor becomes

$$S_{LEM,tot} = \frac{\sum_{i=1}^{3} N_i \tan \varphi_i}{\sum_{i=1}^{3} T_i}, \quad (26)$$

where T_i is the shear force acting in the plane between the pillar and the foundation, N_i is the normal load acting from the dam on the foundation, and the index i denotes the pillar number.

In both cases the only difference between the new method and the traditional single pillar approach is that the new method takes the sum of the stabilizing forces within a section and divides it by the sum of the resisting forces. The resulting combined sliding safety factors are listed in Table 7.

Table 7: Combined sliding safety factors for cases 1, 2 and 3.

	$S_{SFM,tot}$	$S_{LEM,tot}$
Case 1	1.1	1.1
Case 2	1.3	1.2
Case 3	1.4	1.4

In case 1, all the pillars have zero inclination and the benefit of the combined method is limited. Since it is assumed that concrete exhibits linear elastic behaviour, this method provides almost no information that cannot be obtained from a rigid body calculation performed by hand; the safety factors obtained from the rigid body calculation and the finite element analysis are identical. In case 2, one side pillar has an inclination of $\alpha = 10^{\circ}$. The safety factor for the all three sections is 1.2 but that for the weakest pillar is 1.1. In this case, although treatment of the complete sector slightly increases the sliding safety factor, the calculated value remains well below the regulatory minimum of 1.4. Conversely, in case 3, a safety factor of 1.4 is attained when the finite element analysis is performed for all three pillars together. The compressive stresses in all three pillars under these conditions are lower than the typical compressive strength of concrete.

These results indicate that a dam section may have a satisfactory overall sliding stability even if some of its individual pillars would have inadequate sliding stability values if considered in isolation.

7 Conclusions

This paper briefly outlines the different methods used to calculate sliding safety factors for buttress dams, and presents a new method for computing combined sliding safety factors for dam segments spanning multiple pillars in typical Norwegian flat slab buttress dams. It is shown that if there are pillars with high capacity within a plate section of such a dam, it is beneficial to use this simplified three-dimensional method to compute the sliding safety factor if the slab has the capacity to transfer loads.

Although the increase in safety factors achieved by using the new model is relatively modest, it may be enough to avoid expensive rehabilitation of the section.

The new model could also be used to support further, more detailed analyses. Such analyses could, for example, consider the actual geometry of the plate foundation and fixation. Asperities in the pillar foundation, walkway openings, rock bolts, and reinforcement could also be considered, together with nonlinear concrete properties. The data needed to support such efforts could be obtained by performing an on-site survey of the dam to gather and test material samples and measure geometries. In general, the more information that is to be included in the analysis, the greater the need to document the dam's current state. A natural first step in extending the model presented here would be to include the plate foundation in the analysis.

8 Acknowledgments

The present study was supported by the national Large-scale programme for energy research programme (ENERGIX) of the Research Council of Norway, through the project Stable Dams (244029).

9 References

[1] IHA, *2017 Hydropower Status Report, Retrived feb. 2019*. https://www.hydropower.org/2017-hydropower-status-report: The International Hydropower Association, 2017.

[2] NVE, "Damdatabasen SIV." https://www.nve.no/damsikkerhet-og-energiforsyningsberedskap/damsikkerhet/innrapportering-og-damdatabasen-siv/, 2017.

[3] C. F. Grøner, "Modern Techique Of Concrete Dams for wide Valleys and ancillary works. Q. 26 - R. 21," *7th ICOLD Congr.*, 1961.

[4] FERC, "Engineering Guidelines for the Evaluation of Hydropower Projects," *Chapter 10 - Other Dams*. Federal Energy Regulatory Commission, https://www.ferc.gov/industries/hydropower/safety/guidelines/eng-guide/chap10.pdf, 1997.

[5] W. P. Creager, J. D. W. Justin, and J. Hinds, *Engineering for Dams: Concrete dams*, vol. 2. John Wiley & Sons, 1945.

[6] R. B. Jansen, *Advanced dam engineering for design, construction, and rehabilitation*. New York : Van Nostrand Reinhold, 1988.

[7] I. Møller, *Norske dammer : B. 1 : Norske vannkraftdammer i Østfold, Akershus, Hedmark, Oppland, Buskerud, Telemark, Aust-Agder, Vest-Agder og Rogaland*, vol. B. 1. Oslo: Energi forl., 2008.

[8] Olje- og Energidepartementet, "Forskrift om sikkerhet ved vassdragsanlegg (damsikkerhetsforskriften)," *I 2009 hefte 14 (Merknader)*. Olje- og Energidepartementet, 2010.

[9] NVE, "Retningslinjer for betongdammer." Norges Vassdrags- og Energidirektorat, 2005.

[10] USACE, "ETL 1110-2-256: Sliding Sability For Concrete Structures," U.S. Army Corps of Engineers, 1981.

[11] D. C. Henny, "Stability of Straight Concrete Gravity Dams," *Trans. Am. Soc. Civ. Eng.*, vol. 99, no. 1, pp. 1041–1061, 1934.

[12] G. A. Nicholson and U. S. A. C. of Engineers, "Design of gravity dams on rock foundations : sliding stability assessment by limit equilibrium and selection of shear strength," 1983.

[13] E. M. Bretas and T. A. Jenssen, "A DEM-Based Tool For Safety Analysis of Gravity Dams Q. 99 - R. 25," in *25th ICOLD Congress*, 2015, pp. 331–348.

[14] R. Malm, "GUIDELINE FOR FE ANALYSES OF CONCRETE DAMS," 2016.

[15] NVE, "Retningslinje for laster og dimensjonering." Norges Vassdrags- og Energidirektorat, 2003.

[16] Stone and W. E. Corporation, "Uplift Pressures, Shear Strengths and Tensile Strengths for Stability Analysis of Concrete Gravity Dams: Final Report," Electric Power Research Institute, 1992.

[17] R. M. Stangvik, "Shear strength of the rock-concrete interface at Kalhovd dam," NTNU, 2017.

[18] *ANSYS Academic Research Mecahical APDL, Release 17.2*. .

[19] *ANSYS Academic Research Mecahical APDL, Release 17.2, Help System, Element Reference, ANSYS, Inc*. .

Paper C

New thoughts on and discussion of numerical methods for assessing concrete dams under static loading

Andreas Seger

Submitted for publication.

C

New thoughts on and discussion of numerical methods for assessing concrete dams under static loading.

Andreas Seger[1,2]

[1]*Department of Computer Science and Computational Engineering, UiT The Artic University of Norway, Narvik,*
[2]*Sintef Narvik, Rombaksveien 47, N-8517 Narvik, Norway.*

Abstract

In this paper we present some new thoughts on and a discussion of an overview of different numerical methods that may be applied to dam structures. In particular, in this light we discuss and compare with 14 different case studies from the literature where numerical methods have been used to study the behaviour of gravity and plate dams. Finally, we show how different failure modes can be modelled. The main aim is that this paper can be an important basis when investigating dams not only in our research at NORUT Technologies in Norway but also worldwide to analyse, investigate and solve similar problems.

Keywords: Numerical modelling, structural stability, Finite Element Method, failure modes, static loading, dams

2010 AMS classification: 74S05, 74G99

1. Introduction

In Norway, 95 % of the total power production is produced from hydropower. Norway has the largest installed hydropower capacity in Europe with 31 626 MW [1]. The Norwegian Water Resources and Energy Directorate (NVE) is the governmental authority of dams in Norway and ensures that the owners of the dams complies with the dam safety regulation (Damsikkhertsforskriften) [2]. NVE has currently 4002 registered dams in Norway. Concrete dams accounts for 51.2 %, out of which 1220 are gravity dams, 322 are flat slab buttress dams , 130 are arc dams and 376 are other types of concrete dams [3].

The main aim is that this paper shall be an important basis when investigating dams not only in our research on stability assessment of typical Norwegian concrete dams under static loading conditions at NORUT Technologies but also worldwide to analyse, investigate and solve similar problems.

To ensure the dam safety throughout the lifetime of the dams, the dam safety regulation requires that all dams are reassessed at a time interval of 15 - 20 year, depending on the consequence of failure. The safety regulations cover the stability demands and how the safety factors should be calculated. NVE also provides a set of guidelines [4] and [5] that gives a more detailed description of how the stability computation should be performed. These guidelines are based on a rigid body assumption (also called the limit equilibrium method).

Figure 1 shows a typical cross section of a gravity dam, and Figure 2 shows a typical flat slab buttress dam (plate dam). With the rigid body assumption, the dam body is assumed to be rigid and resting on a rigid foundation. When assessing the stability of a dam there are three failure modes that should be checked: Overturning, sliding and overstressing, shown in Figure 3. The last of which is a local failure such as cracking or crushing of the concrete dam or rock, while overturning and sliding are global failure modes. It is assumed that for overturning, the whole dam body rotates about the toe, see Figure 3a.

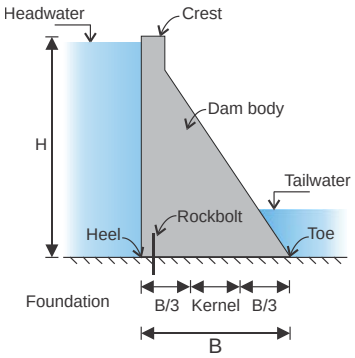

Figure 1: A typical cross-section of a gravity dam, with headwater, tail water and rock bolt.

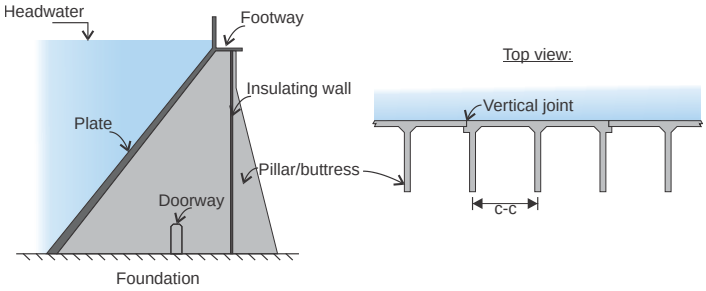

Figure 2: The components of a flat slab buttress dam (plate dam).

For sliding, it is assumed a failure plane in the dam-foundation interface and that the whole dam slides, using Mohr-Coulomb failure criteria for contact (a description of which can be found in [6]). It should be noted that overstressing might lead to a global failure of the dam, which for example is if a crack propagates through the dam body this may cause the whole dam to fail. There are two common situations when the strength/stability of a dam is computed; (1) when it is designed, and (2) when it is reassessed. A Norwegian dam that is reassessed should satisfy the current regulations. If the regulations have changed since the dam was designed (increased/change loading conditions, increased safety factors etc.), the dam might not meet the stability requirements when it is reassessed.

The cost of the corrective measures needed to satisfy the regulations might motivate a more detailed analysis of the dam. In recent history there are four known failures in concrete dams. In Norway [7], there have been no failures in dams built according to the "Damsikkerhetsforskriften" introduced in 2001. Numerical methods or more detailed and accurate analytical (mathematical) models can be useful tools in this process. Rock bolts are often used to improve the stability of the dam foundation, but in Norway these should not be included in the stability calculation if the dam is taller than 7 m (by the current guidelines [5]). The rock bolts are placed close to the upstream side on a gravity dam, and in a buttress dam the bolts are placed in the interface between the plate and foundation. In addition, there might be placed bolts along the pillars.

We finish this introduction by shortly describing loads acting on gravity and flat slab buttress dams:

Typical loading and boundary conditions are shown in Figure 3. *Hydrostatic pressure* is applied to the dam body, if there is water on the downstream (tail-water) side of the dam it applied there as well. The *uplift pressure* is assumed to have trapezoidal shape and is assumed as stress in tension in the dam-foundation interface. It is assumed to be a crack in the (interface between the foundation and) dam, the uplift pressure is assumed to be equal to the hydrostatic pressure at the heel of the dam. The uplift is then linearly decreasing towards the toe of the dam. The *ice pressure* is assumed to be 200 to 300 kPa and is acting at the top 0.5 m below the headwater level [4]. For a flat slab buttress dam, the loading is mostly the same as for a gravity dam. The main differences are that the uplift is usually assumed to act only under the plate and to be zero under the buttress. This is done if there is good drainage around the buttresses, and it is therefore assumed that there will be no build-up of uplift pressure.

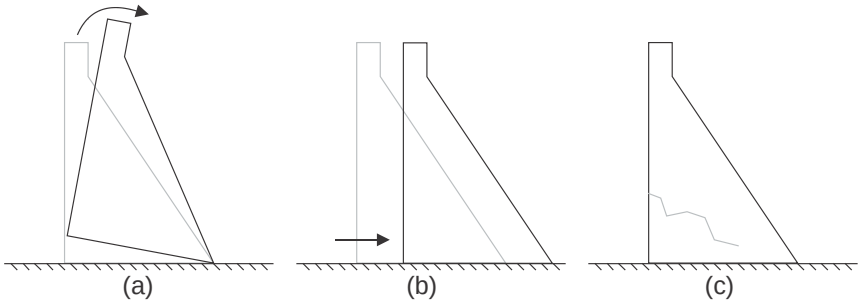

Figure 3: The failure mechanism: (a) Overturning about the toe. (b) Sliding in the dam-foundation interface. (c) Overstressing (cracking).

The paper is organized as follows: In Section 2 we present, analyse and discuss both linear and non-linear models of and seven different numerical methods, which can be useful for investigating various dam constructions. In the same spirit, in Section 3 we focus on numeric analysis in design of new dams or reassessment of existing dams. Moreover, also some error

analysis and a first case study (the La Breña II dam) are included. Moreover, in Section 4 we present and discuss 13 more interesting case studies all over the world. Section 5 is reserved for presenting and analysing the important concept overstressing, procedures for evaluating stability and modelling of failure modes. Our final discussion together with some concluding remarks can be found in Section 6.

2. Numerical analysis of dam structures: models and methods

In this section we present and discuss different numerical models and methods that can be suitable for analysing and treating problems related to dams.

2.1. Linear and non-linear numerical models

A *linear numerical model* (such as finite element model) of a dam provides a more detailed and accurate stress distribution in the dam than a limit equilibrium analysis. But a linear numerical analysis is not suitable to model the redistribution of stress due to cracking or crushing in the dams. However, it can be used to assess where in the dam it is likely that tension and shear stresses above the capacity of the materials occur. A linear numerical model should also be used as a starting point if a nonlinear model of the dam should be developed. The results from the linear analysis can then be used as a reference in the nonlinear analysis.

There are several types of *nonlinear numerical models*. One type of such model is a nonlinear material model that allows for cracking and crushing in the material. Another type is a nonlinear connection between the foundation and the dam, and can be applied for both linear and nonlinear material models.

Brand et al. [8] showed by an example that the benefits of using numerical models are not always that great. In the example, a two-dimensional analysis of a gravity dam was carried out. If the model can be reduced to a rigid body analysis, such as a gravity dam with a planar base, then a limit equilibrium analysis, which gives the cheapest analyses to perform, can be adequate for the dam. On the other hand, if the base of the dam is not planar and/or has asperities, then the failure can be best modelled with a nonlinear contact model. When an irregular base surface was introduced in the same example, the nonlinear analysis of the dam gave a friction angle of 18.3 degrees in order for the dam to be stable. If the irregularities are ignored and a limit equilibrium analysis was used, the required friction angle was 51.6 degrees. It should be noted that the irregularity causes a very different distribution of the stress, and a four times higher peak normal stress, than the one assumed in the limit equilibrium analyses. The results in the report showed that the geometry in the dam-foundation interface was clearly influencing the results of the numerical analysis.

Léger et. al. [9] showed that the similarity of the results between the ones obtained from the limit equilibrium analysis and a nonlinear finite element analysis (FE-analysis) might depend on how the dam-foundation interface was modelled in the FE-analysis and what was analysed. A gravity dam with the height of 52 meters and a typical cross section was considered. A two-

dimensional plain stress FE-analysis was performed, and showed how the choice of dam-foundation interface model affected the resulting crack length. Hydrostatic pressure (water level: 52 meters), gravity and a triangular uplift pressure were applied to the dam (updated according to crack development). A linear material model was used for both the dam and the foundation. The boundary conditions applied on the foundation was set to zero displacement in the normal direction to the boundary. First, the crack length was computed by the gravity method. Assuming no tension capacity in the concrete, the authors found that the crack expanded to 28 % of the base length. Furthermore, the authors performed the following two FE-analysis: (i) The dam-foundation interface was bounded together. If the tensile stress exceed the strength of the concrete, then the elastic modulus in the normal direction to the interface was set to zero. By using this method, we obtain the same crack length as in the case mentioned above when the elastic modulus was changed equal to 28 % of the base. (ii) The dam-foundation interface was modelled with a model that utilized a cracking criterion based on principal tensile stresses instead of normal tensile stresses as was used in the gravity method. The crack length obtained in this analysis was 83 % of the base length. This shows that the crack length is highly dependent on how the interface is modelled.

Numerical models can be expensive to develop. In general, the more complex an analysis is, the more it costs. As indicated in the example above (with planar base), the nonlinear model will not give any more information about the stability of the dam than the limit equilibrium analysis. The level of details included in the model should be such that the real structure can be approximated in the best possible way for the analysis in question. Details that do not affect the results should not be included. The more complex an analysis is, the higher the potential sources of errors is. Therefore, a more complex model does not necessarily give a more accurate result. The following three sections summarizes some of the key aspects to consider when applying the different methods to dams. These key aspects are described in the bulletin B155 - Guidelines of use of numerical models in dam engineering [10]. We will give a brief overview of some of the different numerical methods used to analyse dam constructions.

2.2. Numerical methods

a) The ***finite element method*** **(FEM)** has its origin in structural engineering; it was used to perform approximate computation of the behaviour of trusses, beams etc. subjected to external loading. Today it is also a widely used method in many fields of engineering. The basic concept of FEM is that a continuous body is dived into a finite number of parts (elements) described through nodes with different behaviour. The behaviour of each of these elements is then described with a finite number of parameters. The solution of the complete system is the result of the assembly of each elements behaviour. A more precise and detailed description of the FEM can be found in e.g. [11] and the references therein. The basic assumption of a continuous body used in FEM is also a valid assumption for concrete dams. For other types of dams such as embankment or masonry dams, where the body is not continuous, this assumption may not be justifiable. Effects such as cracking in the

concrete that introduces discontinuity into the otherwise continuous domain can be accounted for by using nonlinear material models. Today there are several commercially available finite element (FE)-software, such as ANSYS [12], ATENA [13], ABAQUS [14], LS-DYNA [15], Catia [16] and many others.

b) The ***distinct element method*** (DEM) differs from the FEM by representing a discontinuous media as an assembly of blocks that mechanical interact with each other. The development of DEM was motivated by problems in rock mechanic to which the basic continuum assumption used in FEM was not applicable. The method was first proposed by Cundall in [17]. DEM might be used for concrete and masonry dams. During the last years, DEM has been further developed, and today there is a possibility to combine FEM and DEM. This "combination", treats each block as deformable (FEM) and mechanical connected to each other (DEM), is described in details in [18]. Modelling of dams by using DEM is a good approach to evaluate the stability of dams, as shown in some examples later in this paper. There exists commercially available software that has the option of DEM, such as LS-DYNA [15].

c) The ***particle finite element method*** (PFEM) has shown to be useful when investigating problems relating to fluid - structure interaction. The nodes (in each element) are considered to be particles that can move freely and even be separate from the main domain of the analysis. An overview of the method can be found in [19], which also presents several examples where the PFEM is shown to be a more accurate tool when the different problems are considered. One of the examples presented involves large motion of free surface and splashing of waves. PFEM might be a good tool to examine the interaction between the water and embankment dams.

d) The ***finite volume method*** (FVM) is mainly used to model the behaviour of fluids, but it has also been used to model structures, see [20] and the references given there. Modelling structures by using FVM is mainly motivated by its ability to model the fluid-structure interaction by using the same numerical methods for all parts of the model. This method might be of interest in dam engineering but it is depending on the capability of the FVM to model structures and what the aim of the analysis is. For example, if the analysis aim is to assess the multi-physics problem of water – dam interaction, then the FVM might be of interested.

e) The ***extended finite element method*** (XFEM) is a numerical method that was developed to model the crack growth in an domain. A detailed description of the method can be found in [21]. XFEM is based on the framework of FEM by using discontinuous fields across the crack faces. This gives the possibility to model crack growth without re-meshing the domain.

f) The ***smooth particle hydrodynamics*** (SPH) method was originally developed to solve astrophysical and cosmological problems. A detailed description of the method can be found in [22] and the reference within. As the name of the method suggests, the domain is discretized using particles. Furthermore, it is a mesh free method. This makes SPH capable

of handling large displacements and fractures in a better way than numerical methods that depend on a mesh, such as FEM. The SPH is implemented in some commercial available software, e.g. LS-DYNA [23]. Mesh free methods do not discretize the domain into elements/volumes to provide a relationship between the nodes as for example FEM does. Some of the benefits of this is that re-meshing of a domain if cracking occurs is not required, and errors due to element distortions are avoided [24].

g) The ***isogoemetric analysis*** (IGA) method was first proposed in 2005 [25]. The main concept of IGA is to create a model for the numerical analysis based on geometry created in a computer aided design tool. This can be achieved by constructing the mesh using for example Non-Uninform Rational B-Splines. This will give a better representation of the exact geometry in the numerical model. This might be of interest for dam engineering if more details of the geometry should be included in the models. There exists a plug-in called abqNURBS [26] that utilizes IGA with in ABAQUS.

3. Numeric analysis in design of new or reassessment of existing dams

3.1. Numerical analysis in design of new concrete dams

It is not only the geometry of the dam body that should be considered in a numerical model. Also the foundation of the dam should be included in the analysis. For linear analysis with static loads the Saint - Venant principle [27] can be used as a guideline for how much of the surroundings that should be included in the analysis. This principle implies that the foundation that is included in the model should at least have the same dimensions as the characteristic dimensions of the dam body. Normal practice is to let the foundation be 1.5H high (H is the height of dam), and it should also be of H length on both the upstream and downstream side of the dam, see Figure 4. The modelling of the foundation should of course be more detailed if it is the behaviour of the foundation that is of interest in the analysis.

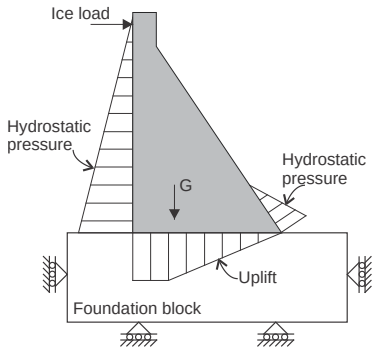

Figure 4: Typical loading and boundary conditions for a gravity dam.

The stress state in the dam that is caused by the hydration heat distribution should also be considered when modelling concrete dams. The initial stress-strain state in the dam is one of

the most complex problems to analyse for existing structures. The two main reasons for the complexity of the problems are; the lack of knowledge about the construction phase and the thermo-visco-mechanical parameters that can introduce stresses. For dams, it is also important to take into account that the dead load and stiffness are added to the structure during the construction phase. The effect of this is of great importance for the initial stress-strain state in the structure. When using numerical analysis in the design of a new dam there will always be a challenge with the calibration of the numerical model, and the geometry of the dam-foundation interface is often unknown until construction of the dam has begun.

Case study 1: The La Breña II dam

Rueda et al. [28], presented a preliminary result on how to conduct a detailed thermo-chemical study of a roller compacted concrete (RCC) gravity dam during the construction phase. The dam model in the analyses is the La Breña II dam, located in Spain. It is 124 meters high and the crest is 673 meters long, divided into 25 monoliths. The consecutive lifts between new layers of concrete were assumed to be fully bounded. The dam-foundation interface was modelled as adjacent surfaces, which allows them to slip and separate from each other. The software used to analyse the problem was the finite element method program ABAQUS/Standard [14]. The construction process was divided into 207 steps. First, the thermal dissipation in the dam was simulated by using transient heat transfer in the time domain. Second, the result from the first step was introduced as thermal loads in a mechanical analysis. The input air temperature was the averaged measured temperature at the site. The curve of heat used in the analysis was approximated as the heat generated of concrete setting. The thermal properties of the materials were assumed to be independent of time. In the mechanical analysis, the dam-foundation interface was modelled as a friction contact. Small values of sliding were assumed. On the vertical sides of the monolith, the boundary conditions were defined such that the domain can contract in the cross valley direction, but cannot expand. The “underground” boundaries in the foundation could not move in the normal direction and was free in the other. The temperature distribution obtained in the thermal analysis was applied as thermal loads. They were applied stepwise according to the new concrete lift (layering of concrete) added and the magnitude was time-dependent (computed in the thermal analysis). The self-weight of the dam was also considered. The material properties of concrete were defined as a piecewise function of time in order to account for the fact that the concrete's properties change very much in the early stages of setting. Both the Poisson's ratio and the thermal expansion coefficient were assumed constant with respect to time. In this analysis, the authors were able to show that there were high tensile stresses near the base of the dam and at the exposed faces on both the upstream and downstream side. These tensile stresses may lead to cracks in the concrete, allowing water to penetrate into the crack and concrete (seepage) which causes uplift loads. As noted by the authors, this numerical analysis was done before the dam was built and that physical experiments in order to verify the numerical model were not carried out.

3.2. Numerical analysis in reassessment of existing concrete dams

There are two commonly used approaches when applying numerical methods in the reassessment process of an existing dam. The first approach is to use the data obtained from measurements of the dams geometry and behaviour. Then the analysis is carried out as if the dam was new. By using this method, the safety factors for different load cases can be obtained. If the results of the analysis correspond with the observed behaviour of the dam, then it is likely that the results are accurate. This approach is useful if the calculation from the design phase of the dam is lost, or if the calculation method, loading conditions and criteria have changed since the dam was built.

If for example, dams were constructed without considering the effect of uplift, or if the ice load was not considered designing the dam, then this method could be used.

The second approach is the back-calculation method, which was performed on the Upper Stillwater Dam located in Northern Utah, USA. The dam failed during the initial filling the summer of 1988 [29]. The cause of the failure was horizontal shearing along a weak layer of rock in the foundation. Results from numerical analysis were compared with the observed behaviour during failure. The numerical analysis (linear elastic and plain strain) predicted larger displacement than the observed displacement of the dam before the failure, but after the failure occurred the numerical model showed less displacement of the dam than the real behaviour in the dam. The back calculation of the stability showed that it was the lowest strength measured in the foundation that could predict the shearing in the foundation.

3.3. Limitation of numerical methods and common errors in numerical analysis of dams

Numerical methods are often simplified and partial methods are often used to compute the behaviour of a real physical system [10]. The geometry is simplified by not including details. Often, finite boundaries are assumed and imposed. The material models used are approximations of the real behaviour of the material. It is difficult to include the space-wise variation of the material properties in the model. The displacements are assumed to follow some shape functions, usually of first or second degree. The loading of the structure is systemized with respect to both space and time. All of these simplifications and limitations of the numerical model are not limited to dam engineering. However, they are important to remember when evaluating the results obtained from the model.

There are some common errors in numerical analysis of dams that are highlighted in the report [8]:

- *Unrealistic boundary conditions.* Dams are large structures that may span over an entire valley. Therefore, to reduce the size of the model, often only a representative section of the dam can be considered in the numerical model. It should be considered if the section is allowed translation in the cross valley or in downstream (and upstream) direction. The same should be considered for rotation. If a connection/boundary in the dam is not rigid in the real world, then it should not be modelled as a fixed connection/boundary. Free

translations and rotations should not be assumed if the dam is constructed such that these movements are not possible.

- *Mesh density (FEM).* If the geometry is poorly meshed, then stress concentrations may be missed. Sharp corners and edges often result in high stresses and it is important that the model is meshed such that these stress concentration areas are visible in the results.
- *Strength*. It is often tempting to utilize the tensile strength of the concrete if the numerical analysis show that there are tension forces acting in the dam. During the construction of the dam, the construction sequencing, curing and cooling of the concrete and different foundations deformation may have caused stresses in the dam that are not included in the analysis. Because of these unknown stresses, the tensile strength of the concrete should not be utilized. It should be assumed that the concrete has no tensile strength.

4. Further important case studies

In this Section we present some case studies, where numerical methods have been used on gravity dams and plate dams. In additions to this, some cases where the aim of the analysis is to study the effect of passive anchors is also included.

4.1. Concerning gravity dams

A gravity dam which has a fairly constant cross section and that is long compared to the height of the dam can be modelled by using a two-dimensional numerical model. This will be a good simplification and approximation to use when computing the behaviour of the dam [10]. If the dam spans a narrow valley, and the support on the sides of the dam is assumed to influence the behaviour of the dam, then a three-dimensional model is required to create a good model of the dam.

Case study 2: The Norfork dam in USA

The analysis of the stress distribution in the Norfork dam in USA, presented in the paper [30] and the report [31], is one of the earliest applications of finite element method on problems concerning dams. The Norfork dam is a concrete gravity dam. Extensive cracking in the dam was discovered during the construction of the dam and over 18 years after the completion of the dam, an extensive survey of the size and distribution of principal cracks was carried out. In one of the monoliths (or sections) a vertical crack was discovered. It spanned almost the complete height of the cross section. This section is about 60 meters high (196 feet) and was considered in the analysis. The purpose of the analysis was to assess how the crack affected the stress distribution in the dam body. Plain stress in the cross section was assumed in the finite element (FE) analysis, and a unit length in the cross-valley direction was considered. Both an un-cracked and a cracked cross section were modelled with the following loads: hydrostatic pressure, temperature and gravity. The results showed a stress concentration around the top and bottom of the crack that was not present in the un-cracked cross section. The principal stresses in the

areas of stress concentration did not exceed 3.4 MPa (500 psi), and was concluded to be not severe.

Case study 3: The Fratel spillweir dam

The Fratel spillweir dam in Tagus River in Portugal was investigated in the paper [32]. The dam is approximately 147 meter long and has six gates(that can control the water flow) placed on spillways (part of the dam where the water can flow) 12 meter high, and piers that are 33 meter high support the gates. The spillway section of the dam is a gravity dam. Both a finite element analysis and an physical experiment using a three dimensional model (model made of plaster material in scale 1/75) was used to analyse the effect of pre-stressing needed in the piers to support the gates. A linear isotropic material model was used for the concrete. The spillway part of the dam was modelled with two-dimensional plain strain elements, and the pier was modelled with plain stress elements. In the FE-analysis the dead load, water load on the spillway dam and gate, and the pre-stressing forces were included. Furthermore, the concrete block that supports the axes of the gates was modelled using plain strain elements. It was found that the results from the FE-analysis and the plaster model have good agreement.

Case study 4: The Djerdap 1 dam

The displacement in the Djerdap 1 dam located on the Danube River on the common stretch between Yugoslavia and Romania was studied in the paper [33]. The dam has an extensive monitoring system and measurements over a 30-year period have been collected. The author used the measured displacements as a reference for the behaviour of the dam. A concrete overflow section of the dam was modelled in a two-dimensional FE-analysis. The displacements obtained from this numerical analysis were compared to the historical measurements. The horizontal displacement computed using the finite element method (FEM) was in good agreement with the recorded data. The vertical displacement computed with FEM was a bit larger than the actual historical displacement. Measurements taken in the construction phase and initial phase of operation of the dam showed that 70% of the deformation of the rock in the foundation occurred during that time. The remaining 30% of the deformation has occurred during the 30 years of operation.

Case study 5: The Hiyoshi and the Urayama dams

The behavior of Hiyoshi dam and Urayama dam in Japan during their first filling was studied in the paper [34]. The Hiyoshi Dam is a Roller Compacted (RC) gravity dam with the height 67.4 meter. The Urayama is also a RC gravity dam, and it is 156 meter high. During the first filling, there were no issues with any of the dam's behaviour. The largest cross-section of both dams was used in the analysis. The temperature and displacement of both dams were measured during the first filling. The authors compared these measurements with the computations performed with a two-stepped FE-analysis. The first step was an analysis of the temperature distribution in the dam. The result from this analysis was then used in the second step as a temperature load in the concrete in addition to the hydrostatic pressure. In the thermal analysis, a two-dimensional FE-analysis was performed considering the air temperature and

temperatures in the water on-site. The heat of hydration of the concrete, sunshine and other weather effects were not considered. In the static analysis, a plane stress FE-analysis was used, and the loads applied were temperature (in air and water), hydrostatic pressure, uplift and gravity. A segment of the foundation was also included in the analysis. For both of the dams the authors achieved numerical results that corresponded well with the actual measured behaviour of the dam. Furthermore, how the temperature and hydrostatic loading individually affected the behaviour of the dam, were also investigated. The result closest to the actual measured behaviour was the result obtained by a computation that included temperature loads, hydrostatic loads and gravity.

Case study 6: The Ternay dam

The Ternay dam in France is a 41 meters high old (completed in 1864) gravity masonry dam. A numerical analysis of the Ternay dam was presented in the paper [35]. A two-dimensional FE-analysis with an elastic foundation was performed with the FEM program FARC-DAM. The dam-foundation interface was modelled using a Mohr-Coulomb contact model with the friction angle of 46 degrees and a cohesion of 81 kPa. A poro-fracture analysis with a smeared nonlinear fracture mechanic concrete model was used to compute the cracking. The fracturing process was described using a tensile strain softening law when the tensile stresses exceeded the strength of the concrete. The foundation was constrained at the dam edges by setting the displacement to zero in the normal direction to the edge. When the water level reached 35.6 meters, an unstable crack developed. It was concluded that a water level of 35.6 meters gave the failure load, and the failure was overstressing. These results were compared to previously work presented in [36], which used a poro-plastic formulation, and the obtained failure load in that work gave a crack at water level 36.4 meters. The differences between the two studies were assumed to be some differences in the effective porosity coefficient and the evolution of internal water pressure. It was concluded that by comparing the failure water level to the normal operating water level, a safety margin can be obtained. Furthermore, the authors noted some important aspects of numerical modelling of concrete dams; e.g. that the possibility of a crack jumping from one lift joint to the next should be considered. Moreover, the benefit of a numerical analysis, compared with the limit equilibrium method, was that it can compute the critical cracking profile. The numerical analysis can also handle several cracks, voids in the dam, varying material properties in the cross-section, discontinuities in the dam/foundation or the interface between them, temperature effects, and other actions done to improve the performance of the dam.

Case study 7: The Itaipu dam

The Itaipu dam located on the Praná River between Brazil and Paraguay is 7.8 kilometres long and has a maximum height of 196 meters. The dam consists of a concrete hollow gravity, a concrete buttress, a concrete mass gravity, a rock fill and an earth fill section. In the paper [37] the authors used the measurements taken over 17 years, to calibrate the finite element models connected to some of the sections of the dam. Two-dimensional FE-analysis was performed on

10 different cross-sections of the dam. In addition, a three-dimensional FE-analysis of the whole dam was conducted. It was assumed a monolithic connection between the dam and foundation, i.e. the two parts acted as one body. Gravity, temperature and hydrostatic loads were applied to the dam. Based on the FEA, it was concluded that the evaluated sections of the dam have the necessary safety margins.

4.2. Concerning plate dams

A plate dam (or flat slab buttress dam) can be modelled in different ways. One approximation is a two part plain stress model. First, the plate can be modelled, and the stresses obtained from the analysis can then be used in an analysis of the pillar, see [38], as the second step. Another method is to model one pillar and a section of the plate using either shell elements or solid elements (one pillar and a section of a plate method). The analysis performed on the Storfinnforsen is an example of this, which is summarized below.

Case study 8: The Målset dam

In the paper [39], the finite element method was used to investigate the sliding stability of four sections in the Målset dam, located on Vikafjellet on the west coast of Norway. The dam was built in 1954. It has one buttress section (34 pillars with a distance of 5 meter) and two sections that are gravity dams. The buttress section is up to 17 meter high. The sliding stability of two relative low sections (5.7 meter and 6 meter) was assessed by using a two-dimensional numerical model in the FEM-software ATENA. The pillars were modelled with plain stress elements. The plate and the rock foundation were modelled using plain strain elements. A fracture-plastic constitutive model was used in the model in order to include cracking and/or crushing. The loads were hydrostatic pressure, see Figure 1b, gravity and ice load. The uplift pressure was modelled by reducing the gravitational load of the plate. The traditional method of computing the safety factor with FEM, both with a smooth planar inclined dam-foundation interface and an interface that was close to the actual one (asperities etc. was included) was compared. The results showed that the FEM analysis gave higher safety factors against sliding than the shear-friction method, for the planar interface. The actual interface has a lower safety factor than the planar interface, but it is still higher than what you get from the shear-friction method.

Case study 9: The Storfinnforsen dam

In this case, a numerical analysis of a buttress dam was performed to investigate the cause of crack development in the dam. The Storfinnforsen dam, located in Sweden, were completed in 1954. The dam has a maximum height around 40 meters. In 1961, the first survey of cracks in the dam was completed, and a second one was done in 1981. During that time three times as many cracks had developed, and the length of the cracks had doubled. One of the hypotheses was that it was the temperature difference between the upstream side and downstream side that caused these cracks. This was described in the references [40]–[42], where numerical modelling of thermal expansion in buttress dams was used. The starting point in the papers was a linear model, which was further developed into to a nonlinear model. In the report [41], a 40-

meter-high section of the dam was considered. The numerical model consisted of one pillar and a plate segment. A finite element analysis was performed using shell elements with the effect of steel reinforcement and the FEM-software Abaqus. The plate was rigidly connected to the pillar and free on the sides that are in contact with the plates of the adjacent pillars. Moreover, the pillar was rigidly connected to the rock foundation, see Figure 2. The rock foundation was modelled as a 2 meter thick plate. This was done to reduce the stress close to the foundation when it was modelled as rigid surface. This was done to avoid unrealistic stresses at the base of the pillar. Due to the lack of elasticity if the foundation it was modelled as a rigid foundation. A nonlinear material model based on plasticity theory (called concrete damaged plasticity) was used to model the concrete. Gravity, hydrostatic pressure and temperature loads were applied. The temperature load was time dependent. The seasonal variation in the air/water temperate was considered as one temperature cycle, and a total of five cycles was applied to the dam. The results of the analysis showed that the cracks from the analysis corresponded well with the ones observed in the dam, and that the 3D shell elements provided higher accuracy than a 2D FE-analysis. This also showed that the placement of the insulation wall had a significant effect on how the stresses due to thermal loads were distributed in the dam.

4.3. Concerning arch dams

We also describe some concrete examples concerning numerical analysis of arc dams.

Case study 10: Sarvsfossen dam

In the design process of Sarvsfossen dam (completed in 2014), a 50 meter high double curved concrete arch dam located in Bykle, Norway, a FE-analysis was used to assess the capacity of the dam [43]. It was assumed that the concrete and bedrock are linear elastic isotropic materials, the interface between the concrete dam body and bedrock were modelled with contact elements, hence uplift and sliding in the interface were included in the model. The motivation for performing a FEA on the dam was to get a more accurate representation of the geometry in the model than the one used in the currently used analytical calculations. The FEA showed that the dam body was lifted at the heel when the water pressure was added. Therefore, sensors were installed during the construction, and after the first filling of the dam the measurements showed that the heel lifted 2.5 - 3.5 mm under the highest water pressure. These measurements were close to what the numerical model predicted.

Case study 11: The Xiaowan concrete arch dam

Y. Pan et. al. [44] implemented an unbalanced force method in a FE-model to study the crack development in the Xiaowan high concrete arch dam, located in China. It was an existing crack in the dam which was assumed to be the results of thermal induces stresses. Both numerical and physical experiments were conducted to study the stability of the dam, and to determine the most likely failure mechanism. Both the numerical and the physical experiments showed that the cracking at the heel of the dam should be of the greatest concern and that the existing cracks seemed to be stable.

4.4. Passive anchors

Passive anchors (or rock bolts) are often used in a concrete dam. Below follows two different methods of implementing rock bolts in a numerical analysis of a dam.

Case study 12: DEM used to assess passive anchors

E.M. Bretas et al. [45] used a small gravity dam model located in Canada with passive anchors by using DEM as a case study. The dam is 2.9 meter high and has a base width of 3.65 meter. The section was reinforced with a passive anchor 0.6 meters from the upstream heel. The load case used in the analysis was a flooding scenario with a headwater of 4.81 meters on the upstream and 1.81 meters downstream. The hydrostatic pressure was applied on the upstream face of the dam, but discarded on the downstream side, since that would have a stabilizing effect on the dam. Uplift and gravity were also included. The dam-foundation interface was based on the Mohr-Coulomb contact model and the foundation “block” was fixed in place. Full uplift pressure was applied in a crack that was computed to be one meter from the upstream heel. A parametric study of both the strength of the anchor and friction angel was conducted. It was concluded that the parameter that had the largest effect on the shear load acting on the anchor, was the friction angle. The effect of multiple anchors was also studied and was found to increase the normal force and related shear force in the bolts; this was due to reduction in the distance from the bolt to the toe of the dam.

Case study 13: A typical Swedish buttress monolith

R. Malm et al. [46] performed a case study on a typical Swedish buttress monolith to examine how the rock bolts contributes to the stability of concrete dams. The height and width was 8 meters, the thickness of the plate was 1.2 meter, and the buttress had a thickness of 3 meter. The monolith has 20 rock bolts as anchors (steel bars, with a diameter of 25 millimetres) which are drilled 2 meters into the concrete and 3 meters into the rock. The water level was 7.5 meters. The geometry consisted of one pillar and the corresponding part of the plate. Four cases were assessed in this study, performed by FE-analysis; (1) Without bolts, (2) Bolts with maximum allowed stress level of 140 MPa, (3a) Bolts with a yield stress level of 370 MPa and no corrosion, and (3b) Bolts with yield strength of 370 MPa and considering corrosion. The used software was Abaqus. The dam body and rock foundation were modelled with a 8-noded linear brick element. The FE-model of the dam body consisted of 32640 elements with an average size of 0.2 meters. The rock foundation consisted of 40960 elements with the average size of 0.25 meters. The rock bolts were modelled with a three-dimensional 2-noded linear Timoshenko beam element, with an element size of 0.035 meters. The loading considered in this analysis was gravity (i.e. dead load), hydrostatic pressure and uplift pressure. The dam-rock interface was modelled as a "hard contact" for compressive loads that allowed separation, and the friction coefficient was set to 1.0. The boundary conditions were applied to the rock foundation, except the top surface that was constrained in the normal direction. The rock bolts were defined in such a way that a 0.1 millimetre axial deformation was allowed before failure. A push-over procedure (described in more details later) was used in all cases. The hydrostatic

pressure and uplift were increased by increasing the density of water, i.e. only the horizontal component was increasing. The results showed a combined failure mode of sliding and overturning. The numerical safety factors (combined) for all cases are listed in Table 1, together with the safety factor obtained by analytical calculations (sliding and overturning).

Table 1: The safety factors for the different load cases.

Case	Combined	Sliding*	Overturning*
1	1.00	1.03	1.43
2	1.98	1.49	2.02
3	3.00	2.22	2.54

*Analytical results

The conclusion of the study was that the rock bolts have a significantly effect on the stability on concrete dams. In this study, it was included also a presentation of and a discussion on how degradation influence the strength of the rock bolts.

Case study 14: The Nygårdsvatn dam

E.M. Bretas et al., [47], used the discrete element method (DEM) in a case study of a two-dimensional numerical analysis. The method of reducing the friction angle was used to evaluate the stresses in passive rock bolts instead of the more commonly known FEM that was based on joint elements to represent the bolts. The Nygårdsvatn dam located near Narvik in the northern part of Norway was used as a case study. The construction of the dam was completed in 1932. It is a small dam consisting of one arched section and two gravity dam sections. In 2002 the owner of the dam concluded that one of the sections needed to be rehabilitated. The 48 meter long gravity dam with the height of 5 meters, needed more grouting and reinforcement due to a horizontal crack of 2 meters below the crest of the dam. In the analysis, the rock bolts were included as one-dimensional elements. The dam was loaded with hydrostatic pressure and ice load. The friction angle was reduced from 55 degrees to 25 degrees, and the failure in the dam-foundation interface occurred at 30 degrees. By using the DEM model, it was shown that for the selected method of rehabilitation forces acting on the anchors were well within the capacity of the selected solution for the anchors.

5. Overstressing, procedures for evaluating stability and modelling of failure modes

5.1. Overstressing

In this section, a selection of case studies where the aim has been to assess overstressing in dams, is presented. One of the main concern within the field of dam engineering is how cracks that occur in the dam will affect the failure of the dams.

A gravity dam

A. Carpinteri et al. [48] showed that is was a good correlation between the crack propagation in a FE-model and physical lab experiments conducted on a scaled down section of a gravity dam. In the FE-model triangular elements with 6 nodes together with quadratic shape functions were used. A cohesive crack model (see for example [49]) was used to allow for cracks to occur in the FEA. The physical experiments were conducted on scaled down sections (1:40) of a gravity dam with a notch on the upstream side to initiate the crack development (different notch depths were tested). FEA of these experimental tests showed that the FE-model was able to predict the crack trajectories in a satisfactory manner, while the peak load obtained in the FEA was a bit lower than the experimental results.

Smeared crack analysis

S. Bhattacharjee et al. [50] studied how well smeared crack analysis models predicted crack propagation. Both a coaxial rotating crack model (CRCM) and a fixed crack model with a variable shear resistance factor (FCM-VSRF) were implemented in a two-dimensional FEA. The results were compared with available experimental studies in the literature. For both methods (CRCM and FCM-VSRF) of smeared crack analysis, a satisfactory estimation of the crack propagation, when compared to the experimental data, was obtained.

Crack propagation

G. Bolzon et. al. [51] performed a comparative study of crack propagation in a two dimensional buttress dam. Two different formulations of the boundary element method and finite element method were compared with experimental data. It was shown that both of the boundary element methods were able to fairly close predict the actual peak load. The finite element analysis using a cohesive fracture model with linear springs was also predicting the peak load fairly good, but the method cannot be used to predict the crack propagation. The smeared crack method was also tested. This method gave a peak load approximate 1.4 higher than the experimental results.

S.N. Roth et. al. [52] showed good results when simulating the crack propagation in concrete structures, such as dams, by combining XFEM with the damage mechanics approach. Both the crack paths and peak load correlated well with the experimental results.

Y. Wang et. al. [53] investigated the hydraulic fracturing in high concrete dams both with physical and numerical experiments. The results from FEA were compared with physical experiments carried out, and showed good correlation between the results. Furthermore, the importance of considering hydraulic fracture in high concrete dams was shown.

S. Kai et. al [54] used a hybrid finite element mesh-free method to investigate the cracking in concrete dams. The effect of the hydraulic pressure in the cracks was also considered. It was found that the crack surfaces increased and the crack paths were smoother. The numerical model without hydraulic pressure was validated by comparing the results to existing results from physical experiments.

In the next subsection some different procedures for modelling failure modes that have been identified in the reviewed case studies are presented.

5.2. Four procedures for evaluating the stability of dams

Procedure 1: Increasing the head water level until failure.

As seen in the case study [35], a method for computing the capacity of the dam is to increase the headwater until failure. The safety margin can then be obtained by comparing the headwater level that causes failure with the normal operational headwater.

Procedure 2: Push-over.

A procedure called "push-over" to obtain the maximum capacity for a dam is described in Guideline for FE-Analysis of concrete dams [55]. This is an iterative procedure that has two main steps. *Step one:* Apply the normal loads. *Step two:* Increase the "driving" loads until failure occurs. The "driving" loads are the forces that decrease the stability of the dam, such as the horizontal component of the hydrostatic pressure, the ice load, the uplift etc. One way of doing this is to increase the density of the water. Loads that contribute to the stability, such as the weight of the dam or vertical competent of the hydrostatic pressure, should not be increased during the analysis. Both step one and two can be divided into the necessary sub-load steps. The main idea in this procedure is to keep the lever arm of the "driving" forces in the same location, and only increase the size of the loads. By doing this it is argued that the results obtained by this method can be compared with results obtained from a rigid body analysis of the dam. Figure 5 shows the steps in the procedure, the driving forces are increased until failure occurs (indexed with * in Figure 5).

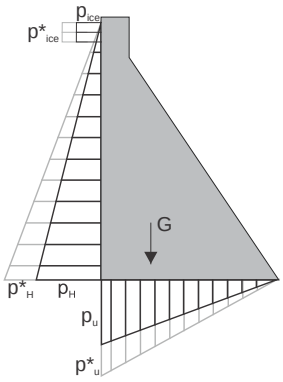

Figure 5: The push-over method.

Procedure 3: Reducing the friction angle.

One method to examine/assess the sliding failure, is by reducing the friction angle (or coefficient of friction) until sliding occurs. This is an iterative process, starting with the actual friction angle between the dam and the foundation and stepwise reduce it until the dam start to

slide. The safety factor for sliding can then be obtained by comparing the lowest friction angle needed for the dam not to start sliding with the actual friction angle. The advantage with this procedure is that the loads are not manipulated. In both Procedures 1 and 2 the failure mechanism is not isolated. By reducing the friction angle the most likely failure is sliding. A disadvantage with this method is that it may require several analyses (one for each friction angle) depending on how close (assumed) to failure the iterative process was started.

Procedure 4: Resultant forces.
The resultant force can be used to compute the safety factor for overturning. The position of the resultant force can be computed from the results obtained from the numerical model. If the resultant force is within the kernel (see Figure 1a) of the dam base, then there will be no overturning. This method uses the same principles as the limit equilibrium method and can also be used for sliding. In this procedure, the contact is modelled by using a suitable contact model, such as the Mohr - Coulomb contact model.

5.3. Numerical modelling of failure modes

This subsection focuses on how the following three failure events can be modelled by using numerical methods:

- overturning about the toe of the dam,
- sliding in the connection between the dam and the foundation,
- overstressing in the dam or foundation.

In addition to this, some common procedures for loading the dam to failure are presented.

Failure of a dam is often defined as an uncontrolled release of the reservoir. Two main events can cause this: overturning and sliding. Both of which can occur in any place and in any plane in the dam and foundation. For this to occur a third event is needed: overstressing that causes cracks or crushing in the structure. A numerical model that includes every possible failure plane is a complex model. Therefore, the numerical models can often by simplified by studying each failure mode one by one. This gives a motivation for modelling the different failure modes that is twofold: (1) Reduce the complexity of the model. (2) To fulfil the NVE regulation [5], which demands that the overturning (about the toe) stability, the sliding (dam-foundation interface) stability and the stress distribution must be checked.

There is a difference in the level of details which are needed in this analysis. The material strength is not of importance for the stability against overturning of the dam about the toe and sliding between the dam and foundation. These failure modes depend only on the density of the material and the coefficient of friction. This justifies the use of linear material models when analysing these failure modes. Overstressing, on the other hand, is highly dependent on the material strength. Hence, a more detailed material model is required. It should be noted that if the dam-foundation interface is modelled using a model that depends on friction, some numerical software require that the contact pressure must be established in a load step before the loads that may cause friction stresses, are applied. For dams, this can easily be achieved by

applying forces in a natural order. In the first step, the gravity load is applied (this generates the contact pressure), and in the second step, the hydrostatic pressure, uplift, ice pressure etc., will gradually be applied.

Overturning

Overturning of the dam about the toe can be modelled by using Procedure 2 (push-over). If using the push-over procedure, there should be no slip between the dam body and the foundation. This is achieved by modelling the contact between the foundation and dam with vertical springs and horizontal springs [55]. The vertical springs are used to represent the deformability of the foundation and the extension stiffness is then set to zero, i.e. it can only be activated in compression. The stiffness of the horizontal springs is used to model the friction between the dam body and the foundation. The load that causes overturning is then compared to the actual load acting on the dam, and the safety factor is obtained. Procedure 4 (resultant force) can be used to compute the safety factor for overturning. The benefit of this method is that there is no need to load the dam to failure, hence the modelling algorithm/method requires fewer iterations compared with Procedure 2 (push-over).

Sliding

Sliding in the plane between the dam and foundation can be modelled by using the Procedure 2 (push-over), Procedure 3 (reducing the friction angle), and procedure 4 (resultant forces.). Common for all procedures is that the contact should be modelled by using a contact model such as, e.g. a Mohr - Coulomb or others. As in the limit equilibrium method, it is common to assume a planar connection surface between the dam and the foundation. Both the push-over procedure and reduction of the friction angle procedure require several iterations to obtain the failure load or friction angle. The result can then be compared with the actual loads/friction angles, and the safety factor can be obtained.

Similar as in the case for overturning one can obtain the safety factor by retrieving the normal stress and friction stress from the numerical model under normal loading, and compute the safety factor in the same way as when using the limit equilibrium method (Procedure 4). Procedure 3 will most likely produce a pure sliding failure. Procedure 2, on the other hand, might result in a combination of both overturning and sliding.

Overstressing.

Overstressing (or crushing) and cracking are local failure modes, which can occur if local stresses exceed the strength of the material. If it is of interest to study how a local failure progresses, then a nonlinear material model is often required. This will also make it possible to study the redistribution of stresses after a part of the dam is crushed or cracked. The contact between the foundation and the dam (dam-foundation interface) should be modelled by a contact model such as Mohr - Coulomb. Geometrical discontinuities, such as asperity and gallery openings, that can cause stress concentrations in the dam, should be included in the model [56]. These stress concentration areas are potential starting points for material failure. Therefore, the actual

shape of the dam-foundation interface should be modelled in some detail. If there is cracking in the dam on the waterside, there should be applied an uplift/hydrostatic pressure inside the crack. This should be done for both overturning and sliding analysis if there are areas in the dam where tension stress occurs (assumed crack). How to model the crack propagation in concrete structures, such as concrete dams, belongs to the research field fracture mechanics. The details of this is not the main scope of this paper. However, this is an important topic within the field of dam engineering and will be described and discussed in more detail in a forthcoming paper

6. Final discussion and concluding remarks

In this paper a review of how numerical methods can be used in dam engineering is given and discussed. Some of the case studies show that the results obtained by using numerical methods, such as FEM, are close to the measurements of the behaviour of the dam. In some cases, the numerical methods have been used to show that the dams are stable. It seems that FEM is the most commonly used numerical method to model concrete dams.

In particular, the use of numerical analyses of dams in Norway has been motivated by the cost of rehabilitation (strengthening) of dams that appears to be stable but do not pass the reassessment calculations performed according to the current regulations and by using rigid body assumptions. This has motivated the dam owners to start looking for less conservative methods such as numerical methods. The goal is to develop better methods for computing the stability, and numerical analyses/methods might an especially suitable approach for doing this, but this requires that the assumptions used for the models are in fact correct. Numerical models that use the same assumptions that the rigid body method might not give any more information about behaviour of the dam.

In some of the case studies presented here, it is often difficult to understand what the assumptions that are made for the numerical analysis, and what boundary conditions and loads that are applied on the model. Hence, the results are not easily repeatable and verifiable. This is a result of poor documentation of the numerical analysis. A better documentation would be very beneficial within the field of dam engineering.

As shown in the example by Brand et al. [8] the geometry of the dam-foundation interface has a big impact on how the stresses are transferred from the dam body to the foundation. This interface might be difficult to check on site for a gravity dam, but for a buttress dam where the surrounding area of the pillar often is exposed, the interface geometry can be measured on site for an existing dam. For gravity dams this must probably be done before they are built. By including the geometry of the foundation asperities this might act as shear keys and will contribute to the sliding stability if the foundation is of a strong material, such as good rock. On the other hand, these shear keys might lead to stress concentration points that can lead to overstressing.

The Procedures 1 - 3, described in subsection 5.2, all try to obtain the maximum / minimum capacity of a dam. In Procedure 1, the water level is increased until failure. This will move the resultant force of the water further away from the toe (in the vertical direction) and accelerate the overturning movement in the dam. On the other hand, if the dam has a sloping upstream face, increasing water level will also increase the deadweight of water that will contribute to the stability. This is avoided in Procedure 2 (push-over), where only the horizontal component of the "driving" forces are increased. As seen from the last case study by Malm et al. [55], this procedure gives a combined failure of overturning and sliding. By using Procedure 3 (reducing the friction angle in the dam-foundation interface), the most likely failure to occur is sliding. This method does not alter the loads in any way.

The main reason for all these procedures is to find the capacity of the dam, but for Procedures 1 and 2 the loads are changed in a somewhat unnatural way. In Procedure 1, there is a risk for ending up with a headwater level far above the crest of the dam. In Procedure 2, the increase of the horizontal component can be viewed as increasing the density of the water, which might result in a very dense water. Both the water level and density of water are known parameters, but if unknown, it is easy to measure. Procedure 4 (the use of the resultant forces), does not require any changes in the loads. However, then the maximum capacity of the dams is not obtained.

As shown by the reviewed case studies from the literature, several numerical methods can be used to assess the crack propagation in concrete dams. For an engineer considering these types of problems one important task will be to validate the numerical method which can be chosen to model the problem at hand. One of the main aims of this paper is that it can be used as a basis when doing this crucial choice.

Finally we remark that another approach to tackle problems of the type described in this paper is to use Fourier based methods. A recent review article on this subject is that by A. Singh and N. Grip [57], where also a fairly complete list of references are included and a concrete case study from a bridge in Sweden is presented.

7. References

[1] IHA, *2017 Hydropower Status Report, Retrived feb. 2019*. https://www.hydropower.org/2017-hydropower-status-report: The International Hydropower Association, 2017.

[2] Olje- og Energidepartementet, “Forskrift om sikkerhet ved vassdragsanlegg (damsikkerhetsforskriften),” *I 2009 hefte 14 (Merknader)*, 2010.

[3] NVE, “Damdatabasen SIV.” https://www.nve.no/damsikkerhet-og-energiforsyningsberedskap/damsikkerhet/innrapportering-og-damdatabasen-siv/, 2017.

[4] NVE, “Retningslinje for laster og dimensjonering.” Norges Vassdrags- og Energidirektorat, 2003.

[5] NVE, “Retningslinjer for betongdammer.” Norges Vassdrags- og Energidirektorat, 2005.

[6] J. F. Labuz and A. Zang, “Mohr–Coulomb Failure Criterion,” *Rock Mech. Rock Eng.*, vol. 45, no. 6, 975–979, 2012.

[7] T. Konow, “Vurdering av bergrunnen,” *NVE Workshop - Veileder for betongdamer*. Gardemoen, Oslo, Norway, April 2018.

[8] B. Brand *et al.*, “Selecting Analytic Tools for Concrete Dams Adressing Key Events Along Potential Failure Mode Paths,” FEMA (Federal emergency Mangemet Agency), 2014.

[9] P. Leger, R. Tinawi, M. Leclerc, and S. Rheault, “A progressive methodology for structural safety evaluation of gravity dams subjected to floods.,” in *Proceedings of Canadian Dam Safety Conference*, 2–16, 1996.

[10] ICOLD, *B155 - Guidelines for use of numerical models in dam engineering*, no. B155. International Commission On Large Dams, 2013.

[11] O. C. Zienkiewicz, R. L. Taylor, and J. Z. Zhu, *The Finite Element Method: Its Basis and Fundamentals*, 6th ed. Elsevier Butterworth-Heinemann, 2005.

[12] ANSYS Inc., *ANSYS Mechanical APDL Theory Reference 14.5*. 2012.

[13] V. Červenka, L. Jendele, and J. Červenka, *ATENA Program Documentation Part 1 - Theory*. Prague,Czech Republic: Červenka Consulting s.r.o., 2018.

[14] Abaqus, *Theory manual. Abaqus 6.6*. Simulia, Providence, RI, USA., 2006.

[15] *LS-DYNA Theory Manual*. Livermore Software Technology Corporatio, 2006.

[16] Dassault Systemes, *CAA V5 Encyclopaedia*. Dassault Systemes, 2009.

[17] P. A. Cundall, “A Computer Model for Simulating Progressive, Large-Scale Movements in Blocky Rock Systems, Symposium Soc,” *Internat. Mech. des Roches, Nancy, Pap. II-8*, 1971.

[18] A. A. Munjiza, *The Combined Finite-Discrete Element Method*. Hoboken: Wiley, 2004.

[19] E. Oñate, S. R. Idelsohn, F. Del Pin, and R. Aubry, “The Particle Finite Element Method. An Overview.,” *Int. J. Comput. Methods*, vol. 1, no. 2, 267–307, 2004.

[20] N. A. Fallah, C. Bailey, M. Cross, and G. A. Taylor, “Comparison of finite element and finite volume methods application in geometrically nonlinear stress analysis,” *Appl. Math. Model.*, vol. 24, no. 7, 439–455, 2000.

[21] N. Moës, J. Bolbow, and T. Belytschko, “A Finite Element Method For Crack Growth Without Remeshing,” *Int. J. Numer. Methods Eng.*, vol. 46, no. 1, 131–150, 1999.

[22] P. W. Randles and L. D. Libersky, “Smoothed Particle Hydrodynamics: Some recent improvements and applications,” *Comput. Methods Appl. Mech. Eng.*, vol. 139, no. 1, 375–408, 1996.

[23] J. L. Lacome, “Smooth particle hydrodynamics (SPH): a new feature in LS-DYNA,” in *6th International LS-DYNA Users Conference,* 29–34, 2000.

[24] G. R. Liu, *Mesh Free Methods: Moving Beyond the Finite Element Method*. CRC Press, 2002.

[25] T. J. R. Hughes, J. A. Cottrell, and Y. Bazilevs, “Isogeometric analysis: CAD, finite elements, NURBS, exact geometry and mesh refinement,” *Comput. Methods Appl. Mech. Eng.*, vol. 194, no. 39–41, 4135–4195, October 2005.

[26] T. Elguedj, A. Duval, F. Maurin, and H. Al-Akhras, “Abaqus user element implementation of NURBS based isogeometric analysis,” in *6th European Congress On Computational Methods In Applied Sciences And Engineering, Vienna, Austria*, 10–14, 2012.

[27] A. E. H. Love, *A treatise on the mathematical theory of elasticity,* 2. London: Cambridge University Press, 1906.

[28] F. Rueda, N. Camprubi, G. Garcia, and J. M. Padro, “Thermomechanical Analysis of La Breña II Dam During its Construction Process: Evaluation Of potetial Thermal Cracking, Q.84 - R. 31,” in *22th ICOLD Congress*, 513–523, 2006.

[29] C. Anderson, C. Mohorovic, L. Mogck, B. Cohen, and G. Scott, “Concrete Dams Case Histories of Failures and Nonfailures with Back Calculations,” 1998.

[30] R. W. Clough and E. L. Wilson, “Stress Analysis of a Gravity Dam by the Finite Element Method,” *RILIM Bull.*, vol. 19, 45–54, 1963.

[31] R. W. Clough, “The stress distribution of norfork dam,” CALIFORNIA UNIV BERKELEY INST OF ENGINEERING RESEARCH, 1962.

[32] A. M. Heitor and J. O. Pedro, “Prestressed Piers For High Radial Gates - Fratel Spillweir Dam, Q.43 - R. 11,” in *11th ICOLD Congress*, 1127–1142, 1973.

[33] M. Tucovis, “Djerdap 1 Dam Behavior And Comparison With Project Predictions, Q. 78 - R. 9,” in *20th ICOLD Congress*, 2000, pp. 121–131.

[34] M. Nonaka, T. Hara, and J. Kamimura, “Numerical Analysis On Displacement Behavior Of Concrete Gravity Dams Measured During Impoundment, Q. 78 - R. 76,” in *20th ICOLD Congress*, 1235–1260, 2000.

[35] P. Léger, R. Tinawi, S. S. Bhattacharjee, and M. Leclerc, “Failure Mechanism Of Gravity Dams Subjected To Hydrostatic Overload: Influence Of Weak Lift Joints, Q. 75 - R. 2,” in *19th ICOLD Congress*, 11–37, 1997.

[36] B. Fauchet, O. Coussy, A. Carrére, and B. Tardieu, “Poroplastic analysis of concrete dams and their foundations,” *Dam Eng.*, vol. II, no. 3, 165–192, 1991.

[37] M. Juliani, L. Becocci, J. F. S. Rodrigues, C. Piasentin, and A. S. Fiorini, “Itaipu Dam Monitoring Reevaluation Of Instrumentation Control Values, Q. 78 - R. 83,” in *20th ICOLD Congress*, 1403-1416, 2000.

[38] ICOLD, *B030A - Finite Elements Methods In Analysis And Design Of Dams*, no. B030A. International Commission On Large Dams, 1987.

[39] G. Sas, E. M. Bretas, and L. Lia, "Advanced Sliding Assessment of Målset Dam: Tests and Numerical Analysis of Unbonded Joints, Q. 99 - R. 30," in *25th ICOLD Congress*, 331–348, 2015.

[40] A. Ansell, J. Björnström, T. Ekström, M. Hassanzadeh, and M. Unosson, "Spricktillväxt i lamelldamm Tillämpning av icke-linjära modeller – Del I," 2007.

[41] A. Ansell, T. Ekström, M. Hassanzadeh, and R. Malm, *Crack propagation in buttress dams Application of non-linear models – Part II*, vol. 10:69. Elforsk, 2010.

[42] J. Björström, T. Ekström, and M. Hassanzadeh, *Spruckna betongdammar - Översikt och beräkningsmetoder*, vol. 06:29. Elforsk, 2006.

[43] J. Lindemark, E. E. AAsheim, R. O. Mork, and T. Bjønnes, "Sarvsfossen Dam – Design of a Norwegian Concrete Arch Dam," in *Hydropower'15*, June 2015.

[44] Y. Pan, Y. Liu, Z. Cui, X. Chen, and Q. Yang, "Fracture Analysis of Brittle Materials Based on Nonlinear FEM and Application in Arch Dam with Fractures," *J. Appl. Math.*, vol. 2013, no. November 2015, 1–12, 2013.

[45] E. M. Bretas, P. Léger, and J. V Lemos, "Analysis Of Gravity Dam Considering The Application Of Passive Reinforcement.," in *Dam Maintenance and Rehabilitation II*, 809–819, 2010.

[46] R. Malm, F. Johansson, R. Hellgren, and F. R. Bayona, "Load capacity of grouted rock bolts due to degradation," 2017.

[47] E. M. Bretas and T. A. Jenssen, "A DEM-Based Tool For Safety Analysis of Gravity Dams Q. 99 - R. 25," in *25th ICOLD Congress*, 331–348, 2015.

[48] A. Carpinteri, S. Valente, G. Ferrara, and L. Imperato, "Experimental and Numerical Fracture Modelling of a Gravity Dam," in *Special Publication*, vol. 143, 351–360, 1992.

[49] A. Carpinteri, P. Cornetti, F. Barpi, and S. Valente, "Cohesive crack model description of ductile to brittle size-scale transition: dimensional analysis vs. renormalization group theory," *Eng. Fract. Mech.*, vol. 70, no. 14, 1809–1839, September 2003.

[50] S. S. Bhattacharjee and P. Léger, "Application of NLFM Models to Predict Cracking in Concrete Gravity Dams," *J. Struct. Eng.*, vol. 120, no. 4, 1255–1271, 1994.

[51] G. Bolzon, G. Cocchetti, G. Maier, G. Novati, and G. Giuseppetti, "Boundary element and finite element fracture analysis of dams by the cohesive crack model: a comparative study," in *The International Workshop on Dam Fracture and Damage*, 69–78, 1994.

[52] S.-N. Roth, P. Léger, and A. Soulaïmani, "A combined XFEM–damage mechanics approach for concrete crack propagation," *Comput. Methods Appl. Mech. Eng.*, vol. 283, 923–955, 2015.

[53] Y. Wang and J. Jia, “Experimental study on the influence of hydraulic fracturing on high concrete gravity dams,” *Eng. Struct.*, vol. 132, 508–517, 2017.

[54] K. Su, X. Zhou, X. Tang, X. Xu, and Q. Liu, “Mechanism of Cracking in Dams Using a Hybrid FE-Meshfree Method,” *Int. J. Geomech.*, vol. 17, no. 9, 1–14, 2017.

[55] R. Malm, “GUIDELINE FOR FE ANALYSES OF CONCRETE DAMS,” 2016.

[56] USBR, *State-of-Practice for the Nonlinear Analysis of Concrete Dams at the Bureau of Reclamation, January 2006*. U.S. Department of the Interior, Bureau of Reclamation, 2006.

[57] H. Singh and N. Grip, “Recent trends in operation modal analysis techniques and its application on a steel truss bridge,” *Nonlinear Stud. (to Appear December 2019)*.

Paper D

Some Fourier inequalities for orthogonal systems in Lorentz–Zygmund spaces

G. Akishev, L.E. Persson and A. Seger

Published in *Journal of Inequalities and Applications*, 2019, Article number: 2019:171, DOI: 10.1186/s13660-019-2117-4.

D

Journal of Inequalities and Applications
a SpringerOpen Journal

RESEARCH Open Access

Some Fourier inequalities for orthogonal systems in Lorentz–Zygmund spaces

G. Akishev[1,2], L.E. Persson[3*] and A. Seger[3]

*Correspondence:
larserik6pers@gmail.com
[3]Department of Computer Science and Computational Engineering Campus Narvik, The Artic University of Norway, Narvik, Norway
Full list of author information is available at the end of the article

Abstract

A number of classical inequalities and convergence results related to Fourier coefficients with respect to unbounded orthogonal systems are generalized and complemented. All results are given in the case of Lorentz–Zygmund spaces.

MSC: 42A16; 42B05; 26D15; 26D20; 46E30

Keywords: Inequalities; Fourier series; Fourier coefficients; Unbounded orthogonal systems; Lorentz–Zygmund spaces

1 Introduction

Let $q \in (1, +\infty)$, $r \in (0, +\infty)$ and $\alpha \in \mathbb{R}$. Moreover, let $L_{q,r}(\log L)^{\alpha}$ denote the Lorentz–Zygmund space, which consists of all measurable functions f on $[0,1]$ such that

$$\|f\|_{q,r,\alpha} := \left\{ \int_0^1 \left(f^*(t)\right)^r \left(1 + |\ln t|\right)^{\alpha r} \cdot t^{\frac{r}{q}-1}\, dt \right\}^{\frac{1}{r}} < +\infty,$$

where f^* is a nonincreasing rearrangement of the function $|f|$ (see e.g. [1]).

If $\alpha = 0$, then the Lorentz–Zygmund space coincides with the Lorentz space: $L_{q_1,q_2}(\log L)^{\alpha} = L_{q_1,q_2}$. If $\alpha = 0$ and $q_1 = q_2 = q$, then $L_{q_1,q_2}(\log L)^{\alpha}$ space coincides with the Lebesgue space $L_q[0,1]$ (see e.g. [2]) with the norm

$$\|f\|_q := \left(\int_0^1 |f(x)|^q\, dx \right)^{\frac{1}{q}}, \quad 1 \le q < +\infty.$$

Moreover, $L_{\infty}[0,1]$ denotes the space, which consists of all measurable function on $[0,1]$ such that

$$\|f\|_{\infty} := \operatorname*{ess\,sup}_{x \in [0,1]} |f(x)| < \infty.$$

We consider an orthogonal system $\{\varphi_n\}$ in $L_2[0,1]$ such that

$$\|\varphi_n\|_s \le M_n, \quad n \in \mathbb{N}, \tag{1}$$

and

$$\mu_n = \sup\left\{ \left\| \sum_{k=1}^{n} c_k \varphi_k \right\|_s : \sum_{k=1}^{n} c_k^2 = 1 \right\}, \qquad \rho_n = \left(\sum_{k=n}^{\infty} |a_k|^2 \right)^{\frac{1}{2}}, \tag{2}$$

for some $s \in (2, +\infty]$. Here $M_n \uparrow$ and $M_n \geq 1$ (see [3], [4, p. 313]).

An orthonormal system $\{u_n\}$ is called uniformly bounded if there is a constant $M > 0$ such that $\|u_n\|_\infty \leq M$, $\forall n \in N$. Note that any uniformly bounded system $\{u_n\}$ satisfies condition (1) but the reversed implication is false.

For one variable function Marcinkiewicz and Zygmund [4] proved the following theorems.

Theorem A (see [4]) *Let the orthogonal system $\{\varphi_n\}$ satisfy the condition (1) and $2 \leq p < s$. If the real number sequence $\{a_n\}$ satisfies the condition*

$$\sum_{n=1}^{\infty} |a_n|^p M_n^{(p-2)\frac{s}{s-2}} n^{(p-2)\frac{s-1}{s-2}} < +\infty,$$

then the series

$$\sum_{n=1}^{\infty} a_n \varphi_n(x)$$

converges in L_p to some function $f \in L_p[0,1]$ and

$$\|f\|_p \leq C_{p,s} \left(\sum_{n=1}^{\infty} |a_n|^p M_n^{(p-2)\frac{s}{s-2}} n^{(p-2)\frac{s-1}{s-2}} \right)^{\frac{1}{p}}.$$

Theorem B (see [4]) *Let the orthogonal system $\{\varphi_n\}$ satisfy the condition (1), and $\frac{s}{s-1} = \mu < p \leq 2$. Then the Fourier coefficients $a_n(f)$ of the function $f \in L_p[0,1]$ with respect to the system $\{\varphi_n\}$ satisfy the inequality*

$$\left(\sum_{n=1}^{\infty} |a_n(f)|^p M_n^{(p-2)\frac{s}{s-2}} n^{(p-2)\frac{s-1}{s-2}} \right)^{\frac{1}{p}} \leq C_{p,s} \|f\|_p.$$

Nowadays there are several generalizations of Theorems A and B for different spaces and systems (see e.g. [5–8] and the corresponding references).

Here we just mention that Flett [8] generalized this to the case of Lorentz spaces and that Maslov [5] proved generalizations of Theorem A and Theorem B in Orlicz spaces.

The problem concerning the summability of the Fourier coefficients by bounded orthonormal system with functions from some Lorentz spaces were investigated e.g. by Stein [9], Bochkarev [10], Kopezhanova and Persson [11] and Kopezhanova [12] (cf. also Persson [13]).

Moreover, Kolyada [6] proved the following improvement of Theorem A.

Theorem C (see [6]) *Let an orthogonal system* $\{\varphi_n\}$ *satisfy the condition* (1), *let the sequence* $\{a_n\} \in l_2$ *and* $\rho_n = (\sum_{k=n}^{\infty} |a_k|^2)^{\frac{1}{2}}$, $2 < q < s \le +\infty$. *If*

$$\Lambda_q(a) = \left[\sum_{n=1}^{\infty} \mu_n^{\frac{(q-2)s}{s-2}} \left(\rho_n^q - \rho_{n+1}^q \right) \right]^{\frac{1}{q}} < +\infty,$$

then the series $\sum_{n=1}^{\infty} a_n \varphi_n(x)$ *converges in the space* L_q *to some function* $f \in L_q$ *and the following inequality holds*: $\|f\|_q \le C_{q,s} \Lambda_q(a)$.

This result was further generalized by Kirillov [7] as follows.

Theorem D (see [7]) *If* $2 < q < s$, $r > 0$, $\delta = \frac{r(q-2)s}{q(s-2)}$ *and the sequence* $\{a_n\} \in l_2$ *satisfies the following condition*:

$$\Omega_{q,r}(a) = \left(\sum_{n=1}^{\infty} \left(\rho_n^r - \rho_{n+1}^r \right) \mu_n^{\delta} \right)^{\frac{1}{r}} < \infty \qquad \left(\mu_n \equiv \mu_n^{(s)}, \qquad \rho_n = \left(\sum_{k=n}^{\infty} |a_k|^2 \right)^{\frac{1}{2}} \right),$$

then the series $\sum_{n=1}^{\infty} a_n \varphi_n(x)$ *converges in space* $L_2[0,1]$ *to some function* f *and the inequality* $\|f\|_{q,r} \le C_{q,r,s} \Omega_{q,r}(a)$ *holds*. (*Here* μ_n *and* ρ_n *are defined by* (2).)

The following well-known lemma is used in our proofs.

Lemma E *Let* $0 < p < \infty$, *and* $\{a_k\}_{k=0}^{\infty}$ *and* $\{b_k\}_{k=0}^{\infty}$ *are non-negative sequences.*

(i) *If*

$$\sum_{n=k}^{\infty} a_n \le C a_k, \quad k = 0, 1, 2, \ldots, \tag{3}$$

then

$$\sum_{n=0}^{\infty} a_n \left(\sum_{k=0}^{n} b_k \right)^p \le C p^p \sum_{n=0}^{\infty} a_n b_n^p.$$

(ii) *If*

$$\sum_{n=0}^{k} a_n \le C a_k, \quad k = 0, 1, 2, \ldots, \tag{4}$$

then

$$\sum_{n=0}^{\infty} a_n \left(\sum_{k=n}^{\infty} b_k \right)^p \le C p^p \sum_{n=0}^{\infty} a_n b_n^p,$$

where C *is a positive number independent of* n.

In this paper we both generalize and complement the statements in Theorems A–D in various ways and always to the case with Lorentz–Zygmund spaces involved. In particular, in Sect. 2 such a generalization of Theorem D (and, thus, of Theorems A and C) is

proved (see Theorem 2.1). In Sect. 3 such a complement of Theorem B to the case $q < 2$ is given (see Theorem 3.1). Finally, in Sect. 4 we present and prove some further results for uniformly bounded systems and give some concluding remarks. In particular, we compare our results with some other recent research. For the reader's convenience we also include a proof of Lemma E in the Appendix.

2 Generalization of Theorem D

In this section we state and prove the following generalization of Theorem D.

Theorem 2.1 *Let $2 < q < s \le +\infty$, $\alpha \in \mathbb{R}$, $r > 0$ and $\delta = \frac{rs(q-2)}{q(s-2)}$. If $\{a_n\} \in l_2$ and*

$$\Omega_{q,r,\alpha}(a) = \left\{ \sum_{n=1}^{\infty} \left(\rho_n^r - \rho_{n+1}^r\right) \mu_n^{\delta} \left(1 + \frac{2s}{s-2} \ln \mu_n\right)^{\alpha r} \right\}^{\frac{1}{r}} < +\infty,$$

where ρ_n and μ_n are defined by (2), then the series

$$\sum_{n=1}^{\infty} a_n \varphi_n(x)$$

with respect to an orthogonal system $\{\varphi_n\}_{n=1}^{\infty}$, which satisfies the condition (1), converges to some function $f \in L_{q,r}(\log L)^{\alpha}$ and $\|f\|_{q,r,\alpha} \le C\Omega_{q,r,\alpha}$.

Corollary 2.2 *For the case $\alpha = 0$, Theorem 2.1 coincides with Theorem D.*

Proof Since the sequence $\{\mu_n\}$ is increasing, let us define the sequence $\{\nu_n\}$ in the following way (see [7]):

$$\nu_1 = 1, \qquad \nu_{n+1} = \min\{k \in \mathbb{N} : \mu_k \ge 2\mu_{\nu_n}\}, \quad n = 1, 2, 3, \ldots.$$

Then $\mu_{\nu_{n+1}} \ge 2\mu_{\nu_n}$, $\mu_{\nu_{n+1}-1} < 2\mu_{\nu_n}$, $n = 1, 2, \ldots$.

Let $t_n = \mu_n^{-\frac{2s}{s-2}}$,

$$u_j(x) = \sum_{k=\nu_j}^{\nu_{j+1}-1} a_k \varphi_k(x),$$

$$S_n(x) = \sum_{k=1}^{n} u_j(x) \quad \text{and} \quad R_n(x) = f(x) - S_n(x).$$

Since $t_n \downarrow 0$ for $n \to +\infty$, by the property of nonincreasing rearrangement of the function (see [14, p. 83]), we get

$$\begin{aligned} \|f\|_{q,r,\alpha}^r &= \sum_{n=1}^{\infty} \int_{t_{n+1}}^{t_n} \left(f^{**}(t)\right)^r \left(1 + |\ln t|\right)^{\alpha r} t^{\frac{r}{q}-1} dt \\ &\le C \left[\sum_{n=1}^{\infty} \int_{t_{n+1}}^{t_n} \left(S_n^{**}(t)\right)^r \left(1 + |\ln t|\right)^{\alpha r} t^{\frac{r}{q}-1} dt \right. \\ &\quad \left. + \sum_{n=1}^{\infty} \int_{t_{n+1}}^{t_n} \left(R_n^{**}(t)\right)^r \left(1 + |\ln t|\right)^{\alpha r} t^{\frac{r}{q}-1} dt \right] := C[I_1 + I_2] \end{aligned} \tag{5}$$

and, moreover,

$$S_n^{**}(t) \le \frac{1}{t}\sum_{j=1}^{n}\int_0^t u_j^*(y)\,dy.$$

By applying Hölder's inequality we obtain

$$\int_0^t u_j^*(y)\,dy \le t^{1-\frac{1}{s}}\rho_{\nu_j}\mu_{\nu_{j+1}-1}.$$

Therefore,

$$S_n^{**}(t) \le t^{-\frac{1}{s}}\sum_{j=1}^{n}\rho_{\nu_j}\mu_{\nu_{j+1}-1}.$$

By using this estimate we find that

$$\begin{aligned} I_1 &\le \sum_{n=1}^{\infty}\int_{t_{n+1}}^{t_n}\left(\sum_{j=1}^{n}\rho_{\nu_j}\mu_{\nu_{j+1}-1}\right)^r\left(1+|\ln t|\right)^{\alpha r}t^{r(\frac{1}{q}-\frac{1}{s})-1}\,dt \\ &\le C\sum_{n=1}^{\infty}\left(\sum_{j=1}^{n}\rho_{\nu_j}\mu_{\nu_{j+1}-1}\right)^r\left(1+|\ln t_n|\right)^{\alpha r}\left(t_n^{r(\frac{1}{q}-\frac{1}{s})}-t_{n+1}^{r(\frac{1}{q}-\frac{1}{s})}\right). \end{aligned}$$

Thus, by taking into account the definition of t_n, we can conclude that

$$I_1 \le \sum_{n=1}^{\infty}\left(\sum_{j=1}^{n}\rho_{\nu_j}\mu_{\nu_{j+1}-1}\right)^r\left(1+\left|\frac{2s}{s-2}\ln\mu_{\nu_n}\right|\right)^{\alpha r}\mu_{\nu_n}^{-r\frac{2(s-q)}{q(s-2)}}. \tag{6}$$

Since for any $\varepsilon>0$ the function $t^{-\varepsilon}\ln t\downarrow 0$ for $t\to+\infty$, according to the definition of the numbers ν_n, we see that

$$\begin{aligned} &\sum_{k=n}^{\infty}\left(1+\left|\frac{2s}{s-2}\ln\mu_{\nu_k}\right|\right)^{\alpha r}\mu_{\nu_k}^{-r\frac{2(s-q)}{q(s-2)}} \\ &\quad\le\left(\frac{1+|\frac{2s}{s-2}\ln\mu_{\nu_n}|}{\mu_{\nu_n}^{\varepsilon}}\right)^{\alpha r}\mu_{\nu_n}^{-r(\frac{2(s-q)}{q(s-2)}-\varepsilon\alpha)}\sum_{k=n}^{\infty}2^{-(k-n)r(\frac{2(s-q)}{q(s-2)}-\varepsilon\alpha)}. \end{aligned}$$

Now choose the number ε such that $\frac{2(s-q)}{q(s-2)}-\varepsilon\alpha>0$. Then

$$\sum_{k=n}^{\infty}2^{-(k-n)r(\frac{2(s-q)}{q(s-2)}-\varepsilon\alpha)} \le \sum_{l=0}^{\infty}2^{-lr(\frac{2(s-q)}{q(s-2)}-\varepsilon\alpha)} < +\infty.$$

Hence,

$$\sum_{k=n}^{\infty}\left(1+\left|\frac{2s}{s-2}\ln\mu_{\nu_k}\right|\right)^{\alpha r}\mu_{\nu_k}^{-r\frac{2(s-q)}{q(s-2)}} \le C\left(1+\left|\frac{2s}{s-2}\ln\mu_{\nu_n}\right|\right)^{\alpha r}\mu_{\nu_n}^{-r\frac{2(s-q)}{q(s-2)}}.$$

Therefore, by Lemma E, we have

$$\sum_{n=1}^{\infty}\left(\sum_{j=1}^{n}\rho_{v_j}\mu_{v_{j+1}-1}\right)^r\left(1+\left|\frac{2s}{s-2}\ln\mu_{v_n}\right|\right)^{\alpha r}\mu_{v_n}^{-r\frac{2(s-q)}{q(s-2)}}$$
$$\le C\sum_{n=1}^{\infty}(\rho_{v_n}\mu_{v_{n+1}-1})^r\left(1+\left|\frac{2s}{s-2}\ln\mu_{v_n}\right|\right)^{\alpha r}\mu_{v_n}^{-r\frac{2(s-q)}{q(s-2)}}.$$

Thus, from (6) it follows that

$$I_1\le C\sum_{n=1}^{\infty}(\rho_{v_n}\mu_{v_n})^r\left(1+\left|\frac{2s}{s-2}\ln\mu_{v_n}\right|\right)^{\alpha r}\mu_{v_n}^{\delta}, \tag{7}$$

where $\delta = r\frac{2(s-q)}{q(s-2)}$. Since $\rho_n\to 0$ for $n\to+\infty$, it yields $\rho_{v_n}^r=\sum_{k=n}^{\infty}(\rho_{v_k}^r-\rho_{v_{k+1}}^r)$. Therefore, by changing the order of summation, we get

$$\sum_{n=1}^{\infty}\rho_{v_n}^r\left(1+\left|\frac{2s}{s-2}\ln\mu_{v_n}\right|\right)^{\alpha r}\mu_{v_n}^{\delta}=\sum_{k=1}^{\infty}(\rho_{v_k}^r-\rho_{v_{k+1}}^r)\sum_{n=1}^{k}\left(1+\left|\frac{2s}{s-2}\ln\mu_{v_n}\right|\right)^{\alpha r}\mu_{v_n}^{\delta}. \tag{8}$$

Since $\delta>0$ and $\mu_{v_{n+1}}\ge 2\mu_{v_n}$, we have $\sum_{n=1}^{k}\mu_{v_n}^{\delta}\le C\mu_{v_k}^{\delta}$. Hence, by again using Lemma E, from (8) it follows that

$$\sum_{n=1}^{\infty}\rho_{v_n}^r\left(1+\left|\frac{2s}{s-2}\ln\mu_{v_n}\right|\right)^{\alpha r}\mu_{v_n}^{\delta}\le C\sum_{k=1}^{\infty}\rho_{v_k}^r\left(1+\left|\frac{2s}{s-2}\ln\mu_{v_k}\right|\right)^{\alpha r}\mu_{v_k}^{\delta}. \tag{9}$$

By now combining inequalities (7) and (9) we obtain

$$I_1\le C\sum_{k=1}^{\infty}\rho_{v_k}^r\left(1+\left|\frac{2s}{s-2}\ln\mu_{v_k}\right|\right)^{\alpha r}\mu_{v_k}^{\delta}. \tag{10}$$

Next we estimate I_2. By using Hölder's inequality we find that $R_n^{**}(t)\le Ct^{-\frac{1}{2}}\|R_n\|_2$. Therefore,

$$I_2\le C\sum_{n=1}^{\infty}\|R_n\|_2\int_{t_{n+1}}^{t_n}\left(1+|\ln t|\right)^{\alpha r}t^{r(\frac{1}{q}-\frac{1}{2})-1}\,dt$$
$$\le C\sum_{n=1}^{\infty}\|R_n\|_2\left(1+|\ln t_n|\right)^{\alpha r}\int_{t_{n+1}}^{t_n}t^{r(\frac{1}{q}-\frac{1}{2})-1}\,dt$$
$$\le C\sum_{n=1}^{\infty}\rho_{v_{n+1}}^r\left(1+\left|\frac{2s}{s-2}\ln\mu_{v_{n+1}}\right|\right)^{\alpha r}\mu_{v_{n+1}}^{\delta}. \tag{11}$$

Next, by repeating the proof of Eq. (9) we obtain

$$\sum_{n=1}^{\infty}\rho_{v_{n+1}}^r\left(1+\left|\frac{2s}{s-2}\ln\mu_{v_{n+1}}\right|\right)^{\alpha r}\mu_{v_{n+1}}^{\delta}\le C\sum_{k=1}^{\infty}\rho_{v_k}^r\left(1+\left|\frac{2s}{s-2}\ln\mu_{v_k}\right|\right)^{\alpha r}\mu_{v_k}^{\delta}. \tag{12}$$

By combining the inequalities (11) and (12) we have

$$I_2 \le C\sum_{k=1}^{\infty}\rho_{\nu_k}^r\left(1+\left|\frac{2s}{s-2}\ln\mu_{\nu_k}\right|\right)^{\alpha r}\mu_{\nu_k}^{\delta}. \tag{13}$$

Moreover, in view of inequalities (10) and (13), from (5) it follows that

$$\|f\|_{q,r,\alpha}^r \le C\sum_{k=1}^{\infty}\rho_{\nu_k}^r\left(1+\left|\frac{2s}{s-2}\ln\mu_{\nu_k}\right|\right)^{\alpha r}\mu_{\nu_k}^{\delta} \tag{14}$$

in the case $\alpha > 0$. Since $\alpha > 0$ and $\mu_n \uparrow$, we see that

$$\begin{aligned}
&\sum_{n=1}^{\infty}(\rho_n^r-\rho_{n+1}^r)\mu_n^{\delta}\left(1+\frac{2s}{s-2}\ln\mu_n\right)^{\alpha r}\\
&\quad=\sum_{k=1}^{\infty}\sum_{n=\nu_k}^{\nu_{k+1}-1}(\rho_n^r-\rho_{n+1}^r)\mu_n^{\delta}\left(1+\frac{2s}{s-2}\ln\mu_n\right)^{\alpha r}\\
&\quad\ge\sum_{k=1}^{\infty}\mu_{\nu_k}^{\delta}\left(1+\frac{2s}{s-2}\ln\mu_{\nu_k}\right)^{\alpha r}\sum_{n=\nu_k}^{\nu_{k+1}-1}(\rho_n^r-\rho_{n+1}^r)\\
&\quad=\sum_{k=1}^{\infty}\mu_{\nu_k}^{\delta}\left(1+\frac{2s}{s-2}\ln\mu_{\nu_k}\right)^{\alpha r}(\rho_{\nu_k}^r-\rho_{\nu_{k+1}}^r).
\end{aligned}$$

Hence, from the inequality (14) it follows that

$$\|f\|_{q,r,\alpha}^r \le C\sum_{n=1}^{\infty}(\rho_n^r-\rho_{n+1}^r)\mu_n^{\delta}\left(1+\frac{2s}{s-2}\ln\mu_n\right)^{\alpha r} \tag{15}$$

in the case $\alpha > 0$.

Let $\alpha < 0$. Then, for any number $\varepsilon > 0$, the function $y^{\varepsilon}(1+\ln y)^{r\alpha}$ increases on $(1,\infty)$. Therefore, by taking into account that $\mu_n \uparrow$, we obtain

$$\begin{aligned}
&\sum_{n=1}^{\infty}(\rho_n^r-\rho_{n+1}^r)\mu_n^{\delta}\left(1+\frac{2s}{s-2}\ln\mu_n\right)^{\alpha r}\\
&\quad=\sum_{k=1}^{\infty}\sum_{n=\nu_k}^{\nu_{k+1}-1}(\rho_n^r-\rho_{n+1}^r)\mu_n^{\delta}\left(1+\frac{2s}{s-2}\ln\mu_n\right)^{\alpha r}\\
&\quad\ge\sum_{k=1}^{\infty}\mu_{\nu_k}^{\varepsilon}\left(1+\frac{2s}{s-2}\ln\mu_{\nu_k}\right)^{\alpha r}\sum_{n=\nu_k}^{\nu_{k+1}-1}(\rho_n^r-\rho_{n+1}^r)\mu_n^{\delta-\varepsilon}.
\end{aligned} \tag{16}$$

Choose $\varepsilon > 0$ such that $\delta - \varepsilon > 0$. Since $\mu_n^{\delta-\varepsilon} \uparrow$, according to the inequality (16), we have

$$\sum_{n=1}^{\infty}(\rho_n^r-\rho_{n+1}^r)\mu_n^{\delta}\left(1+\frac{2s}{s-2}\ln\mu_n\right)^{\alpha r} \ge \sum_{k=1}^{\infty}\mu_{\nu_k}^{\delta}\left(1+\frac{2s}{s-2}\ln\mu_{\nu_k}\right)^{\alpha r}\sum_{n=\nu_k}^{\nu_{k+1}-1}(\rho_n^r-\rho_{n+1}^r)$$

in the case $\alpha < 0$. Therefore (15) holds also for case $\alpha < 0$ and the proof is complete. □

Corollary 2.3 *Let* $\{\varphi_n\}_{n=1}^{\infty}$ *be an uniformly bounded orthogonal system and let* $2 < q < +\infty$, $\alpha \in \mathbb{R}$ *and* $r > 0$.

If

$$\Omega_{q,r}(a) = \left(\sum_{n=1}^{\infty} \left(\rho_n^r - \rho_{n+1}^r\right) n^{\frac{r(q-2)}{2q}} (1 + \ln n)^{\alpha r} \right)^{\frac{1}{r}} < \infty,$$

where ρ_n *are defined by* (2), *then the series* $\sum_{n=1}^{\infty} a_n \varphi_n(x)$ *converges to some function* $f \in L_{q,r}(\log L)^{\alpha}$ *and* $\|f\|_{q,r,\alpha} \le C \cdot \Omega_{q,r,\alpha}$.

Proof Since $\{\varphi_n\}_{n=1}^{\infty}$ is an uniformly bounded orthogonal system, we have $s = +\infty$. Therefore

$$\lim_{s \to +\infty} \frac{rs(q-2)}{q(s-2)} = \frac{r(q-2)}{q}.$$

Now, given that $M_n \le M$, $\mu_n \le \sqrt{n} M$, $n \in \mathbb{N}$, we have

$$\sum_{n=1}^{\infty} \left(\rho_n^r - \rho_{n+1}^r\right) \mu_n^{\delta} \left(1 + \frac{2s}{s-2} \ln \mu_n\right)^{\alpha r} \le C \sum_{n=1}^{\infty} \left(\rho_n^r - \rho_{n+1}^r\right) n^{\frac{r(q-2)}{2q}} (1 + \ln n)^{\alpha r} \tag{17}$$

if $\alpha \ge 0$.

If $\alpha < 0$, then we choose a number ε such that $0 < \varepsilon < \frac{(q-2)}{q}$. Then, by considering the function $(1 + \ln t)^{\alpha} t^{\varepsilon} \uparrow$ on $[1, +\infty)$, we can verify that the inequality (17) holds also for $\alpha < 0$. Consequently, by Theorem 2.1, the statement is true. □

3 A complement of Theorem B. The case $q < 2$

In this section we prove a result which was formulated but not proven in [15]. It may be regarded as a complement of Theorem B relevant for a more general situation.

Theorem 3.1 *Let* $s \in (2, +\infty]$, $\frac{s}{s-1} < q < 2$, $r > 1$, $\alpha \in \mathbb{R}$ *and* $\delta = \frac{r(q-2)s}{q(s-2)}$. *If* $f \in L_{q,r}(\log L)^{\alpha}$, *then the inequality*

$$\left[\sum_{n=1}^{\infty} \left(\sum_{k=\nu_n}^{\nu_{n+1}-1} a_k^2(f) \right)^{\frac{r}{2}} (1 + \log \mu_{\nu_n})^{r\alpha} \mu_{\nu_n}^{\delta} \right]^{\frac{1}{r}} \le C \|f\|_{q,r,\alpha}$$

holds, where μ_{ν_n} *are defined by* (2) *and* $a_n(f)$ *denote the Fourier coefficients of* f *with respect to an orthogonal system* $\{\varphi_n\}_{n=1}^{\infty}$ *satisfying condition* (1).

Remark 3.2 Theorem 3.1 was formulated, but not proved, in [15]. Here we present the details of the proof.

Proof Choose an increasing sequence $\{\nu_n\}$ of natural numbers such that $\nu_1 = 1$, $\nu_{n+1} = \min\{k : \mu_k \ge 2\mu_{\nu_n}\}$, $n = 1, 2, 3, \ldots$. Then $\mu_{\nu_{n+1}} \ge 2\mu_{\nu_n}$, $\mu_{\nu_{n+1}-1} < 2\mu_{\nu_n}$. Since the system

$\{\varphi_n\}$ is orthogonal we have

$$\left|\int_0^1 f(x)g(x)\,dx\right| = \left|\sum_{k=1}^{\infty} a_k(f)b_k(g)\right|$$

for any function $g \in L_{q',r'}(\log L)^{-\alpha}$, $\frac{1}{r}+\frac{1}{r'}=1$ and $\frac{1}{q}+\frac{1}{q'}=1$. Let

$$b_k := \left[\sum_{n=1}^{\infty}\left(\sum_{k=\nu_n}^{\nu_{n+1}-1} a_k^2(f)\right)^{\frac{r}{2}}(1+\log\mu_{\nu_n})^{r\alpha}\mu_{\nu_n}^{\delta}\right]^{-\frac{1}{r'}} \times \left(\sum_{k=\nu_n}^{\nu_{n+1}-1}\left|a_k(f)\right|^2\right)^{\frac{r-2}{2}}(1+\log\mu_{\nu_n})^{r\alpha}\mu_{\nu_n}^{\delta}a_k(f) \tag{18}$$

for $k=\nu_n,\dots,\nu_{n+1}-1$, $n=1,2,\dots$, and consider a function $g \in L_{q',r'}(\log L)^{-2}$ with Fourier coefficients $b_k(g)=b_k$. Then

$$\left|\int_0^1 f(x)g(x)\,dx\right| = \left|\sum_{n=1}^{\infty}\sum_{k=\nu_n}^{\nu_{n+1}-1} a_k(f)b_k(g)\right| = \left[\sum_{n=1}^{\infty}\left(\sum_{k=\nu_n}^{\nu_{n+1}-1} a_k^2(f)\right)^{\frac{r}{2}}(1+\log\mu_{\nu_n})^{r\alpha}\mu_{\nu_n}^{\delta}\right]^{\frac{1}{r}}. \tag{19}$$

Taking into account that $rr'=r+r'$, by Theorem 2.1 and (18), we have

$$\begin{aligned}
\|g\|_{q',r',-\alpha} &\le C\left\{\sum_{n=1}^{\infty}\left(\sum_{k=\nu_n}^{\nu_{n+1}-1} b_k^2(g)\right)^{\frac{r'}{2}}(1+\log\mu_{\nu_n})^{-r'\alpha}\mu_{\nu_n}^{\frac{s(q'-2)}{(s-2)q'}\cdot r'}\right\}^{\frac{1}{r'}} \\
&= C\left[\sum_{n=1}^{\infty}\left(\sum_{k=\nu_n}^{\nu_{n+1}-1} a_k^2(f)\right)^{\frac{r}{2}}(1+\log\mu_{\nu_n})^{r\alpha}\mu_{\nu_n}^{\delta}\right]^{-\frac{1}{r'}} \\
&\quad\times\left\{\sum_{n=1}^{\infty}\left(\sum_{k=\nu_n}^{\nu_{n+1}-1} a_k^2(f)\right)^{\frac{r'}{2}}\left(\sum_{k=\nu_n}^{\nu_{n+1}-1} a_k^2(f)\right)^{\frac{r'}{2}(r-2)}\right. \\
&\quad\left.\times(1+\log\mu_{\nu_n})^{-r'\alpha}\mu_{\nu_n}^{\frac{s(q'-2)}{(s-2)q'}\cdot r'}(1+\log\mu_{\nu_n})^{rr'\alpha}\mu_{\nu_n}^{\frac{s(q-2)}{(s-2)q}rr'}\right\}^{\frac{1}{r'}} \\
&= C\left[\sum_{n=1}^{\infty}\left(\sum_{k=\nu_n}^{\nu_{n+1}-1} a_k^2(f)\right)^{\frac{r}{2}}(1+\log\mu_{\nu_n})^{r\alpha}\mu_{\nu_n}^{\delta}\right]^{-\frac{1}{r'}} \\
&\quad\times\left[\sum_{n=1}^{\infty}\left(\sum_{k=\nu_n}^{\nu_{n+1}-1} a_k^2(f)\right)^{\frac{r}{2}}(1+\log\mu_{\nu_n})^{r\alpha}\mu_{\nu_n}^{\delta}\right]^{\frac{1}{r'}} = C.
\end{aligned}$$

Thus, the function $g_0 := C^{-1}g \in L_{q',r'}(\log L)^{-\alpha}$ and $\|g_0\|_{q',r',-\alpha} \le 1$. Next, by the property of the norm in the Lorentz–Zygmund space and using equality (19), we get

$$\|f\|_{q,r,\alpha} \asymp \sup_{\substack{g\in L_{q',r'}(\log L)^{-\alpha} \\ \|g\|_{q',r',-\alpha}\le 1}} \left|\int_0^1 f(x)g(x)\,dx\right| \ge \left|\int_0^1 f(x)g_0(x)\,dx\right|$$

$$= C^{-1}\left[\sum_{n=1}^{\infty}\left(\sum_{k=\nu_n}^{\nu_{n+1}-1} a_k^2(f)\right)^{\frac{r}{2}}\mu_{\nu_n}^{\delta}\right]^{\frac{1}{r}}.$$

The proof is complete. □

4 Further results and concluding remarks

In this section we first prove some results which are closely related to but not covered by the results in the previous sections (Propositions 4.1 and 4.2). After that, we present some results of a similar kind (see [11, 12] and Theorem F) and in remarks we point out how these results can be compared with our results in some special cases when such a comparison is possible.

Proposition 4.1 *Let $\{\varphi_n\}_{n=1}^{\infty}$ be an uniformly bounded orthogonal system and $2 < q < +\infty$, $\alpha \in \mathbb{R}$ and $r > 1$. If*

$$\Omega_{q,r,\alpha}(a) = \left(\sum_{n=1}^{\infty} |a_n|^r n^{r(1-\frac{1}{q}-\frac{1}{r})}(1+\ln n)^{\alpha r}\right)^{\frac{1}{r}} < \infty,$$

then the series $\sum_{n=1}^{\infty} a_n\varphi_n(x)$ converges to some function $f \in L_{q,r}(\log L)^{\alpha}$ and $\|f\|_{q,r,\alpha} \le C\Omega_{q,r,\alpha}(a)$.

Proof Since $\rho_n \downarrow 0$ when $n \to +\infty$, we can choose numbers $n_1 = 1$,

$$n_{k+1} = \min\left\{n \in \mathbb{N} : \rho_{n_{k+1}} \le \frac{1}{2}\rho_{n_k}\right\}, \quad k = 1, 2\ldots.$$

Therefore, if $\alpha \ge 0$, it yields

$$\sum_{n=1}^{\infty}\left(\rho_n^r - \rho_{n+1}^r\right)n^{\frac{r(q-2)}{2q}}(1+\ln n)^{\alpha r} = \sum_{k=2}^{\infty}(n_k-1)^{\frac{r(q-2)}{2q}}(1+\ln n_k)^{\alpha r}\left(\rho_{n_{k-1}}^r - \rho_{n_k}^r\right). \tag{20}$$

For any numbers $k = 2, 3, \ldots$, the following inequality holds:

$$\rho_{n_{k-1}}^r - \rho_{n_k}^r \le \rho_{n_{k-1}}^r \le 2^r\left(\rho_{n_{k-1}}^2\right)^{\frac{r}{2}}. \tag{21}$$

Since $\rho_{n_{k+1}} \le \frac{1}{2}\rho_{n_k} \le \frac{1}{2}\rho_{n_k-1}$, we have

$$\rho_{n_k-1}^2 - \rho_{n_{k+1}}^2 \ge \rho_{n_k-1}^2 - \left(\frac{1}{2}\rho_{n_k-1}\right)^2 = \frac{3}{4}\rho_{n_k-1}^2. \tag{22}$$

By using (21) and (22), we can obtain the following inequality:

$$\rho_{n_{k-1}}^r - \rho_{n_k}^r \le 2^r \left(\frac{4}{3}\right)^{\frac{r}{2}} \left(\sum_{n=n_k-1}^{n_{k+1}-1} |a_n|^2\right)^{\frac{r}{2}}. \tag{23}$$

Therefore, from (20) it follows that

$$\sum_{n=1}^{\infty} \left(\rho_n^r - \rho_{n+1}^r\right) n^{\frac{r(q-2)}{2q}} (1+\ln n)^{\alpha r} \le C_r \sum_{k=2}^{\infty} (n_k-1)^{\frac{r(q-2)}{2q}} (1+\ln n_k)^{\alpha r} \left(\sum_{n=n_k-1}^{n_{k+1}-1} |a_n|^2\right)^{\frac{r}{2}} \tag{24}$$

when $\alpha \ge 0$.

If $\alpha < 0$, then we can choose a number ε which satisfies $0 < \varepsilon < \frac{q-2}{2q}$. We note that $(1+\ln n)^{\alpha} n^{\varepsilon} \uparrow$ and we obtain the following inequality:

$$\begin{aligned}
&\sum_{n=n_{k-1}}^{n_k-1} \left(\rho_n^r - \rho_{n+1}^r\right) n^{\frac{r(q-2)}{2q}} (1+\ln n)^{\alpha r} \\
&= \sum_{n=n_{k-1}}^{n_k-1} \left(\rho_n^r - \rho_{n+1}^r\right) n^{\frac{r(q-2)}{2q} - r\varepsilon} \left((1+\ln n)^{\alpha} n^{\varepsilon}\right)^r \\
&\le (n_k-1)^{\frac{r(q-2)}{2q} - r\varepsilon} \left((1+\ln(n_k-1))^{\alpha} (n_k-1)^{\varepsilon}\right)^r \sum_{n=n_{k-1}}^{n_k-1} \left(\rho_n^r - \rho_{n+1}^r\right) \\
&= (n_k-1)^{\frac{r(q-2)}{2q}} \left(1+\ln(n_k-1)\right)^{\alpha r} \left(\rho_{n_{k-1}}^r - \rho_{n_k}^r\right).
\end{aligned} \tag{25}$$

By now combining the inequalities (20), (23) and (25), we conclude that (24) holds also for the case $\alpha < 0$.

If $r > 2$, then, by using Hölder's inequality with $\theta = \frac{r}{2}$, $\frac{1}{\theta} + \frac{1}{\theta'} = 1$, we obtain

$$\sum_{n=n_k-1}^{n_{k+1}-1} |a_n|^2 \le \left(\sum_{n=n_k-1}^{n_{k+1}-1} |a_n|^r n^{r(1-\frac{1}{q})-1}\right)^{\frac{2}{r}} \left(\sum_{n=n_k-1}^{n_{k+1}-1} n^{\theta'(\frac{1}{\theta}-2(1-\frac{1}{q}))}\right)^{\frac{1}{\theta'}}. \tag{26}$$

Since $2 < q$, we have $1 + \theta'(\frac{1}{\theta} - 2(1-\frac{1}{q})) = \theta'(\frac{2}{q} - 1) < 0$. Therefore,

$$\begin{aligned}
\sum_{n=n_k-1}^{n_{k+1}-1} n^{\theta'(\frac{1}{\theta}-2(1-\frac{1}{q}))} &\le C_{r,q} \int_{n_k-1}^{n_{k+1}} t^{\theta'(\frac{1}{\theta}-2(1-\frac{1}{q}))}\, dt \\
&\le \frac{C_{r,q}}{\theta'(2(1-\frac{1}{q}) - \frac{1}{\theta}) - 1} (n_k-1)^{1+\theta'(\frac{1}{\theta}-2(1-\frac{1}{q}))}
\end{aligned} \tag{27}$$

for $k = 2, 3, \ldots$. From inequalities (26) and (27), we can derive the following inequality:

$$\sum_{n=n_k-1}^{n_{k+1}-1} |a_n|^2 \le C (n_k-1)^{\frac{1}{\theta'} + \frac{1}{\theta} - 2(1-\frac{1}{q})} \left(\sum_{n=n_k-1}^{n_{k+1}-1} |a_n|^r n^{r(1-\frac{1}{q})-1}\right)^{\frac{2}{r}} \tag{28}$$

for $k = 2, 3, \ldots$, in the case of $2 < r < \infty$.

Now, by combining (26) and (28), we obtain the following inequality:

$$\sum_{n=1}^{\infty}\left(\rho_n^r-\rho_{n+1}^r\right)n^{\frac{r(q-2)}{2q}}(1+\ln n)^{\alpha r}$$
$$\le\sum_{k=2}^{\infty}(n_k-1)^{\frac{r(q-2)}{2q}}(1+\ln n_k)^{\alpha r}(n_k-1)^{\frac{r}{2}(1-2(1-\frac{1}{q}))}\sum_{n=n_k-1}^{n_{k+1}-1}|a_n|^r n^{r(1-\frac{1}{q})-1} \tag{29}$$

in the case of $2<r<\infty$, $0<\alpha<\infty$.

Since

$$\frac{r(q-2)}{2q}+\frac{r}{2}\left(1-2\left(1-\frac{1}{q}\right)\right)=0,$$

it follows from (29) that

$$\sum_{n=1}^{\infty}\left(\rho_n^r-\rho_{n+1}^r\right)n^{\frac{r(q-2)}{2q}}(1+\ln n)^{\alpha r}\le C\sum_{k=2}^{\infty}\sum_{n=n_k-1}^{n_{k+1}-1}|a_n|^r n^{r(1-\frac{1}{q})-1}(1+\ln n)^{\alpha r} \tag{30}$$

in the case $2<r<\infty$, $0<\alpha<\infty$.

Furthermore,

$$\sum_{k=2}^{\infty}\sum_{n=n_k-1}^{n_{k+1}-1}|a_n|^r n^{r(1-\frac{1}{q})-1}(1+\ln n)^{\alpha r}$$
$$\le\sum_{k=2}^{\infty}\sum_{n=n_{k-1}}^{n_k-1}|a_n|^r n^{r(1-\frac{1}{q})-1}(1+\ln n)^{\alpha r}+\sum_{k=2}^{\infty}\sum_{n=n_k}^{n_{k+1}-1}|a_n|^r n^{r(1-\frac{1}{q})-1}(1+\ln n)^{\alpha r}$$
$$\le 2\sum_{n=1}^{\infty}|a_n|^r n^{r(1-\frac{1}{q})-1}(1+\ln n)^{\alpha r} \tag{31}$$

in the case $2<r<\infty$, $0<\alpha<\infty$.

If $\alpha<0$, then we choose a number ε which satisfies $0<\varepsilon<\frac{q-2}{2q}$. By using the Hölder inequality, we obtain ($\theta=\frac{r}{2}$, $\frac{1}{\theta}+\frac{1}{\theta'}=1$)

$$\sum_{n=n_k-1}^{n_{k+1}-1}|a_n|^2\le\left(\sum_{n=n_k-1}^{n_{k+1}-1}|a_n|^r n^{r(1-\frac{1}{q})-\varepsilon\theta-1}\right)^{\frac{2}{r}}\left(\sum_{n=n_k-1}^{n_{k+1}-1}n^{\theta'(\frac{1}{\theta}-2(1-\frac{1}{q})+\varepsilon)}\right)^{\frac{1}{\theta'}}. \tag{32}$$

According to the choice of the number ε it shows that

$$1+\theta'\left(\frac{1}{\theta}-2\left(1-\frac{1}{q}\right)+\varepsilon\right)=\theta'\left(\frac{2}{q}-1+\varepsilon\right)<0.$$

Therefore (as in the case of $\alpha>0$) we obtain the following inequality:

$$\sum_{n=n_k-1}^{n_{k+1}-1}n^{\theta'(\frac{1}{\theta}-2(1-\frac{1}{q})+\varepsilon)}\le C_{r,q}\int_{n_k-1}^{n_{k+1}}t^{\theta'(\frac{1}{\theta}-2(1-\frac{1}{q})+\varepsilon)}\,dt$$
$$\le\frac{C_{r,q}}{\theta'(2(1-\frac{1}{q})-1-\varepsilon)}(n_k-1)^{1+\theta'(\frac{1}{\theta}-2(1-\frac{1}{q})+\varepsilon)} \tag{33}$$

for $k = 2, 3, \ldots$. Thus, in view of (32) and (33), the following inequality holds:

$$\sum_{n=n_k-1}^{n_{k+1}-1} |a_n|^2 \le C(n_k-1)^{1+\theta'(\frac{1}{\theta}-2(1-\frac{1}{q})+\varepsilon)} \left(\sum_{n=n_k-1}^{n_{k+1}-1} |a_n|^r n^{r(1-\frac{1}{q})-\varepsilon\theta-1} \right)^{\frac{2}{r}}$$

for the case of $2 < r < \infty$, $\alpha < 0$. Hence, we can consider the function $(1+\ln n)^{\alpha} n^{\frac{\varepsilon}{2}} \uparrow$, and from the inequality (24), we obtain the following inequality:

$$\begin{aligned} &\sum_{n=1}^{\infty} \left(\rho_n^r - \rho_{n+1}^r\right) n^{\frac{r(q-2)}{2q}} (1+\ln n)^{\alpha r} \\ &\quad \le C \sum_{k=2}^{\infty} \left(1+\ln(n_k-1)^{\alpha r} (n_k-1)^{\frac{r}{2}\varepsilon}\right) \sum_{n=n_k-1}^{n_{k+1}-1} |a_n|^r n^{r(1-\frac{1}{q})-1} \\ &\quad \le C \sum_{k=2}^{\infty} \sum_{n=n_k-1}^{n_{k+1}-1} |a_n|^r n^{r(1-\frac{1}{q})-1} (1+\ln n)^{\alpha r} \end{aligned} \tag{34}$$

for the case of $2 < r < \infty$, $\alpha < 0$. Thus, it follows from inequalities (30), (31) and (34) that

$$\sum_{n=1}^{\infty} \left(\rho_n^r - \rho_{n+1}^r\right) n^{\frac{r(q-2)}{2q}} (1+\ln n)^{\alpha r} \le C \sum_{n=1}^{\infty} |a_n|^r n^{r(1-\frac{1}{q})-1} (1+\ln n)^{\alpha r}$$

and the proof is complete. □

Our next result reads as follows.

Proposition 4.2 *Let $\{\varphi_n\}_{n=1}^{\infty}$ be an uniformly bounded orthogonal system, $2 < q < +\infty$, $\alpha \in \mathbb{R}$ and $r > 0$. If $|a_n| \downarrow 0$, $n \to \infty$, $\{a_n\} \in l_2$ and*

$$\sum_{n=1}^{\infty} |a_n|^r n^{r(1-\frac{1}{q})-1} (1+\ln n)^{\alpha r} < +\infty,$$

then the series $\sum_{n=1}^{\infty} a_n \varphi_n(x)$ converges to some function $f \in L_{q,r}(\log L)^{\alpha}$ and

$$\|f\|_{q,r,\alpha} \le C \left\{ \sum_{n=1}^{\infty} |a_n|^r n^{r(1-\frac{1}{q})-1} (1+\ln n)^{\alpha r} \right\}^{\frac{1}{r}}.$$

Proof It is easy to see that

$$\begin{aligned} &\sum_{n=1}^{\infty} \left(\rho_n^r - \rho_{n+1}^r\right) n^{\frac{r(q-2)}{2q}} (1+\log n)^{\alpha r} \\ &\quad \le C \sum_{k=1}^{\infty} 2^{k\frac{r(q-2)}{2q}} (1+k)^{\alpha r} \left(\rho_{2^{k-1}}^r - \rho_{2^k}^r\right) \\ &\quad = C \sum_{k=1}^{\infty} 2^{k\frac{r(q-2)}{2q}} (1+k)^{\alpha r} \left(\sum_{\nu=k}^{\infty} \sum_{l=2^{\nu-1}}^{2^{\nu}-1} |a_l|^2 \right)^{\frac{r}{2}}. \end{aligned} \tag{35}$$

Since $2 < q < \infty$, we have

$$\sum_{k=1}^{\nu} 2^{k\frac{r(q-2)}{2q}}(1+k)^{\alpha r} \le C 2^{\nu\frac{r(q-2)}{2q}}(1+\nu)^{\alpha r}, \quad \nu = 1,2\ldots.$$

Therefore, by Lemma E, we obtain

$$\sum_{k=1}^{\infty} 2^{k\frac{r(q-2)}{2q}}(1+k)^{\alpha r}\left(\sum_{\nu=k}^{\infty}\sum_{l=2^{\nu-1}}^{2^{\nu}-1}|a_l|^2\right)^{\frac{r}{2}} \le \sum_{k=1}^{\infty} 2^{k\frac{r(q-2)}{2q}}(1+k)^{\alpha r}\left(\sum_{l=2^{k-1}}^{2^{k}-1}|a_l|^2\right)^{\frac{r}{2}}. \tag{36}$$

Moreover, since $|a_n| \downarrow 0$, $n \to \infty$, it yields

$$\left(\sum_{l=2^{k-1}}^{2^{k}-1}|a_l|^2\right)^{\frac{r}{2}} \le \left(2^{k-1}\right)^{\frac{r}{2}}|a_{2^{k-1}}|^r, \quad k = 1,2,\ldots.$$

Thus,

$$\sum_{k=1}^{\infty} 2^{k\frac{r(q-2)}{2q}}(1+k)^{\alpha r}\left(\sum_{l=2^{k-1}}^{2^{k}-1}|a_l|^2\right)^{\frac{r}{2}} \le C\sum_{k=1}^{\infty} 2^{kr(1-\frac{1}{q})}(1+k)^{\alpha r}|a_{2^{k-1}}|^r. \tag{37}$$

Furthermore, since the sequence $\{|a_n|\}$ is monotonic, we can easily verify that

$$\sum_{n=2^{k-2}}^{2^{k-1}-1}|a_n|^r n^{r(1-\frac{1}{q})-1}(1+n)^{\alpha r} \ge C|a_{2^{k-1}}|^r 2^{kr(1-\frac{1}{q})}(1+k)^{\alpha r}, \quad k = 2,3,\ldots.$$

Therefore, it follows from inequality (37) that

$$\sum_{k=1}^{\infty} 2^{k\frac{r(q-2)}{2q}}(1+k)^{\alpha r}\left(\sum_{l=2^{k-1}}^{2^{k}-1}|a_l|^2\right)^{\frac{r}{2}} \le C\left\{|a_1|^r + \sum_{n=1}^{\infty}|a_n|^r n^{r(1-\frac{1}{q})-1}(1+n)^{\alpha r}\right\}. \tag{38}$$

Now, from the inequalities (35), (36), and (38) we can deduce that

$$\sum_{n=1}^{\infty}\left(\rho_n^r - \rho_{n+1}^r\right)n^{\frac{r(q-2)}{2q}}(1+\log n)^{\alpha r} \le C\sum_{n=1}^{\infty}|a_n|^r n^{r(1-\frac{1}{q})-1}(1+n)^{\alpha r}.$$

Therefore, in view of Corollary 2.3, the statement in the proposition holds. □

Remark 4.3 We may ask wether it is possible to generalize the results obtained in this paper to more general Lorentz–Zygmund type spaces by replacing the weight $(1+|\ln t|)^{\alpha r}t^{r/q-1}$ by a more general weight $\lambda(t)$. Of course, we must still have some control of the growth properties of the weight. Below we will just briefly describe one such a possibility namely the quasi-monotone weights, used in recent work of Kopezhanova and Persson (see [11, 12]).

Let $0 < r < \infty$, $0 < \beta < \infty$ and $\lambda = \lambda(t)$ be a positive function defined on $(0, \infty)$. Consider all functions f for which

$$\|f\|_{\Lambda_\beta(\lambda)} := \left\{ \int_0^1 \left(f^*(t) t \lambda\left(\frac{1}{t}\right)\right)^\beta \frac{dt}{t} \right\}^{\frac{1}{\beta}} < +\infty.$$

Note that if $\lambda(y) = y^{1-\frac{1}{q}} (\log(2y))^\alpha$, $\alpha \in \mathbb{R}$, then, for $t \in (0,1]$, the function $t\lambda(\frac{1}{t}) = t^{\frac{1}{q}}(1 + \log \frac{1}{t})^\alpha$. Therefore

$$\|f\|_{\Lambda_\beta} = \left\{ \int_0^1 \left(f^*(t)\right)^\beta t^{\frac{\beta}{q}} \left(1 + \log \frac{1}{t}\right)^{\alpha\beta} \frac{dt}{t} \right\}^{\frac{1}{\beta}}$$

so that Λ_β is just the Lorentz–Zygmund space $L_{q,\beta}(\log L)^\alpha$.

We consider the following classes of functions $B = \bigcup_{\delta>0} B_\delta$ and $A = \bigcup_{\delta>0} A_\delta$:

$$B_\delta = \left\{ \lambda : \lambda(y) y^{-\frac{1}{2}-\delta} \uparrow \text{ and } \lambda(y) y^{-1+\delta} \downarrow \text{ on } [1,\infty) \right\},$$

$$A_\delta = \left\{ \lambda : \lambda(y) y^{-\frac{1}{2}-\delta} \uparrow \text{ and } \lambda(y) y^{-1+\delta} \downarrow \text{ on } [1,\infty) \right\}.$$

The following result was proved by Kopezhanova and Persson (see [11, Theorem 2] and [12, p. 45]).

Theorem F *Let $0 < \beta < \infty$, and assume that the orthonormal system $\Phi = \{\varphi_k\}_{k=1}^\infty$ is uniformly bounded.*

(a) *If $\lambda(t)$ belongs to the class A, then*

$$\left(\sum_{n=1}^\infty \left(a_n^* \lambda(n)\right)^\beta \frac{1}{n} \right)^{\frac{1}{\beta}} \le c_1 \|f\|_{\Lambda_\beta(\lambda)},$$

where $\{a_n^*\}$ is the nonincreasing rearrangement of the sequence $\{|a_k|\}_{k=1}^\infty$ of Fourier coefficients of f with respect to the system Φ.

(b) *If $\lambda(t)$ belongs to the class B and $f \overset{\text{a.e.}}{=} \sum_{n=1}^\infty a_n \varphi_n$, then*

$$\|f\|_{\Lambda_\beta(\lambda)} \le c_2 \left(\sum_{n=1}^\infty \left(a_n^* \lambda(n)\right)^\beta \frac{1}{n} \right)^{\frac{1}{\beta}}. \tag{39}$$

Here the constants c_1 and c_2 do not depend on f.

In the case of $\lambda(y) = y^{1-\frac{1}{q}} (\log(2y))^\alpha$, $\alpha \in \mathbb{R}$, from part (b) of Theorem F we obtain the following assertion.

Corollary 4.4 *Let $0 < \beta < \infty$, and assume that the orthonormal system $\Phi = \{\varphi_k\}_{k=1}^\infty$ is bounded. If $2 < q < \infty$, $0 < \beta < \infty$, and $f \overset{\text{a.e.}}{=} \sum_{n=1}^\infty a_n \varphi_n$, then*

$$\|f\|_{q,\beta,\alpha} \le C \left(\sum_{n=1}^\infty \left(a_n^*\right)^\beta n^{\beta(1-\frac{1}{q})-1} (1 + \ln n)^{\alpha\beta} \right)^{\frac{1}{\beta}}.$$

Proof For the function $\lambda(y) = y^{1-\frac{1}{q}}(\log(2y))^{\alpha} \in B$ there exists a number $\delta > 0$ such that $\lambda(y) \in B_{\delta}$. If $\frac{1}{2} - \frac{1}{q} - \delta > 0$, then $\lambda(y)y^{-\frac{1}{2}-\delta} = y^{\frac{1}{2}-\frac{1}{q}-\delta}(1 + \log y)^{\alpha} \uparrow$ on the interval $[1, \infty)$. Hence $2 < q < \infty$.

Further, the function $\lambda(y)y^{-1+\delta} = y^{\delta-\frac{1}{q}}(1 + \log y)^{\alpha} \downarrow$ on the interval $[1, \infty)$ if $\delta - \frac{1}{q} < 0$.

Thus, there is a number $\delta \in (0, \min\{\frac{1}{q}, \frac{1}{2} - \frac{1}{q}\})$ such that the function $\lambda(y) = y^{1-\frac{1}{q}}(1 + \log y)^{\alpha} \in B_{\delta}$. Therefore, by using (39), we see that the statement holds. □

Remark 4.5 Obviously, Proposition 4.2 is more general than Corollary 4.4. We also note that in the case when the sequence $\{a_n\}_{n=1}^{\infty}$ is non-negative and decreasing the assertions of Proposition 4.2 and Corollary 4.4 coincide.

Remark 4.6 In [12] (see Theorem 2.1, Theorem 2.3), theorems on the convergence of series of the Fourier coefficients of a function from the generalized Lorentz space $\Lambda_{\beta}(\lambda)$ with respect to regular systems are proved. It is known that a regular system is uniformly bounded (see [16, p. 117]). Therefore, the assertions of Theorem 2.1 and Theorem 3.1 of this paper do not follow from the results of [12]. Since $\|f\|_s \le \|f\|_{\infty}$, for the functions $f \in L_{\infty}[0, 1]$, if orthogonal system $\{\varphi_n\}$ satisfies the condition (1), then $\{\varphi_n\}$ is uniformly bounded.

Appendix: Proof of Lemma E

The proof of Lemma E is a consequence of a well-known inequality of Leindler [17]. For the reader's convenience we present a proof which is similar to but simpler than that in the research report [18] by Johansson.

(i) If $0 < p < 1$, then

$$\left(\sum_{k=0}^{n} b_k\right)^{p} \le \sum_{k=0}^{n} b_k^{p}.$$

By using this inequality, changing the order of summation and taking into account the condition (3) we get

$$\sum_{n=0}^{\infty} a_n \left(\sum_{k=0}^{n} b_k\right)^{p} \le \sum_{n=0}^{\infty} a_n \sum_{k=0}^{n} b_k^{p} = \sum_{k=0}^{\infty} b_k^{p} \sum_{n=k}^{\infty} a_n \le C \sum_{k=0}^{\infty} a_k b_k^{p},$$

in the case $0 < p < 1$.

Let $1 \le p < \infty$. The following inequalities are proved in [17]:

$$\sum_{n=0}^{\infty} a_n \left(\sum_{k=0}^{n} b_k\right)^{p} \le p^{p} \sum_{n=0}^{\infty} a_n^{1-p} \left(\sum_{k=n}^{\infty} a_k\right)^{p} b_n, \tag{40}$$

$$\sum_{n=0}^{\infty} a_n \left(\sum_{k=n}^{\infty} b_k\right)^{p} \le p^{p} \sum_{n=0}^{\infty} a_n^{1-p} \left(\sum_{k=0}^{n} a_k\right)^{p} b_n. \tag{41}$$

Now it is easy to verify that condition (3) and inequality (40) imply statement (i) also in the case of $1 \le p < \infty$.

(ii) If $0 < p < 1$, then

$$\left(\sum_{k=n}^{\infty} b_k\right)^p \le \sum_{k=n}^{\infty} b_k^p.$$

Using this inequality, changing the order of summation and taking into account the condition (4), we obtain

$$\sum_{n=0}^{\infty} a_n \left(\sum_{k=n}^{\infty} b_k\right)^p \le \sum_{n=0}^{\infty} a_n \sum_{k=n}^{\infty} b_k^p = \sum_{k=0}^{\infty} b_k^p \sum_{n=0}^{k} a_n \le C \sum_{k=0}^{\infty} a_k b_k^p$$

in the case $0 < p < 1$.

If $1 \le p < \infty$, then statement (ii) follows from (4) and (41).

Acknowledgements
We thank the referees and Professors Dag Lukkasson and Annette Meidell for some good advice which improved the final version of the paper. Moreover, the first author is grateful for the support of this work given by the Russian Academic Excellence Project (agreement no. 02.A03.21.0006 of August 27, 2013, between the Ministry of Education and Science of the Russian Federation and Ural Federal University).

Funding
Not applicable.

Availability of data and materials
Not applicable.

Competing interests
The authors declare that they have no competing interests.

Authors' contributions
The authors contributed equally to the writing of this paper. All authors approved the final version of the manuscript.

Author details
[1]Department of Fundamental Mathematics, L.N. Gumilyov Eurasian National University, Astana, Republic of Kazakhstan. [2]Institute of Mathematics and Computer Science, Ural Federal University, Yekaterinburg, Russia. [3]Department of Computer Science and Computational Engineering Campus Narvik, The Artic University of Norway, Narvik, Norway.

Publisher's Note

Received: 6 February 2019 Accepted: 30 May 2019 Published online: 13 June 2019

References

1. Sharpley, R.: Counterexamples for classical operators on Lorentz–Zygmund spaces. Stud. Math. **58**, 141–158 (1980)
2. Nikol'ski, S.M.: Approximation of Classes of Functions of Several Variables and Embedding Theorems. Nauka, Moscow (1977)
3. Zygmund, A.: Trigonometric Series, vol. II. Izdat. "Mir", Moscow (1965)
4. Marcinkiewicz, J., Zygmund, A.: Some theorems on orthogonal systems. Fundam. Math. **28**, 309–335 (1937)
5. Maslov, A.V.: Estimates of Hausdorff–Young type for Fourier coefficients. Vestnik Moscow Univ. Ser. I Mat. Mekh. **3**, 19–22 (1982) (Russian)
6. Kolyada, V.I.: Some generalizations of the Hardy–Littlewood–Paley theorem. Mat. Zametki **54**(3), 48–71 (1993) (Translation in Math. Notes **51**(3–4), 908–922 (1992))
7. Kirillov, S.A.: Norm estimates of functions in Lorentz spaces. Acta Sci. Math. **65**(1–2), 189–201 (1999)
8. Flett, T.M.: On a theorem of Pitt. J. Lond. Math. Soc. **2**(7), 376–384 (1973)
9. Stein, E.M.: Interpolation of linear operators. Trans. Am. Math. Soc. **83**, 482–492 (1956)
10. Bochkarev, S.V.: The Hausdorf–Young–Riesz theorem in Lorentz spaces and multiplicative inequalities. Tr. Mat. Inst. Steklova **219**, 103–114 (1997) (Translation in Proc. Steklov Inst. Math. **219**(4), 96–107 (1997))
11. Kopezhanova, A.N., Persson, L.-E.: On summability of the Fourier coefficients in bounded orthonormal systems for functions from some Lorentz type spaces. Eurasian Math. J. **1**(2), 76–85 (2010)
12. Kopezhanova, A.: Summability of Fourier transforms of functions from Lorentz spaces. Ph.D. thesis, Department of Engineering Sciences and Mathematics, Luleå University of Technology (2017)
13. Persson, L.-E.: Relation between summability of functions and their Fourier series. Acta Math. Acad. Sci. Hung. **27**(3–4), 267–280 (1976)

14. Krein, S.G., Petunin, Y.I., Semenov, E.M.: Interpolation of Linear Operators. Nauka, Moscow (1978)
15. Mustahaeva, V.M., Akishev, G.: On the Fourier coefficients in Lorentz–Zygmund space. In: Modern Methods of the Theory of Functions and Problems, Voronezh, pp. 155–156 (2013)
16. Nursultanov, E.D.: On the coefficients of multiple Fourier series from L_p-spaces. Izv. Ross. Akad. Nauk, Ser. Mat. **64**(1), 95–122 (2000) (Russian) (Translation in Izv. Math. **64**(1), 93–120 (2000))
17. Leindler, L.: Generalization of inequalities of Hardy and Littlewood. Acta Sci. Math. **31**, 279–285 (1970)
18. Johansson, H.: Embedding of H_p^ω in some Lorentz spaces. Research Report 6, Department of Mathematics, Umeå University, 36 pp. (1975)

Paper E

On the Torsion Problem for Anisotropic Periodic Plate Structures

Dag Lukkassen, Annette Meidell and Andreas Seger

Published in *AIP Conference Proceedings*, 2014, volume 1637, pages 976–981. DOI: 10.1063/1.4904671.

On the torsion problem for anisotropic periodic plate structures

Dag Lukkassen, Annette Meidell, and Andreas Seger

Citation: AIP Conference Proceedings **1637**, 976 (2014); doi: 10.1063/1.4904671
View online: http://dx.doi.org/10.1063/1.4904671
View Table of Contents: http://scitation.aip.org/content/aip/proceeding/aipcp/1637?ver=pdfcov
Published by the AIP Publishing

On the Torsion Problem for Anisotropic Periodic Plate Structures

The paper is dedicated to professor Lars-Erik Persson, on the occasion of his 70th birthday

Dag Lukkassen*, Annette Meidell† and Andreas Seger**

*Narvik University College and
NORUT Narvik, Norway
†Narvik University College and
NORUT Narvik, Norway
**Narvik University College, Norway

Abstract. We consider some mathematical aspects of the torsion problem for anisotropic periodic plate structures where the underlying material is monoclinic. In particular we show in detail how the weak formulation of the problem is derived and express the torsional rigidity in terms its solution.

Keywords: anisotropic periodic plate structures, monoclinic materials, torsional rigidity
PACS: 02.30.Jr, 87.10.-e, 81.40.Jj, 87.10.Pq.

INTRODUCTION

We consider a periodic plate structure of the type principally illustrated in Figure 1. The plate structure is assumed to be a connected set bounded by an upper s^+ and lower surface s^- which are non-intersecting and periodic in the x-variable with period $2x_0$. In Figure 1 we have included a period of the structure in the xz-plane, denoted Y, given by

$$Y = \left\{(x,z) : -x_0 \le x \le x_0, s^-(x) \le z \le s^+(x)\right\}.$$

The boundary ∂Y of Y can be divided into the upper and lower surface denoted ∂Y_f and the vertical sides denoted ∂Y_v. In order to find the effective stiffness parameters of the plate we may deform the structure in such a way that the corresponding displacement-vector $u = u(x,y,z)$ takes the form

$$u = v + w,$$

where $w = w(x,y)$ is quasiperiodic in the x variable and v is a predescribed function which describes the averaged (or homogenized) displacement corresponding to the particular effective parameter we want to compute. Then, by comparing the resultant forces or moments per unit length with the average elongation, curvature or relative twist angle, we find the corresponding effective stiffness parameters.

In this paper we focus on the torsion rigidity per unit length D_{xy}, which is found by twisting the structure as illustrated in Figure 1 and comparing the torsion moment per unit length with the relative twist angle τ. In this case the predescribed function v takes the form $v = [-\tau yz, -\tau xz, \tau xy]$ and $w = [0, \tau\omega(x,z), 0]$.

10th International Conference on Mathematical Problems in Engineering, Aerospace and Sciences
AIP Conf. Proc. 1637, 976-981 (2014); doi: 10.1063/1.4904671

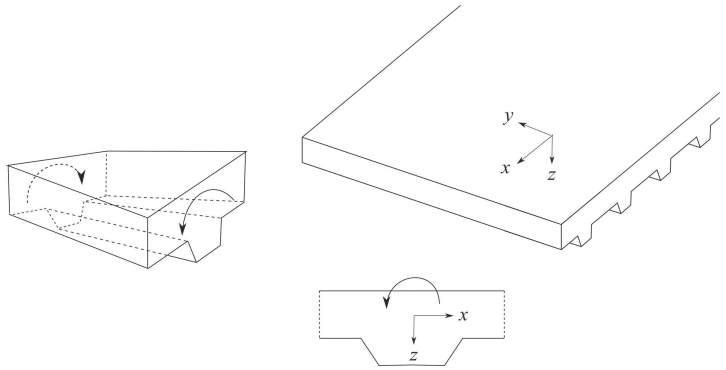

FIGURE 1. The periodic plate-structure.

SOME REMARKS ON MONOCLINIC MATERIALS

We recall that the stress-strain relation for a general anisotropic linear elastic material can be expressed in matrix form as follows:

$$\underbrace{\begin{bmatrix} \sigma_{11} \\ \sigma_{22} \\ \sigma_{33} \\ \sigma_{12} \\ \sigma_{23} \\ \sigma_{13} \end{bmatrix}}_{\sigma} = \underbrace{\begin{bmatrix} C_{1111} & C_{1122} & C_{1133} & C_{1112} & C_{1123} & C_{1113} \\ C_{2211} & C_{2222} & C_{2233} & C_{2212} & C_{2223} & C_{2213} \\ C_{3311} & C_{3322} & C_{3333} & C_{3312} & C_{3323} & C_{3313} \\ C_{1211} & C_{1222} & C_{1233} & C_{1212} & C_{1223} & C_{1213} \\ C_{2311} & C_{2322} & C_{2333} & C_{2312} & C_{2323} & C_{2313} \\ C_{1311} & C_{1322} & C_{1333} & C_{1312} & C_{1323} & C_{1313} \end{bmatrix}}_{C} \underbrace{\begin{bmatrix} e_{11} \\ e_{22} \\ e_{33} \\ \gamma_{12} \\ \gamma_{23} \\ \gamma_{13} \end{bmatrix}}_{e}.$$

Here, the indices 1, 2 and 3 refers to the x, y and z direction, respectively. The stiffness matrix C is symmetric. Let us now consider an orthonormal coordinate system with basis vectors

$$\mathbf{n}_1 = [n_{11}, n_{12}, n_{13}]$$
$$\mathbf{n}_2 = [n_{21}, n_{22}, n_{23}]$$
$$\mathbf{n}_3 = [n_{31}, n_{32}, n_{33}].$$

A vector with coordinates $x = (x_1, x_2, x_3)$ (relative to the usual coordinate system) will then have coordinates $x' = (x'_1, x'_2, x'_3)$ (relative to the new coordinate system) given by the relation

$$\begin{bmatrix} x'_1 \\ x'_2 \\ x'_3 \end{bmatrix} = \begin{bmatrix} n_{11} & n_{12} & n_{13} \\ n_{21} & n_{22} & n_{23} \\ n_{31} & n_{32} & n_{33} \end{bmatrix} \begin{bmatrix} x_1 \\ x_2 \\ x_3 \end{bmatrix}.$$

It is possible to show that the following relation holds between the strain $e = [e_{11}, e_{22}, e_{33,} \gamma_{12}, \gamma_{23,} \gamma_{13}]^T$, $\gamma_{ij} = 2e_{ij}$ (in the usual coordinate system) and $e' = \left[e'_{11}, e'_{22}, e'_{33,} \gamma'_{12}, \gamma'_{23}, \gamma'_{13}\right]^T$, $\gamma'_{ij} = 2e'_{ij}$ (in the new coordinate system):

$$e' = \mathbf{T}_e e,$$

where

$$\mathbf{T}_e = \begin{bmatrix} n_{11}^2 & n_{12}^2 & n_{13}^2 & n_{11}n_{12} & n_{12}n_{13} & n_{11}n_{13} \\ n_{21}^2 & n_{22}^2 & n_{23}^2 & n_{21}n_{22} & n_{22}n_{23} & n_{21}n_{23} \\ n_{31}^2 & n_{32}^2 & n_{33}^2 & n_{31}n_{32} & n_{32}n_{33} & n_{31}n_{33} \\ 2n_{11}n_{21} & 2n_{12}n_{22} & 2n_{13}n_{23} & n_{11}n_{22}+n_{21}n_{12} & n_{12}n_{23}+n_{22}n_{13} & n_{11}n_{23}+n_{21}n_{13} \\ 2n_{21}n_{31} & 2n_{22}n_{32} & 2n_{23}n_{33} & n_{21}n_{32}+n_{31}n_{22} & n_{22}n_{33}+n_{32}n_{23} & n_{21}n_{33}+n_{31}n_{23} \\ 2n_{11}n_{31} & 2n_{12}n_{32} & 2n_{13}n_{33} & n_{11}n_{32}+n_{31}n_{12} & n_{12}n_{33}+n_{32}n_{13} & n_{11}n_{33}+n_{31}n_{13} \end{bmatrix}.$$

Moreover, we can obtain a similar relation between the corresponding stresses σ and σ' :

$$\sigma' = \mathbf{T}_\sigma \sigma,$$

where $\mathbf{T}_\sigma$ is obtained from $\mathbf{T}_e$ by changing the factors of 2 in $\mathbf{T}_e$ symmetrically about the diagonal, i.e.

$$\mathbf{T}_\sigma = \begin{bmatrix} n_{11}^2 & n_{12}^2 & n_{13}^2 & 2n_{11}n_{12} & 2n_{12}n_{13} & 2n_{11}n_{13} \\ n_{21}^2 & n_{22}^2 & n_{23}^2 & 2n_{21}n_{22} & 2n_{22}n_{23} & 2n_{21}n_{23} \\ n_{31}^2 & n_{32}^2 & n_{33}^2 & 2n_{31}n_{32} & 2n_{32}n_{33} & 2n_{31}n_{33} \\ n_{11}n_{21} & n_{12}n_{22} & n_{13}n_{23} & n_{11}n_{22}+n_{21}n_{12} & n_{12}n_{23}+n_{22}n_{13} & n_{11}n_{23}+n_{21}n_{13} \\ n_{21}n_{31} & n_{22}n_{32} & n_{23}n_{33} & n_{21}n_{32}+n_{31}n_{22} & n_{22}n_{33}+n_{32}n_{23} & n_{21}n_{33}+n_{31}n_{23} \\ n_{11}n_{31} & n_{12}n_{32} & n_{13}n_{33} & n_{11}n_{32}+n_{31}n_{12} & n_{12}n_{33}+n_{32}n_{13} & n_{11}n_{33}+n_{31}n_{13} \end{bmatrix}.$$

Moreover, it can be shown that $\mathbf{T}_\sigma^{-1} = \mathbf{T}_e^T$. Concerning these facts we refer to e.g. [1, p. 212]. Letting

$$\sigma' = C'e',$$

denote the stress-strain relation in the new coordinate system, we therefore obtain the following relation between the new and old stiffness matrix:

$$C = \mathbf{T}_e^T C' \mathbf{T}_e = \begin{bmatrix} C'_{1111} & C'_{1122} & C'_{1133} & C'_{1112} & C'_{1123} & C'_{1113} \\ C'_{2211} & C'_{2222} & C'_{2233} & C'_{2212} & C'_{2223} & C'_{2213} \\ C'_{3311} & C'_{3322} & C'_{3333} & C'_{3312} & C'_{3323} & C'_{3313} \\ C'_{1211} & C'_{1222} & C'_{1233} & C'_{1212} & C'_{1223} & C'_{1213} \\ C'_{2311} & C'_{2322} & C'_{2333} & C'_{2312} & C'_{2323} & C'_{2313} \\ C'_{1311} & C'_{1322} & C'_{1333} & C'_{1312} & C'_{1323} & C'_{1313} \end{bmatrix}.$$

In particular, if the new coordinate system is a reflection of xz plane, i.e.

$$\begin{aligned} \mathbf{n}_1 &= [1,0,0], \\ \mathbf{n}_2 &= [0,-1,0], \\ \mathbf{n}_3 &= [0,0,1], \end{aligned}$$

then

$$\mathbf{T}_\sigma = \begin{bmatrix} 1 & 0 & 0 & 0 & 0 & 0 \\ 0 & 1 & 0 & 0 & 0 & 0 \\ 0 & 0 & 1 & 0 & 0 & 0 \\ 0 & 0 & 0 & -1 & 0 & 0 \\ 0 & 0 & 0 & 0 & -1 & 0 \\ 0 & 0 & 0 & 0 & 0 & 1 \end{bmatrix}.$$

Hence,

$$C = \mathbf{T}_e^T C' \mathbf{T}_e = \begin{bmatrix} C'_{1111} & C'_{1122} & C'_{1133} & -C'_{1112} & -C'_{1123} & C'_{1113} \\ C'_{2211} & C'_{2222} & C'_{2233} & -C'_{2212} & -C'_{2223} & C'_{2213} \\ C'_{3311} & C'_{3322} & C'_{3333} & -C'_{3312} & -C'_{3323} & C'_{3313} \\ -C'_{1211} & -C'_{1222} & -C'_{1233} & C'_{1212} & -C'_{1223} & C'_{1213} \\ -C'_{2311} & -C'_{2322} & -C'_{2333} & -C'_{2312} & C'_{2323} & C'_{2313} \\ C'_{1311} & C'_{1322} & C'_{1333} & C'_{1312} & C'_{1323} & C'_{1313} \end{bmatrix}.$$

From this we see that C is invariant under this transformation (meaning that $C = \mathbf{T}_e^T C \mathbf{T}_e$) provided that C is of the form

$$C = \begin{bmatrix} C_{1111} & C_{1122} & C_{1133} & 0 & 0 & C_{1113} \\ C_{2211} & C_{2222} & C_{2233} & 0 & 0 & C_{2213} \\ C_{3311} & C_{3322} & C_{3333} & 0 & 0 & C_{3313} \\ 0 & 0 & 0 & C_{1212} & C_{1223} & 0 \\ 0 & 0 & 0 & C_{2312} & C_{2323} & 0 \\ C_{1311} & C_{1322} & C_{1333} & 0 & 0 & C_{1313} \end{bmatrix}. \tag{1}$$

Materials with this property is called monoclinic. The set of all monoclinic materials is closed under pure rotation about the y-axis. Indeed, putting

$$\begin{aligned}\mathbf{n}_1 &= [\cos\theta, 0, \sin\theta]\\ \mathbf{n}_2 &= [0,1,0]\\ \mathbf{n}_3 &= [-\sin\theta, 0, \cos\theta],\end{aligned}$$

we obtain that

$$\mathbf{T}_e = \begin{bmatrix} n_{11}^2 & 0 & n_{13}^2 & 0 & 0 & n_{11}n_{13} \\ 0 & 1 & 0 & 0 & 0 & 0 \\ n_{31}^2 & 0 & n_{33}^2 & 0 & 0 & n_{31}n_{33} \\ 0 & 0 & 0 & n_{11} & n_{13} & 0 \\ 0 & 0 & 0 & n_{31} & n_{33} & 0 \\ 2n_{11}n_{31} & 0 & 2n_{13}n_{33} & 0 & 0 & n_{11}n_{33}+n_{31}n_{13} \end{bmatrix},$$

and by performing matrix multiplication, we easily find that the zero-elements of (1) are kept under the transformation $C = \mathbf{T}_e^T C' \mathbf{T}_e$.

THE TORSION PROBLEM FOR MONOCLINIC MATERIALS

In the modelling of the torsion problem we assume that the material is locally monoclinic of the form of (1). As mentioned in the introduction, we assume that the displacement is of the form

$$u = [u_1, u_2, u_3] = [-\tau zy, \tau\varphi(x,z), \tau xy], \tag{2}$$

where $\varphi(x,z) = \omega(x,z) - xz$. Moreover, we assume that no body forces are present, i.e. that the following equations of elastic equilibrium are satisfied (see also [2], [3] and [4]):

$$\begin{aligned}\frac{\partial\sigma_{11}}{\partial x} + \frac{\partial\sigma_{12}}{\partial y} + \frac{\partial\sigma_{13}}{\partial z} &= 0,\\ \frac{\partial\sigma_{12}}{\partial x} + \frac{\partial\sigma_{22}}{\partial y} + \frac{\partial\sigma_{23}}{\partial z} &= 0,\\ \frac{\partial\sigma_{13}}{\partial x} + \frac{\partial\sigma_{23}}{\partial y} + \frac{\partial\sigma_{33}}{\partial z} &= 0.\end{aligned} \tag{3}$$

Both the upper and lower surface of the plate are free from external stresses. This implies that all three components of the stress vector on these surfaces vanish, i.e. we get the following boundary conditions

$$\begin{aligned}\sigma_{11}n_1 + \sigma_{12}n_2 + \sigma_{13}n_3 &= 0,\\ \sigma_{12}n_1 + \sigma_{22}n_2 + \sigma_{23}n_3 &= 0,\\ \sigma_{13}n_1 + \sigma_{23}n_2 + \sigma_{33}n_3 &= 0,\end{aligned} \tag{4}$$

where (n_1, n_2, n_3) is the outward normal of the boundary. By (2) the components of the strain vector are: $e_{11} = \partial u_1/\partial x = 0$, $e_{22} = \partial u_2/\partial y = 0$, $e_{33} = \partial u_3/\partial z = 0, \gamma_{12} = \partial u_1/\partial y + \partial u_2/\partial x = -\tau z + \tau\partial\varphi/\partial x$, $\gamma_{23} = \partial u_2/\partial z + \partial u_3/\partial y = \tau x + \tau\partial\varphi/\partial z$ and $\gamma_{13} = \partial u_1/\partial z + \partial u_3/\partial x = -\tau y + \tau y = 0$. Using that the underlying material is monoclinic we therefore obtain from the stress strain relation that

$$\sigma_{11} = \sigma_{22} = \sigma_{33} = \sigma_{13} = 0.$$

Hence, (3) and (4) are satisfied if

$$\operatorname{div}[\sigma_{12}, \sigma_{23}]^T = 0$$

and

$$[\sigma_{12}, \sigma_{23}]^T \cdot n = 0, \tag{5}$$

on the upper and lower side ∂Y_f, where $n=(n_x,n_z)$ is the two dimensional outward normal of the surface and

$$[\sigma_{12},\sigma_{23}]^T = \tau A\left(\operatorname{grad}\varphi + ([-z,x]^T\right),$$

where A is the out-of-plane shear stiffness matrix

$$A=\begin{bmatrix} C_{1212} & C_{1223} \\ C_{2312} & C_{2323} \end{bmatrix}.$$

We will also assume that the average value of the stress vector $[\sigma_{12},\sigma_{23}]^T\cdot n$ on any plane with normal vector $n=(n_x,n_z)=(1,0)$ vanish (otherwise there would be non-zero average shear deformations in the xy-plane), i.e. that

$$\int_{\partial Y_v}\sigma_{12}dz=0. \tag{6}$$

Since, $\varphi=\omega-xz$ where $\omega=\omega(x,z)$ is quasiperiodic in the x-variable (with period $2x_0$) the above partial differential equation can be written as

$$\operatorname{div} A\left(\operatorname{grad}\omega+([-2z,0]^T\right)=0,$$

on Y together with the boundary condition

$$A\left(\operatorname{grad}\omega+([-2z,0]^T\right)\cdot n=0 \tag{7}$$

on the set ∂Y_f and the condition (6), i.e.

$$\int_{\partial Y_v}\left(A\left(\operatorname{grad}\omega+([-2z,0]^T\right)\cdot n\right)dz=0 \tag{8}$$

on the vertical sides of ∂Y. This problem can only be understood in classical sense in parts of Y where the shear stiffness matrix $A=A(x,z)$ is sufficiently smooth. More generally, we have to use the following weak problem:

$$\int_Y A\left(\operatorname{grad}\omega+[-2z,0]^T\right)\cdot\operatorname{grad}v\,dxdz=0,\ \forall v\in W, \tag{9}$$

where W denotes the space of quasiperiodic functions, i.e. the completion, in usual Sobolev space $H^1(Y)$, of the set of smooth functions v of zero average ($\int_Y v(x,z)\,dxdz=0$) of the form $v(x,z)=w(x,z)+kx$, where k is a constant and w satisfies the periodicity property $w(x_0,z)=w(-x_0,z)$.

This formulation can be derived from the classical formulation e.g. when Y is divided into open connected subsets S_i, $\cup_{i=1}^m\overline{S}_i=Y$, with sufficiently smooth boundaries (e.g. Lipschitz), such that the shear modulus matrix $A=A(x,z)$ is x-periodic and possesses smooth components on each set S_i. In this case

$$\operatorname{div}[\sigma_{12},\sigma_{23}]^T=0 \text{ on } S_i, \tag{10}$$

in classical sense. Moreover, on a point of the common boundary between S_i and S_k with normal n^i (pointing out of S_i), the normal component $([\sigma_{12},\sigma_{23}]^T)\cdot n^i$ on the set S_i, denoted $\left[[\sigma_{12},\sigma_{23}]^T\cdot n^i\right]_i$, equals that on the set S_k, which is the negative value of the normal component $[\sigma_{12},\sigma_{23}]^T\cdot n^k$ on the set S_k where $n^k=-n^i$ (the normal is pointing out of S_k), i.e.

$$\left[[\sigma_{12},\sigma_{23}]^T\cdot n^i\right]_i=-\left[([\sigma_{12},\sigma_{23}]^T\cdot n^k\right]_k \text{ on } \partial S_i\cap\partial S_k. \tag{11}$$

Multiplying the equation (10) with an arbitrary function v, which is smooth on Y, we obtain by the Green formula that

$$\int_{S_i}[\sigma_{12},\sigma_{23}]^T\cdot\operatorname{grad}v\,dxdz=\int_{\partial S_i}\left([\sigma_{12},\sigma_{23}]^T\cdot n^i\right)v\,ds.$$

Using this and (11) we find that

$$\int_Y[\sigma_{12},\sigma_{23}]^T\cdot\operatorname{grad}v\,dxdz=\sum_{i=1}^m\int_{S_i}[\sigma_{12},\sigma_{23}]^T\cdot\operatorname{grad}v\,dxdz=$$

$$\int_{\partial Y} \left([\sigma_{12}, \sigma_{23}]^T \cdot n^i \right) v \, ds.$$

The latter integral vanishes. In order to see this, we first note that

$$\int_{\partial Y_f} \left([\sigma_{12}, \sigma_{23}]^T \cdot n^i \right) v \, ds = 0,$$

by (5). Moreover, $[\sigma_{12}, \sigma_{23}]^T$ is periodic since it is constructed by partial derivatives of a quasiperiodic function. Since

$$\left([\sigma_{12}, \sigma_{23}]^T \cdot n \right) v = \left([\sigma_{12}, \sigma_{23}]^T \cdot n \right) kx + \left([\sigma_{12}, \sigma_{23}]^T \cdot n \right) w$$

and

$$\int_{\partial Y_v} \left(\left([\sigma_{12}, \sigma_{23}]^T \cdot n \right) kx \right) dz = kx \int_{\partial Y_v} \left([\sigma_{12}, \sigma_{23}]^T \cdot n \right) dz = 0$$

by (8) and $\left([\sigma_{12}, \sigma_{23}]^T \cdot n \right) w$ has opposite value on opposite sides of the boundary ∂Y_v (due to the periodicity), we see that

$$\sum_{i=1}^{m} \int_{\partial S_i} \left([\sigma_{12}, \sigma_{23}]^T \cdot n^i \right) v \, dxdz = 0.$$

Thus we conclude that

$$\int_{\Omega} [\sigma_{12}, \sigma_{23}]^T \cdot \operatorname{grad} v \, dxdy = \sum_{i=1}^{m} \int_{S_i} [\sigma_{12}, \sigma_{23}]^T \cdot \operatorname{grad} v \, dxdy = 0,$$

which gives (9).

The problem (9) admits a unique solution within an arbitrary additive constant (this fact is easily seen by the Lax-Milgram Lemma), under the assumption that $A : Y \to \mathbb{R}^{2\times 2}$ has Lebesgue measurable components and that there exist constants $\alpha > 0$ and $\beta < \infty$ such that

$$\alpha |\xi|^2 \leq \xi \cdot A(x,y)\xi \leq \beta |\xi|^2 \tag{12}$$

for all $\xi \in R^2$.

The total moment per unit length M_{xz} about the y-axis of the stress vector $[\sigma_{12}, \sigma_{22}, \sigma_{23}]^T$ applied to the surface Y, is given by

$$M_{xz} = \frac{1}{2x_0} \int_Y (-\sigma_{12} z + \sigma_{23} x) \, dxdz.$$

Finally, we have found the expresion for the torsion rigidity per unit length D_{xy} in terms of the solution ω :

$$D_{xy} = \frac{M_{xz}}{\tau} = \frac{1}{2x_0 \tau} \int_Y \left((\sigma_{12}, \sigma_{23})^T (-z, x)^T \right) dxdz =$$

$$\frac{1}{2x_0} \int_Y \left(A \left(\operatorname{grad} \omega + ([-2z, 0]^T \right) (-z, x)^T \right) dxdz.$$

REFERENCES

1. R. D. Cook, D. S. Malkus and M.E. Plesha, "Concepts and applications of finite element analysis," J. Wiley and Sons Inc., 1989.
2. D. Lukkassen, Annette Meidell, A. Piatnitski and A. Shamaev, "Symmetry-relations for elastically deformed periodic rod-structures," Math. Mod. Meth. Appl. Sci. 19, 4, 501-525 (2009).
3. D. Lukkassen, A. Meidell and P. Wall, "New methods for estimating the torsional rigidity of composite bars," Internat. J. Engrg. Sci. 47, 524-536 (2009).
4. D. Lukkassen, A. Meidell and P. Wall, "Mathematical analysis and homogenization of the torsion problem," J. Funct. Spaces Appl. 6, 2, 155-176 (2008).
5. R. Adams, Sobolev Spaces, Academic Press, 1975.
6. W. P. Ziemer, "Weakly Differentiable Functions", Sobolev Spaces and Functions of Bounded Variation. Springer, Berlin, 1989.